UQAC
Université du Québec
à Chicoutimi

Fabrication of Smart Aqueous Self-Lubricating Icephobic Coatings Containing Encapsulated Phase Change Materials (PCM)

By

Mohammadreza Shamshiri

Under supervision of Prof. Reza Jafari and co-supervision of Prof. Gelareh Momen

Manuscript-Based Thesis Presented to Université du Québec à Chicoutimi in Partial fulfillment of the Requirements for the Degree of Doctor of Philosophy Ph.D.

Defended on 14th April, 2023

BOARD OF EXAMINERS:

Professor Yasar Kocaefe, Department of Applied Sciences at UQAC, President of the Board

Professor Véronic Landry, Department of Wood and Forest Sciences at Université Laval, External Member of the Board

Doctor Derek Harvey, Department of Applied Sciences at UQAC, Internal Member of the Board

Professor Reza Jafari, Department of Applied Sciences at UQAC, Internal Member of the Board

Professor Gelareh Momen, Department of Applied Sciences at UQAC, Internal Member of the Board

Québec, Canada

Résumé

Les revêtements glaciophobes intelligents ont attiré beaucoup d'attention en raison de leurs perspectives d'application prometteuses pour réduire l'adhérence de la glace, abaisser la température et retarder le temps de nucléation de la glace. De tels revêtements peuvent ressentir les changements dans les stimuli environnementaux comme la température, la pression et le pH, et fournir une réponse anti-givrage ou dégivrage. Selon le type de stimuli, ces revêtements peuvent être classés en plusieurs groupes. Dans la présente thèse, nous avons choisi deux stratégies glaciophobes intelligentes différentes pour développer de nouveaux revêtements glaciophobes intelligents aux propriétés anti-givrantes et dégivrantes améliorées.

Dans un premier temps, les revêtements autolubrifiants aqueux ont été développés en incorporant le copolymère PEG-PDMS dans une matrice élastomère. La présence des groupes hydrophiles sur les copolymères PEG-PDMS peut contribuer à la formation de la couche quasi liquide (QLL) capable d'améliorer les performances glaçiophobes des revêtements. L'analyse de surface des revêtements fabriqués a confirmé que l'incorporation de ces copolymères dans la matrice élastomère augmentait la surface de contact effective entre la gouttelette d'eau et la surface. De plus, une teneur accrue en copolymère réduit la température de nucléation de la glace et retarde davantage le point de congélation. Deux méthodes différentes d'adhérence, la poussée (push-off) et les tests d'adhérence centrifuge ont été appliquées pour mesure l'adhérence de la glace sur les revêtements. En général, l'ajout de copolymère PEG-PDMS dans la matrice de PDMS produit une couche lubrifiante surfondue, entraînant une diminution de l'adhérence de la glace. Malgré les caractéristiques glaciophobes améliorées grâce à l'ajout de copolymère, une teneur excessive en a saturé le revêtement, ce qui a conduit à la séparation de phase. Par conséquent, la rugosité de la surface s'est accrue donnant lieu à une augmentation de la contrainte d'adhérence de la glace, en raison de l'enclenchement mécanique entre la glace et la surface.

Deuxièmement, compte tenu de la capacité des matériaux à changement de phases (PCM) à emmagasiner et à libérer une grande quantité de chaleur latente au cours de leur processus de changement de phase, un revêtement glaciophobe intelligent a été conçu en incorporant des microcapsules de PCM dans un revêtement à base de PDMS. À cette fin, un mélange de PCM a été encapsulé avec succès dans une coque en polyurée-formaldéhyde (PUF) via une polymérisation in situ. Ensuite, les microcapsules préparées ont été incorporées dans la matrice. Le test de calorimétrie à balayage différentiel (DSC) a confirmé que le mélange PCM a conservé sa capacité de dégagement de chaleur latente lorsqu'il est encapsulé et incorporé dans le revêtement élastomère. Cette analyse a également montré que la présence des microcapsules de PCM réduisait la température de nucléation de la glace, très probablement en raison de la chaleur latente dégagée. Un appareil spécialement conçu, appelé configuration micro-push-off, a été utilisé pour évaluer l'adhérence de la glace pendant une courte période après la congélation complète. La mesure a démontré que l'incorporation de microcapsules PCM peut réduire la contrainte d'adhérence de la glace en raison de l'un ou l'autre des scénarios possibles de production de QLL ou de différences de dilatation thermique. De plus, la quantité réduite de glace accumulée sur les revêtements contenant du PCM proviendraient de la diminution de l'adhérence de la glace.

Enfin, l'effet synergique de la combinaison des stratégies mentionnées ci-dessus en imprégnant des revêtements contenant du copolymère PEG-PDMS avec des microcapsules PCM a été évalué. Pour commencer, un mélange de n-dodécane et de n-tétradécane avec un rapport optimisé a été encapsulé dans la coque PUF. Les microcapsules obtenues ont été incorporées dans le revêtement PDMS contenant en masse 2,5 % m/m de copolymère PEG-PDMS à terminaison hydroxyle. Le test DSC a prouvé que l'incorporation des microcapsules PCM dans le revêtement autolubrifiant aqueux a déplacé la température de nucléation de la glace vers des températures plus froides. L'évaluation du temps de congélation complet a également confirmé les résultats du DSC, car le temps de congélation a été prolongé avec l'incorporation des microcapsules PCM dans le revêtement. Les performances antigivrantes améliorées peuvent être liées au dégagement de chaleur latente par le PCM qui a préservé la QLL pendant une période plus longue. De plus, il a été observé que le revêtement autolubrifiant aqueux contenant des microcapsules PCM présentait une contrainte d'adhérence à la glace inférieure à celle des revêtements autolubrifiants dépourvus de microcapsules. Aussi, des concentrations accrues de microcapsules diminueraient-elles l'adhérence à la glace. Une plus faible contrainte d'adhérence de la glace a également contribué à une réduction de la quantité de glace accumulée sur la surface. La combinaison de dix cycles de givrage/dégivrage et d'un test de micro-poussée a confirmé qu'il n'y avait pas de changements considérables dans la contrainte d'adhérence de la glace au cours des événements de dégivrage ultérieurs. En somme, les revêtements fabriqués peuvent être considérés comme un candidat potentiel pour diverses applications glaciophobes.

Mots-clés: Glaciophobicité, revêtements glaciophobes intelligents, adhérence à la glace, stimuli-sensibles, glace, mouillabilité, copolymère PEG-PDMS, revêtements aqueux autolubrifiants, matériaux à changement de phase (PCM), chaleur latente, accumulation de glace, couche quasi-liquide (QLL), effet synergique.

Abstract

Smart icephobic coatings have attracted much attention owing to their promising application prospects in reducing ice adhesion, decreasing ice nucleation temperature, and delaying freezing time. Such coatings can sense changes in environmental stimuli, such as temperature, humidity, pressure, and pH, and provide an anti-icing or deicing response. These coatings can be categorized into several groups depending on the type of stimuli. In the present thesis, we chose two different smart icephobic strategies to develop novel coatings with enhanced anti-icing and deicing properties.

First, aqueous self-lubricating coatings were developed by incorporating the polyethylene glycol (PEG)–polydimethylsiloxane (PDMS) copolymer in an elastomeric matrix. The presence of hydrophilic groups on PEG–PDMS copolymers can contribute to the formation of a quasi-liquid-like layer (QLL) that can improve the icephobic performance of the coatings. Surface analysis of the fabricated coatings confirmed that blending these copolymers into the elastomeric matrix increased the effective contact area between the water droplet and surface. Moreover, increased copolymer content reduced the ice nucleation temperature and prolonged the freezing-delay time. Two different methods, namely, push-off adhesion and centrifugal adhesion tests, were applied to study ice adhesion on the coatings. In general, adding PEG–PDMS copolymer into the PDMS matrix produced an unfrozen lubricating layer, resulting in decreased ice adhesion. Although excessive copolymer content saturated the coating with copolymer, which led to phase separation. Consequently, the surface roughness heightened; therefore, the ice adhesion strength increased owing to the mechanical interlocking between the ice and surface.

Second, given the capability of phase change materials (PCMs) to restore and release a large amount of latent heat during the phase change process, we designed a smart icephobic coating by embedding PCM microcapsules into the PDMS coating. For this purpose, a mixture of n-dodecane, n-tetradecane was successfully encapsulated in a poly urea–formaldehyde (PUF) shell via in situ polymerization. Then, the prepared microcapsules were incorporated into PDMS. Differential scanning calorimetry (DSC) confirmed that the PCM mixture preserved its capability of latent heat release while being encapsulated and incorporated within the elastomeric coating. This analysis also showed that the presence of PCM microcapsules reduced the ice nucleation temperature very likely due to the released latent heat. A specially designed apparatus called micro-push-off set-up was used to evaluate the ice adhesion for a short period after complete freezing. The measurement demonstrated that embedding PCM microcapsules can reduce the ice adhesion strength because of the possible scenario of producing QLL or thermal expansion differences. Furthermore, the reduced amount of ice accumulated on the PCM-containing coatings stemmed from the decreased ice adhesion.

Finally, we evaluated the synergistic effect of combining the above-mentioned strategies by embedding PCM microcapsules into PEG–PDMS copolymer-containing coatings. A mixture of *n*-dodecane and *n*-tetradecane with an optimized ratio was encapsulated within the PUF shell. The obtained microcapsules were embedded into the PDMS coating containing 2.5 wt.% hydroxyl-terminated PEG–PDMS copolymer.

With DSC, it was verified that incorporating the PCM microcapsules into the aqueous self-lubricating coating shifted the ice nucleation temperature toward colder temperatures. Evaluation of complete freezing time also supported the DSC results, as freezing time was increased by embedding the PCM microcapsules within the coating. The enhanced anti-icing performance can be related to the latent heat released by PCM, which preserved the QLL for a prolonged period. Moreover, it was observed that the aqueous self-lubricating coating containing PCM microcapsules showed lower ice adhesion strength than the self-lubricating coatings lacking microcapsules, and increased concentrations of the microcapsules resulted in decreased ice adhesion. A lower ice adhesion strength also resulted in a reduction in the amount of ice accumulated on the surface. Combining 10 icing/deicing cycles and micro-push-off test confirmed that no considerable changes in ice adhesion strength occurred over the subsequent deicing events. Therefore, the fabricated coatings can be considered a potential candidate for various icephobic applications.

Keywords: Icephobicity, smart icephobic coatings, ice adhesion, stimuli-responsive behavior, ice, wettability, PEG-PDMS copolymer, aqueous self-lubricating coatings, phase change materials (PCMs), latent heat, freezing delay, ice accumulation, quasi liquid-like layer, synergistic effect

Table of Contents

List of figures

List of tables

List of abbreviations

AFM	Atomic force microscopy
Al	Aluminum
ALS	Air/liquid (water)/solid
AMIL	Anti-icing materials international laboratory
ATR	Attenuated total reflection
CAH	Contact angle hysteresis
CAT	Centrifuge adhesion test
DMPA	Dimethylolpropionic acid
DSC	Differential scanning calorimetry
DTA	Differential thermal analysis
EMA	Ethylene maleic anhydride
ETFE	Ethylene tetrafluoroethylene
FTIR	Fourier-transform infrared spectroscopy
GNR	Graphene nanoribbon
IPN	Interpenetrating polymer network
IR	Infrared
MAGSS	Magnetic slippery surfaces
MOF	Metal–organic framework
NIR	Near-infrared
NSERC	Natural sciences and engineering research council of Canada
OH	Hydroxyl
PCM	Phase change materials

PDMS	Poly (dimethylsiloxane)
PEG-PDMS	Poly (ethylene glycol)- poly(dimethylsiloxane)
PFDS	Perfluorodecyltriethoxysilane
PMPS	Poly (methylphenylsiloxane)
PSA	Phosphoric sulfuric anodizing
PTFE	Poly (tetrafluoroethylene)
PUF	Poly (urea–formaldehyde)
PVDF	Poly (vinylidene fluoride)
PZT	Lead zirconate titanate
QLL	Quasi-liquid layer
RTV-SR	Room temperature vulcanized silicone rubber
SA	Sliding angle
SAT	Static accumulation test
SEM	Scanning electron microscopy
SHSS	Superhydrophobic surfaces
SiO_2	Silicone oxide
SLIPS	Slippery liquid-infused porous surfaces
SLUGS	Self-lubricating gels
SLWL	Self-lubricating liquid water layer
SMPS	Shape-memory polymers
UCST	Upper critical solution temperature
UV	Ultraviolet
WCA	Water contact angle

List of symbols

$\boldsymbol{\gamma_{LV}}$	Surface tension
$\boldsymbol{C_p}$	Mass specific heat capacity
$\boldsymbol{F_{\parallel}}$	Tangential component of the gravity force
$\boldsymbol{W_a}$	Practical work of adhesion per unit area
$\boldsymbol{v_m}$	Molecular volume
$\boldsymbol{\gamma_{SL}}$	Solid-liquid interfacial energy
$\boldsymbol{\theta_{rec}}$	Receding contact angle
A	Iced area
h	Planck's constant
I	Thermal effusivity
J_0	Nucleation rate
k	Boltzmann's constant
m	Ice mass
q	Heat flow rate
r	Beam radius
Rq	Root-mean-square deviation of line roughness
Sku	Kurtosis coefficient of area roughness
Sq	Root-mean-square height of area roughness
Ssk	Skewness coefficient of area roughness
T	Absolute temperature
$T_{f,o}$,	Onset temperature on the freezing
T_g	Glass transition temperature

T_m	Melting temperature
$T_{m,o}$	Onset temperature on the heating
T_{ps}	Critical phase separation temperature
W	Weight of the droplet
α	Inclined angle
Δg	Diffusion activation energy
ΔT_s	Supercooling degree
τ	Adhesion shear stress
ω	Angular velocity
$\boldsymbol{k}$	Thermal conductivity
$\boldsymbol{\rho}$	Density

Dedication

To my parents, *Fatemeh Shamshiri* and *Jamshid Shamshiri* for providing me with unfailing support and continuous encouragement throughout my life,

and

to my beloved wife, *Samaneh Heydarian*, for her love and constant support particularly during the last four years.

Acknowledgements

I would like to express my appreciation to my research supervisor, *Prof. Reza Jafari*, for his continuous support, kindness, and suggestions during the planning and development of this research work.

I would like to warmly thank my co-supervisor, *Prof. Gelareh Momen* for her support, guidance, and continuous involvement in my project, and for providing me with the freedom to explore my research interests.

I am deeply grateful to the members of my committee, *Prof. Yasar Kocaefe*, *Prof. Véronic Landry*, and *Dr. Derek Harvey* for their worthwhile guidance and insightful comments.

Special thanks should be given to *Ms. Helene Gauthier*, Chercheuse Métallurgie et génie des Matériaux, IREQ, Hydro Québec, for her feedback and support during this academy-industry collaboration. I would also like to extend my thanks to all the professionals and technicians for their assistance in this project, especially *Dr Jean-Denis Brassard*, *Ms. Caroline Blackburn*, *Ms. Nathalie Gagné,* and *Ms. Shan Yang* at the Anti-icing Materials International Laboratory (AMIL), UQAC, *Mr. Luc Chatigny*, technician of Laboratoire Revêtements glaciophobes et ingénierie des surfaces (LARGIS), and *Ms. Caroline Potvin*, the laboratory assistant of the chemistry department.

I would like to express my sincere appreciation to *Hydro-Québec*, Québec, Canada, Natural Sciences and Engineering Research Council of Canada (NSERC), and le Pôle Recherche Innovation en Matériaux avancés du Québec (PRIMA Québec), Canada, for providing the financial support that made my research possible.

Last but not least, I would like to sincerely thank my family and friends for being there for me during this journey.

Introduction

Definition of the problem

Ice formation and accumulation can result in disastrous blackouts of high-voltage transmission lines. The adhesion of atmospheric ice on exposed objects, such as conductors and insulators, has devastating economical and safety consequences during ice storms [1–13].

Ice accretion on electrical settings can affect electrical efficiency owing to electrical flashover failure [2]. In other words, the formation of an ice layer on their surfaces can lead to electrical flashover failure during the icing period and later during the melting period. Sudden shedding of ice accretion can also mechanically damage power network equipment [2]. In 1998, a freezing rain event caused catastrophic blackouts of transmission lines in Eastern Canada that left many people without electricity for weeks [14]. In Italy, the damages caused by such a special weather condition cost more than 200 million euros per year [11]. In 2008, China faced huge economic losses (about 1.5 billion dollars) because of disruptions in transmission lines [12]. In 2021, winter storm struck Texas that left millions of people without electricity for several days [15].

The strategies used to combat icing on electrical infrastructures, particularly insulators, include preventing the icing of surfaces, avoiding ice accumulation, and reducing the adhesion between ice and the surface. For instance, room temperature-vulcanized silicone rubber coatings are used as hydrophobic coatings on porcelain and glass insulators to enhance their anti-icing performance. However, they have not shown

reliable effectiveness in preventing ice accretion. Besides, the hydrophobicity of silicone rubbers can be affected by humidity, temperature, soluble and insoluble deposits, and UV irradiation [16]. Ceramic semiconducting glaze is another candidate for generating Joule heat and modifying anti-icing properties. However, its main drawback is the continuous loss of energy [17].

In addition, embedding conducting particles, such as zinc oxide, carbon fibers, and carbon black, in silicone coating has been an effective approach to improve the anti-icing characteristics of electrical equipment. They could take advantage of heat generation and hydrophobicity to increase the freezing time of water droplets on the surface. However, high power loss and degradation of organic components are among their major drawbacks [18].

Smart or intelligent coatings have opened a new horizon in high-tech industries owing to their high potential application in harsh environments. Unlike conventional coatings that can provide a constant functionality based on their formulation, smart coatings can sense their surrounding environment and respond to any change in a predictable behavior [19]. Therefore, they can offer the desirable anti-icing characteristics to eliminate problems associated with ice accretion, including power outage and financial losses. Accordingly, this project aimed to develop smart icephobic coatings by impregnating encapsulated phase change materials (PCMs) into aqueous self-lubricating coatings. This project is an academic–industry collaboration between *Université du Québec à Chicoutimi (UQAC)* and *Hydro-Québec Company*.

Overview

Smart coatings show great potential in a wide range of applications owing to their stimuli-responsive behavior. These coatings can respond to any environmental stimulus, such as changes in pressure, temperature, light, and pH, in a desirable way. An ideal smart coating is expected to return to its original state after removing the environmental change [19–21]. Accordingly, a smart icephobic coating can sense and respond to environmental stimuli in a way that would result in reducing the amount of ice accumulated on the surface or lengthening the ice formation time [21].

Various strategies have been followed to fabricate smart icephobic coatings. Based on the type of stimuli, these coatings can be classified into different categories, including thermo-responsive coatings, self-healing icephobic coatings, self-lubricating coatings, and PCMs. Each of these methods has a great potential for developing anti-icing strategies. Most smart icephobic strategies are still in their initial stages. More relevant research needs to be carried out to develop them for large-scale production. Fabrication of aqueous self-lubricating coatings can offer a durable, efficient, and cost-effective method for anti-icing applications. Such a method does not suffer from lubricant-related problems, such as oil depletion, and can be a suitable alternative for many common passive anti-icing methods. Moreover, using PCMs has opened an avenue toward the development of new-generation anti-icing strategies. Releasing huge amounts of latent heat during the phase transition process is considered the outstanding characteristic of PCMs that can remarkably affect ice adhesion and delay ice formation. Besides, each above-mentioned strategy has some probable limits, although the synergistic effects of combining these methods can minimize their

corresponding downsides and promote their icephobic performance. In this project, we first developed an aqueous self-lubricating coating by blending an amphiphilic copolymer in a silicone elastomer. The icephobic characteristics of the prepared coating were evaluated, and the effects of copolymer type and content on the anti-icing performance of the coating were studied. In fact, such coatings can offer an easily operated and inexpensive icephobic strategy to prevent icing on exposed settings. In this research work, we aimed to develop a hybrid anti-icing strategy by combining aqueous self-lubricating coatings and PCMs. Therefore, after identifying the challenges and limits of aqueous self-lubricating coating, we selected a mixture of n-tetradecane, n-hexatriacontane, and then encapsulated it within a chemically compatible shell via in-situ polymerization. The selection of the PCM is essential, because a suitable PCM for anti-icing purpose should meet some criteria, including a desirable melting temperature, high latent heat, supercooling, and reproducible phase change [22,23]. Furthermore, PCM must preserve its ability to release latent heat as its most important characteristic for anti-icing performance. The PCM microcapsules were embedded into aqueous self-lubricating coating with the aim of using the synergistic effect of combining these strategies to enhance anti-icing performance.

Objectives

The main objective of this research work was to develop a hybrid anti-icing strategy using the synergistic effect of combining two approaches, namely, aqueous self-lubricating and PCM. To achieve this main objective, the detailed objectives were to:

- fabricate aqueous self-lubricating coating using amphiphilic copolymers,
- optimize the materials' values to find the desirable icephobic characteristics,
- develop a comprehensive set of characterization methods to evaluate the anti-icing and de-icing properties of the fabricated coatings,
- determine the suitable PCM combination for developing the desired icephobic prosperities,
- evaluate PCM's capability to preserve its phase-change characteristics when encapsulated and embedded within the coating matrix,
- assess the compatibility of the prepared PCM microcapsules with self-lubricating coating, and
- investigate the durability and mechanical properties of the fabricated coatings.

Originality statement

Smart icephobic coatings can provide new insight into designing an efficient strategy to protect many structures, such as wind turbine blades and insulators exposed to harsh cold-weather conditions. Using coatings is considered an efficient and cost-effective method to protect surfaces. Smart icephobic coatings can have a better performance in comparison with conventional coatings owing to their higher capability. Although most studies in this field are still in their initial stages, investment in developing smart icephobic coatings is expected to expand greatly over the next few years. In particular, aqueous self-lubricating coatings and PCMs have shown great potential for anti-icing applications. Moreover, combining these strategies can offer an

effective solution to fulfill market requirements. The originality of the present project can be concluded in the following main items:

- To our knowledge, the synergistic effect of aqueous self-lubricating coating and PCMs was investigated for the first time to develop a new anti-icing strategy. Each anti-icing technique may have some drawbacks and limits. The synergistic effect of combining these techniques can avoid the limits and open a new avenue toward developing anti-icing strategies.

- Most of the previous studies in the field of using PCMs for anti-icing applications were based on directly incorporating the PCMs into the main matrix, and research work on the encapsulation of PCMs for icephobic purpose is, to a large extent, limited. Using encapsulation can remarkably affect the service life of the coating by avoiding PCM leakage. Therefore, the suggested encapsulating procedure can be considered an important step toward producing durable PCM-containing coatings.

- The icephobic characteristics of the coatings in most of the previous studies were evaluated using two or three techniques. The icephobic performance of the produced coatings should be assessed from different aspects, including ice nucleation temperatures, freezing times, and ice accumulation, owing to the complexity of the icing phenomenon. Such an evaluation is rare in previous research works. Therefore, in this study, a comprehensive set of analyzing methods was provided to evaluate the anti-icing (delayed ice nucleation temperature and freezing time) and deicing (ice adhesion strength and ice accumulation) properties of the fabricated coatings.

- Having desired anti-icing characteristics is not enough to achieve an ideal coating; the fabricated coatings should meet other criteria, particularly in terms of mechanical properties. In fact, achieving enhanced icephobic performance may often cause the loss of mechanical properties and therefore decrease durability. This issue can limit the commercialization of icephobic coatings. Therefore, we evaluated the mechanical characteristics of the fabricated coatings, such as hardness, to develop durable icephobic coatings.

Methodology

This study aimed to develop a new anti-icing strategy by considering the synergistic effect of emerging aqueous self-lubricating coatings and phase change materials (PCM). The selection of suitable materials to obtain the desired properties was the most challenging step in the fabricating procedure. To achieve this objective, the research study was divided into three phases.

In the first phase, aqueous self-lubricating coatings were developed by blending two different copolymers in a silicone elastomer. The coatings were prepared with different copolymer contents and applied to substrates using a spin-coater. The variation of water contact angle was studied over time, and the immiscibility of copolymer and the matrix was evaluated using scanning electron microscopy (SEM) and atomic force microscopy (AFM). The effect of copolymer type and percentage on icephobic characteristics was assessed using various test methods.

In the second phase, an optimized combination of two different PCMs, n-dodecane and n-tetradecane, was encapsulated within a PUF shell via in situ

polymerization that was compatible with the coating. The PCM microcapsules were then incorporated into an elastomeric matrix to evaluate PCM performance for the icephobic application. SEM technique and Fourier-transform infrared spectroscopy (FTIR) were used to characterize the obtained PCM microcapsules. Different microcapsule contents were added into an elastomeric matrix, and the coatings were applied to the substrates using a film-applicator. The topographical maps of the coatings and their corresponding surface roughness were obtained using profilometry. The capability of PCM microcapsules to release latent heat was assessed using differential scanning calorimetry (DSC). A comprehensive set of characterizing methods was also conducted to assess the anti-icing performance of the fabricated coatings, including measurements of ice nucleation temperature, freezing-delay time, ice accumulation, and ice adhesion strength.

In the final phase, a mixture of two PCMs, n-dodecane and n-tetradecane, with an optimized ratio of 2:8 was encapsulated within the PUF shell. The obtained microcapsules were then embedded within an elastomeric matrix containing 2.5 wt.% PEG-PDMS copolymer. The cross-sectional micrographs of the coatings were obtained by SEM to evaluate the homogeneity of microcapsules dispersion within the matrix. The capability of encapsulated PCM to release latent heat and also delay ice nucleation were assessed using DSC. Moreover, the ice adhesion and ice accumulation on the coatings were measured by the micro-push-off method and static accumulation test (SAT), respectively. We combined 10 icing/de-icing cycles and micro-push-off test to evaluate the durability of the fabricate samples over subsequent de-icing events.

Thesis outline

The outline section consists a brief overview of the six chapters of this Ph.D. thesis. In the first chapter, a literature review is presented to provide readers a general idea about the smart icephobic coatings. Accordingly, the fundamentals of the icing phenomenon are provided. Then, the definitions of smart icephobic coatings and their subcategories are presented. Existing research works in each group are addressed, and their potential for fabricating an anti-icing strategy is discussed. The approaches of the aqueous self-lubricating coatings and PCMs as the main methods chosen in the present study are also discussed in depth. Notably, a major part of this chapter is related to our review article entitled "*Potential use of smart coatings for icephobic applications: A review*" published in *Surface and Coatings Technology* [21]. The following three chapters correspond to written articles of this Ph.D. research work.

In Chapter 2, the fabrication of aqueous self-lubricating coatings containing PEG–PDMS copolymers is presented. The wettability, morphology, and topography of the fabricated coatings were evaluated using a goniometer, scanning electron microscope, and atomic force microscope, respectively. Furthermore, the icephobic characteristics of the samples were analyzed via differential scanning calorimetry (DSC), push-off test, and centrifugal tests. The obtained results are presented in the journal article "*Icephobic properties of aqueous self-lubricating coatings containing poly(ethylene glycol)–poly(dimethylsiloxane) (PEG–PDMS) copolymers*" published in *Progress in Organic Coatings* [24].

In Chapter 3, a desirable combination of two PCMs were selected and encapsulated in a urea–formaldehyde (UF) shell via in situ polymerization. The microcapsules were characterized by scanning electron microscopy (SEM) and Fourier-transform infrared (FTIR) spectroscopy. The PCM microcapsules were then embedded within a PDMS matrix. A comprehensive set of icephobic characterization methods was carried out to evaluate anti-icing (ice nucleation temperature and delayed ice formation) and de-icing properties (ice accumulation and ice adhesion strength). The results were published with title of "*An intelligent icephobic coating based on encapsulated phase-change materials (PCM)*" in *Colloids and Surfaces A: Physicochemical and Engineering Aspects* [25].

In Chapter 4, the above-mentioned approaches, namely, aqueous self-lubricating coatings and PCMs, were combined to obtain a novel anti-icing strategy. The synergistic effect of combining these approaches was expected to enhance the icephobic performance of the prepared coatings. In fact, using this hybrid strategy presents a novel approach to avoid the downsides and limits corresponding to aqueous self-lubricating coatings or PCMs. All the experimental parts, including material selection, sample preparations, and characterizations, as well as the interpretation of the results by the Ph.D. candidate, are presented. The icephobic characteristics of the fabricated samples were investigated from different aspects. The obtained results are published by *Progress in Organic Coatings* with the title of ''*a novel hybrid anti-icing surface combining an aqueous self-lubricating coating and phase-change materials*'' [26].

In Chapter 5, the main findings of this Ph.D. project are summarized as partial and general conclusions.

In Chapter 6, recommendations that can be helpful for future research are listed based on the results.

Chapter 1: Literature review

1.1 Introduction

Water is a unique substance that exists in three states in nature. Through a change in temperature and/or pressure, liquid water can undergo a phase change to solidify as ice; however, the nature of this solid form can vary (Table 1-1). Moreover, these ice forms can strongly adhere to exposed infrastructures [27,28]. This icing can result in serious safety, operational, and economic issues for a wide range of settings, including road, sea, and rail transportation, power transmission, telecommunications, wind turbines, pumps, and heat exchangers (Figure 1-1) [6–9,29]. For example, wind turbines located in areas of harsh cold-weather conditions must often cease to function during winter because of hazards related to ice accumulation. This stoppage results in the loss of almost half of the annual energy production of these wind turbines [30,31]. Ice build-up on the blade surface increases surface roughness, thereby disrupting airflow around the airfoil and reducing energy production. This phenomenon can prevent the operation of the wind turbine for days and even weeks. Ice adhesion and accumulation can also cause a load imbalance on the blade, and this ice presence accelerates the wear of the turbine components; maintenance costs are therefore heightened, and the service life of the turbine is reduced [10].

Wet snow conditions can also produce catastrophic blackouts of electrical networks involving high-voltage and medium-voltage power lines [32]. The related costs can be quite high. The sudden shedding of accreted ice accretion can also mechanically damage power network equipment [2]. The aircraft industry must deal with major icing problems that, in some cases, have resulted in fatal accidents.

According to the American Safety Adviser, approximately 12% of all flight accidents between 1990 and 2000 involved icing during adverse weather conditions. Moreover, 92% of ice-induced accidents occurred because of in-flight icing [7]. In 1992, approximately $33 US million was spent worldwide on removing ice from navigation equipment [12]. Increased shipping operations in the Arctic over recent decades have increased climate-related accidents in this region [33]. The accreted ice on the surface of some equipment increases the heat-transfer resistance, thereby decreasing the energy transfer rate. Accreted ice also disrupts the airflow within refrigeration systems to reduce system performance and increase energy consumption by approximately 20% [34].

Table 1-1. *The various forms of ice as formed under different environmental conditions.*

Type	Description
Rime	Supercooled water droplets having approximate diameters of 5–70 μm, frozen at low temperatures (T colder than −15 °C) [35] in stratiform clouds or in fog. Their accumulation as rime produces a white, brittle, feather-like ice form [36,37].
Glaze	During freezing rain, partially frozen supercooled water droplets, having diameters between approximately 70 μm and a few millimeters, form a clear, dense, and hard ice known as glaze [36,37].
Snow	Snow can be a mixture of ice crystals and water. Below −1 or −2 °C, it is dry. Closer to the freezing point of water, the crystals are covered by a thin layer of liquid water, and this mixture is wet ice, which shares characteristics of both solid and liquid phases [38,39].
Frost	Frost results through nucleation from the vapor phase through desublimation or condensation, followed by freezing to produce sparse dendritic crystal structures [37].

Figure 1-1. *Ice build-up on an aircraft wing (left), a high-voltage electrical line (middle), and wind turbine blades (right) [6].*

These financial and mechanical issues have led to greater interest in reducing ice accretion on exposed surfaces subjected to harsh cold-weather environments. In the next section, we describe the concept of icephobicity and present icing mitigation strategies that rely on smart icephobic coatings.

1.2 Icephobicity

Much work has focused on understanding the principles of ice formation and growth [40]. As water is cooled to or below 0 °C under atmospheric conditions, a phase transition occurs. As shown in Figure 1-2, ice nucleation begins within a water droplet at the free and solid interfaces as homogeneous and heterogeneous nucleation, respectively [41–43]. Upon the thermodynamic driving force, multiple long-lived hydrogen bonds are spontaneously developed, resulting in the formation of compact ice nuclei. The shape of these nuclei changes as they slowly grow. Then, through the spreading of more stable hydrogen bonds, liquid water transforms into a solid [41,44].

The forming of micro-ice decreases the free energy of the system. However, the growth of ice nuclei increases the interface free energy between the liquid phase and the ice nuclei, and the competition between these effects forms a nuclear energy barrier. In heterogeneous nucleation, ice crystals form on another material. Because of the

presence of impurities and the distinct topography and chemical composition of the interface, heterogeneous nucleation occurs at a higher temperature than homogeneous nucleation. These factors are critical in the design of anti-icing surfaces. Because nucleating agents exist within the water droplets, the formation of critical ice nuclei can be facilitated as the thermodynamically critical nucleation barrier is decreased [41,45].

Thermodynamically, three phase transformation processes must be considered when examining ice formation, namely (1) liquid–solid freezing; (2) vapor–solid desublimation; and (3) vapor–liquid–solid condensation followed by freezing. In developing icephobic surfaces and strategies, the first and second mechanisms are more important than the vapor–liquid–solid process. In the liquid–solid process, ice is formed from supercooled water droplets at or below 0 °C. The vapor–solid ice formation represents the forming of frost from a vapor phase when water vapor desublimates or undergoes nucleation under supersaturated conditions [41,42].

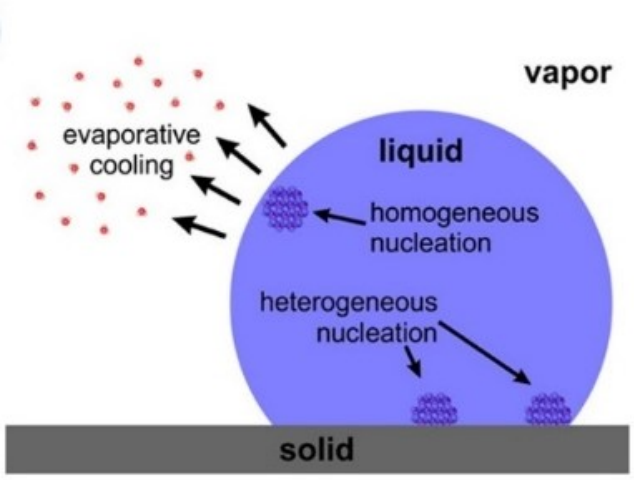

Figure 1-2. *Nucleation within a water droplet [42].*

Various strategies have been pursued to prevent the icing of surfaces, limit ice accumulation, and reduce adhesion between the ice and the surface. The icephobicity of a surface can be measured through ice adhesion strength.

Due to similarity between the binding energies of water and ice molecules to different surfaces, it seems that the work of adhesion corresponding to different ice-surface interfaces can be related to the water contact angle. However, evaluating the relation between shear strength of ice on different surfaces and their corresponding contact angle showed that there is no strong correlation between them due to difference in surfaces' nature and icephobic mechanisms [1,46].

Adhesion between materials can be resulted from different types of intermolecular forces. So, this can make ice adhesion difficult to define. Generally, interactions forces can be divided into short range (0.15-0.3 nm) such as covalent, and electrostatic and long range (more than 0.3 nm) like van der Waals. Furthermore, mechanical interlocking can also produce adhere surfaces. Accordingly, the adhesion between ice and surfaces is a combination of electrostatic forces, hydrogen bonding, van der Waals forces, and mechanical interlocking [1].

The formation of quasi liquid-like layer (QLL) is also considered as an essential factor that can significantly affect ice adhesion. Such a layer is produced below ice melting point, and its thickness varies depending one temperature and surface chemistry [47,48]. More details about QLL will be provided in next sessions.

From a thermodynamic point of view, ice adhesion can be expressed as the difference between the energy of the ice–surface interface and the sum of the surface energies of ice–air and surface–air interfaces [49]. There are multiple definitions of "icephobicity" in the literature. Some researchers have used this term to describe the

low adhesion strength between ice and a surface. Icephobicity can also be defined as the capacity of a surface to prevent ice formation. This definition includes delayed heterogeneous ice nucleation within a supercooled water droplet at the interface [50]. Other definitions identify icephobicity as the capacity of a surface to inhibit the transition from a Cassie to a Wenzel state during supercooling or Wenzel ice formation (see Figure 1-3) on the surface, allowing supercooled water droplets to rebound or roll-off [51].

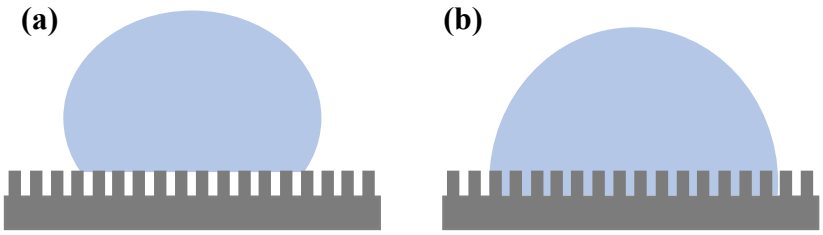

Figure 1-3. *Schematic presenting (a) a Cassie state, and (b) a Wenzel.*

The icephobicity of a surface can be measured by calculating either the critical shear stress or the normal stress [54]. The critical shear stress is the minimum amount of shear stress required to detach a given amount of ice from a surface [54]. The shear stress for a typical icephobic surface is less than 100 kPa. Other researchers, however, consider surfaces having shear strengths less than 10 kPa to be icephobic [55,56]. Icephobicity can represent several mechanisms [57]:

1- Removal of water droplets from a surface to prevent the formation of a frozen layer;

2- Delayed ice nucleation and the creation of a barrier against liquid–solid phase transition;

3- Decreased ice adhesion strength resulting in reduced ice accumulation;

4- Reduced heat transfer between a water droplet and a cold surface;

5- Altered triple point of water toward sub-zero temperatures for water layers in contact with the surface to decrease ice adhesion strength and ease ice removal.

1.2.1 Ice adhesion measurement

The ice adhesion strength is usually measured through three common methods. The first approach is known as peak force method (or push-off adhesion test) in which a cuvette placed on the sample, is filled with deionized water (Figure 1-4a). Then, this sample was kept at subzero temperature condition to obtain an ice cuvette. Ice adhesion strength is obtained by dividing the maximum force needed to remove ice from a surface, obtained via a force meter by the ice–surface interfacial area [58]. The second method is centrifugal method, and in this approach, the sample is bonded to a beam or a wing, and ice is deposited by spraying supercooled water microdroplets on the sample (Figure 1-4b). Then, the sample is placed in the centrifugal apparatus. The ice adhesion force is the centrifugal force needed for ice removal, calculated using Eq. 1-1.

$$F = mr\omega^2 \qquad \text{Eq. 1-1}$$

Where m, r, and ω are the ice mass, the beam radius at center of mass of ice, and angular velocity at which detachment occurs, respectively. Ice adhesion strength can be obtained by dividing the centrifugal force by the cross-sectional area between ice and the sample. The last method is the so-called tensile force test. In this method,

the apparatus consists of two concentric cylinders and a tensile force meter (Figure 1-4c). The coating is applied on the surface of the inner cylinder and the gap between the cylinders is filled with deionized water. When water is frozen, the tensile force is applied until ice detaches at the ice-coating interface. The ice adhesion strength is evaluated by dividing maximum pulling force by iced area [58–60]. It is equally important to consider ice type (non-impact, glaze, etc.) and the iced area when conducting these measurements.

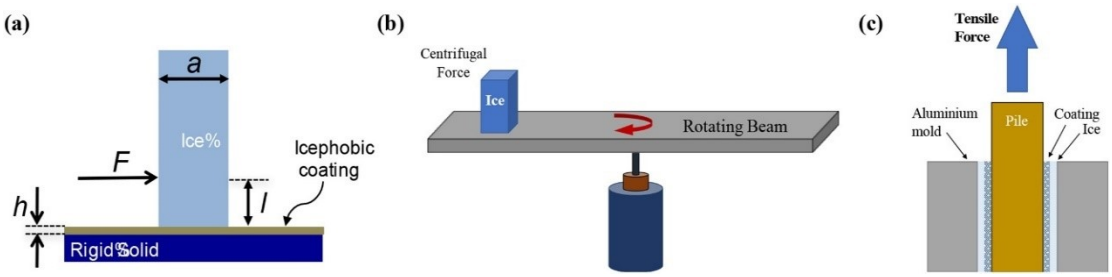

Figure 1-4. *Schematic of (a) the push-off test, (b) the centrifugal test, and (c) tensile test [58].*

1.3 Icephobic strategies

Attempts have been made to determine the relationship between icephobicity and certain surface properties, such as water repellency. Boinovich et al. [61] evaluated the nucleation kinetics of supercooled water droplets on various hydrophilic, hydrophobic, and superhydrophobic surfaces. It is noteworthy that a superhydrophobic surface is usually defined by a water contact angle (WCA) larger than ~150°, a contact angle hysteresis (CAH) of less than ~10°, a roll-off angle of less than ~5°, and the high

stability of a Cassie model state [62–64]. Boinovich et al. found that nucleation kinetics can vary because of the wetted interfacial area, the energy barriers corresponding to heterogenous nucleation at the droplet–surface interface, and the nucleation time lags. Kulinich et al. [65] assessed the adhesion strength in terms of contact angle (CA) and wetting hysteresis. They demonstrated that there was no general correlation between ice adhesion strength and water CA on rough hydrophobic surfaces, and the correlation was only valid for rough hydrophobic surfaces having a low contact angle hysteresis (CAH).

Meuler et al. [66] studied the dynamic impact of water on both smooth and roughened surfaces. They showed that the practical work of adhesion could be related to the receding contact angle using the equation of $W_a = \gamma_{LV}(1 + \cos\theta_{rec})$, where W_a, γ_{LV}, and θ_{rec} are the practical work of adhesion per unit area for water on a surface, the surface tension of water, and the receding water contact angle, respectively. They also found that there was a near-linear correlation between average ice adhesion strength and the practical work of adhesion for liquid water. Therefore, maximizing the receding contact angle should reduce ice adhesion strength [66,67]. Chen et al. [68] claimed, however, that this relationship was not valid for some surfaces, e.g., elastomeric coatings containing polydimethylsiloxane (PDMS)-poly (ethylene glycol) (PEG) amphiphilic copolymers. Jung et al. [68] evaluated water freezing delays on various surfaces, ranging from hydrophilic to superhydrophobic, and identified a relationship between these delays and icephobicity. For superhydrophobic surfaces, a high CA increased the ice delay time, whereas for hydrophilic surfaces, nanometer-scale smooth surfaces provided a much greater delay in ice formation; therefore, the selection of the optimal icephobic characteristics requires considering both wettability

and roughness. Nosonovsky et al. [69] stated that superhydrophobic surfaces do not necessarily show icephobic characteristics because of the different mechanics of ice and water adhesion on a surface. Therefore, mechanical forces acting on both the liquid droplet and ice should be evaluated. For water droplet, applying shear stress can remove the droplet from the surface when the shear force exceeds the counteracting force of contact angle hysteresis. For ice, resistance against shear stress leads to ice detachment because of ice fracturing. Cao et al. [70] fabricated nanoparticle–polymer superhydrophobic composites by mixing organosilane-modified silica particles with a synthesized acrylic polymer. They evaluated the effect of supercooled water on ice accumulation under both laboratory and natural conditions. When subjected to natural freezing rain, the surface of the superhydrophobic composite showed minimal ice accumulation relative to that for an aluminum plate reference; the latter became completely covered by ice under these same conditions. In addition to the superhydrophobicity of the fabricated surfaces, the size of the silica particles played an important role in the icephobic capacity of the composite. As the particle size was in the appropriate range, the composite could prevent ice accretion. They suggested therefore that a direct relationship did not exist between the anti-icing performance of the surfaces and their superhydrophobicity.

As mentioned above, water repellency is an essential characteristic of superhydrophobic surfaces [71–77]; however, these surfaces are not necessarily ice repellent. Indeed, icephobicity is attributed to a delay in icing, lower nucleation temperature, and lower ice adhesion than water repellency. Micro-nanoscale-textured surfaces, for instance, can trap air packets under the water droplets and promote

superhydrophobicity; however, the risk of heterogeneous ice nucleation increases because of the presence of these surficial micro-nanostructures [44].

Given the complex relationship between above-mentioned factors and icephobicity, researchers have applied new approaches, such as machine learning, as means to predict and simulate icing conditions [78–80]. For instance , Fitzner et al. [81] applied a machine-learning technique to produce a predictive set of microscopic descriptors for establishing the possibility of ice nucleation on surfaces. This work confirmed that heterogeneous ice nucleation can be quantitatively predicted. They demonstrated that a quantitative understanding of heterogeneous ice nucleation is possible relying on three factors: the local ordering in liquid water, the reduction in the local density of liquid near the surface, and the corrugation of the adsorption energy landscape in contact with water.

Surface roughness is among the parameters that can significantly influence ice adhesion strength. Nonetheless, the relationship between surface roughness and ice adhesion is quite complex. Approaches such as molecular dynamics simulations and machine learning have been used to improve our understanding of this relationship. Molecular dynamics simulations have shown, for example, that rougher surfaces produce a considerably lower intrinsic ice adhesion strength [82].

Ice adhesion can be reduced through two general approaches, namely active de-icing methods and passive methods. Active methods involve an external energy source, e.g., thermal and mechanical energy, to remove or prevent ice accretion. Passive methods include protecting the surface using engineered surfaces that have anti-icing properties, which reduce ice adhesion strength and/or reduce ice accretion. The advantages of the second strategy are the reduced operational costs relative to the active

methods and an external energy input not being required [1,83]. Moreover, the use of de-icing liquids often involves serious environmental concerns; thus, engineered surfaces, produced either directly using a surface treatment or indirectly by applying a coating, are receiving increased interest [36].

Passive methods involve surface treatments and/or surface modifications, such as etching. These approaches have some limitations, however, including the restricted types of substrate that can be subjected to these treatments. Nonetheless, the application of coatings is generally viewed as one of the best approaches for changing the characteristics of a solid surface. Through this process, a new substance having the desired properties is applied onto a surface with the aim of protecting the substrate [84]. Based on definitions of icephobicity, an icephobic coating must possess some or all of the following characteristics: reduced interaction between the surface and the water to limit water accumulation on the surface (e.g., the capacity of a superhydrophobic surface to repel incoming water droplets), prevention of heterogeneous nucleation, and, very importantly, weakening of the adhesion strength between ice and a surface [50,69]. These definitions of icephobicity and the features of an icephobic coating are presented in Figure 1-5 [54]. Of course, durability, cost-effectiveness, and ease of application should also be added to the final list of the main criteria for an ideal icephobic product [1]. Icephobic coatings can be categorized into different types, including low surface energy coatings, chemically-heterogeneous and composite coatings, porous superhydrophobic coatings, and smart icephobic coatings [1].

Low surface energy can be achieved using materials such as poly(dimethylsiloxane) (PDMS), Teflon and poly(tetrafluoroethylene) (PTFE). The low surface energy of the functional groups of the materials and the low elastic modulus

decrease the adhesion between the ice and the surface; therefore, these coatings exhibit good icephobicity [56]. In the case of PDMS, the polysiloxane-based coatings consist of viscoelastic silicones having a low glass transition temperature (T_g). This characteristic produces a low elastic modulus [38,85] and, therefore, a flexible and soft polymer. The dissimilarity in mechanical properties between ice and these polymers reduces the ice adhesion strength [1].

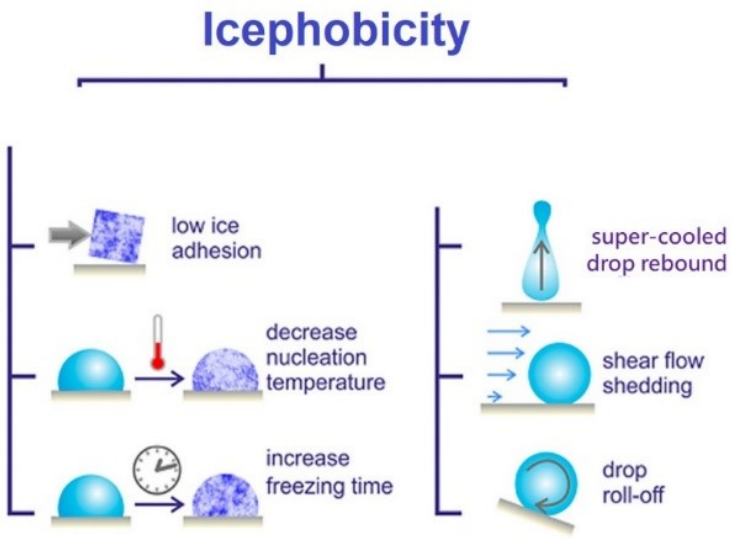

Figure 1-5. *A diagram of the various icephobicity definitions [54].*

Heterogeneous and composite coatings can be fabricated by combining polysiloxane and fluorocarbon groups to produce materials characterized by a very low ice adhesion, even lower than that of surfaces having chemically homogeneous coatings of either of these materials alone [1]. Multiple studies have investigated how chemically heterogeneous and composite coatings reduce ice adhesion [1,86–88];

hydrogen bond lengths and interaction energies were found to be the most important factors. Siloxane groups can, to some extent, repulse water, although there are strong attraction forces between the fluorocarbon groups and water molecules. Furthermore, water molecules differ in their orientation on the surface of fluorocarbon groups from that observed on polysiloxane. These differences in energy bonding and water molecule orientation weaken the adhesion between ice and the surface [1,86,87].

Inspired by natural surfaces (Figure 1-6), superhydrophobic and porous coatings have been developed to obtain icephobic surface characteristics [89]. Combining low surface energy materials and a micro- and/or nanostructured surface topography can produce a superhydrophobic surface having an acceptable WCA and a low CAH. This combination traps air pockets in surface asperities, thereby producing an air–liquid–solid interface and, consequently, a Cassie–Baxter state. These materials characterized by a superhydrophobic surface show great potential for various applications, especially icephobic applications [1,90–97]. Porous superhydrophobic surfaces, using polymers such as polyvinylidene fluoride (PVDF), have relied on combining low surface energy materials and a micro- and/or nanostructured surface topography and can produce anti-icing properties [86].

Although superhydrophobic surfaces can usually reduce ice adhesion strength, repeated icing/de-icing cycles will limit their long-term icephobic performance because of damage to the original rough surface structure [102]. Under real conditions, water molecules in humid air can condense within surface asperities, thereby increasing ice adhesion strength owing to an enhanced mechanical interlocking [103]. Therefore, researchers have focused on improving the durability of superhydrophobic coatings. Boinovich et al. [104], for instance, designed superhydrophobic coatings for stainless

steel surfaces subjected to mechanical stresses. The fabrication process included two stages: first, the chemical etching of the stainless steel, and second, the deposition of silica nanoparticles from a wetting film of a dispersion. The developed superhydrophobic coatings showed much less ice and snow accumulation than untreated stainless steel under heavy snowfall conditions at −3 °C, 99% relative humidity, and a wind velocity of 2 $m \cdot s^{-1}$. The coatings also exhibited an acceptable robustness of the surface morphology after 100 icing/de-icing cycles.

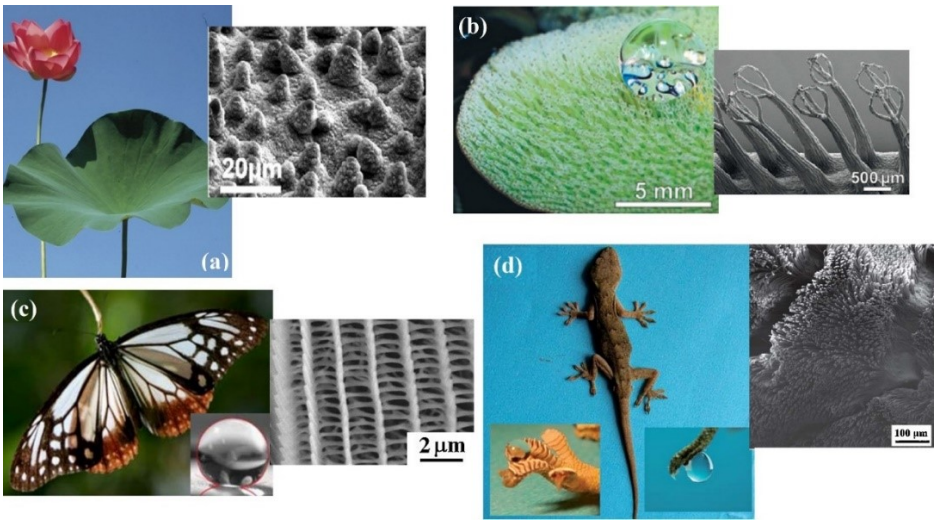

Figure 1-6. *Examples of natural superhydrophobic surfaces: (a) lotus leaves (Nelumbo nucifera) [98]; (b) the surface of Salvinia molesta [99]; (c) the butterfly wings of Parantica [100]; and (d) gecko feet [101].*

New technologies have advanced the development of icephobic coatings. Therefore, smart icephobic coatings, as a new generation of anti-icing strategies, will be detailed in the next section.

1.4 Smart coatings

Smart coatings, also called intelligent coatings, have attracted much interest over the last decades owing to their potential use in high-tech industries. Conventional coatings are fabricated to passively protect the substrate and act as a barrier between the substrate and the environment. These coatings provide a constant functionality, which depends on the formulation of the coating, and this functionality remains present over the coating's lifetime. Progress in the coatings industry has led to more advanced coatings that possess enhanced functionality. Smart coatings are designed to respond in a predictable way to a change in the surrounding conditions [19]. The stimuli-responsive behavior of smart coatings allows these materials to sense the surrounding environment and produce the desired response to stimuli. These stimuli can be a change in pH, pressure, temperature, light, and even variations in electrical or magnetic fields. The coating response can include a change in size, surface area, shape, color, temperature, and mechanical properties. When the stimuli are removed, an ideal smart coating should return to its original state [20].

Smart coatings are already a multibillion-dollar industry, and the importance of this sector is anticipated to reach around $8 billion US by 2021 and expand greatly in the years thereafter (Figure 1-7) [105]. Several types of smart coatings have been developed within academic and industrial settings, including antifouling, self-cleaning, and self-healing coatings. The use of these coatings has improved safety, prolonged product service life, and decreased equipment repair costs [106].

Self-healing coatings represent a very interesting subcategory of stimuli-responsive materials. These particular coatings can repair damage autonomously without any external intervention [107] and thereby prolong the duration of the coating

[106]. Encapsulation is the most commonly used technique to create self-healing characteristics. In this approach, healing agents encapsulated in microcapsules are released within the coating to restore its original properties [108].

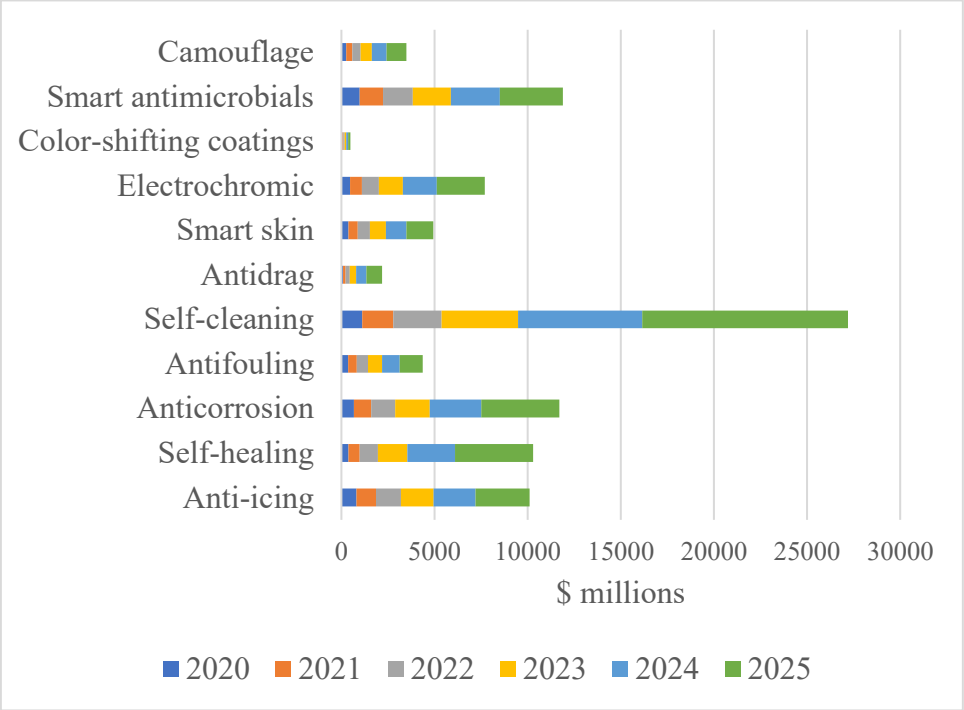

Figure 1-7. *A six-year forecast (2020–2025) for the market of various smart coatings [105].*

Self-cleaning smart coatings are another subcategory of these coatings. These coatings respond to stimuli by maintaining a clean surface. These types of intelligent coatings can be divided into two main groups, namely hydrophilic and hydrophobic coatings. Hydrophobic self-cleaning coatings are used more commonly than hydrophilic smart coatings for self-cleaning applications [13,106,109,110]. Among these smart hydrophobic surfaces are smart icephobic surfaces, which prevent ice accumulation on a surface. The market for smart icephobic coatings is expanding and

is expected to do so over the near future (Figure 1-7). The following sections discuss the types, fabrication strategies, and mechanisms of smart icephobic coatings.

1.5 Smart icephobic coatings

The lack of a universal definition of a smart icephobic coating prevents the clear categorization of these intelligent coatings. Thus, referring to the general definition of smart coatings, a smart icephobic coating senses an environmental stimulus and provides a suitable response; this response results in reduced ice accumulation or a longer delay in ice formation on an exposed surface.

Depending on the types of stimuli and response, smart icephobic coatings can be classified into several categories (Figure 1-8). Some, such as thermoresponsive coatings and phase-change materials (PCMs), generate heat as a response to stimuli; this heat can then serve for anti-icing purposes. In electromechanical de-icing systems, mechanical pulses are generated, which reduce ice adhesion. Self-lubricating coatings as an icephobic strategy have shown great potential in anti-icing applications.

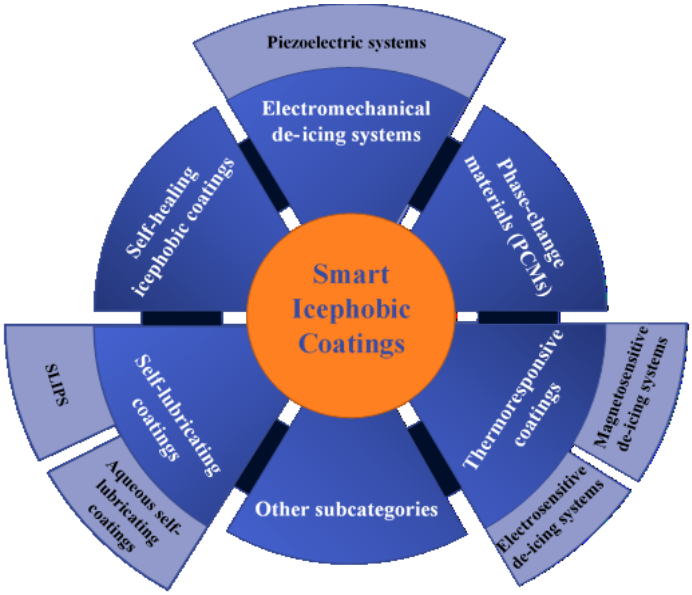

Figure 1-8. *The classifications of the smart icephobic coatings.*

1.5.1 Thermoresponsive coatings

Thermoresponsive coatings are some of the most common smart icephobic coatings. These materials respond to stimuli, such as electric and magnetic fields, and generate the heat required to melt accumulated ice. The thermogenesis phenomenon (process of producing heat in in response to various stimuli) observed in some plants, such as the eastern skunk cabbage (*Symplocarpus foetidus*), has inspired much of the research (Figure 1-9a, Figure 1-9b, and Figure 1-9c). Ramachandran et al. [111] investigated the structures of a few thermogenic plants and their ability to melt ice. To find a correlation between icephobicity and thermogenesis, they developed a heat-transfer model and discussed the biomimetic potential of such plants for fabricating icephobic coatings. This thermogenic process preserves a thin aqueous layer, which causes the ice to slip off readily and then fall off a surface due to gravity. These thermoresponsive systems can be subdivided into electrosensitive and magnetosensitive de-icing systems.

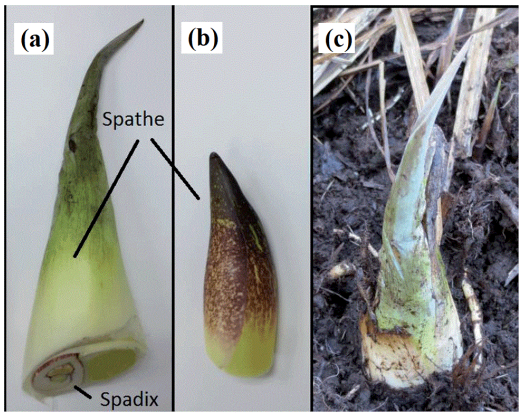

Figure 1-9. *(a and b) The skunk cabbage (Symplocarpus foetidus) in which the spathes enclose spadix; (c) the spadix regulates plant temperature by thermogenesis. A specimen of skunk cabbage in its natural environment [111].*

1.5.1.1 Electrosensitive de-icing systems

Dissipation of electrical energy in electrically conductive materials can appear as Joule or resistive heating, which is an effective method for removing ice from a surface. In this approach, a layer of water forms through the melting of a thin layer of ice near the ice–heated surface interface. Ice adhesion is therefore weakened, facilitating ice removal by an external force, such as gravity or wind [112]. Raji et al. [112] fabricated a conductive composite by filling epoxy with graphene nanoribbon (GNR) stacks. These nanomaterials cause the composite to become electrically conductive (>100 S/m at 5 wt.% of GNR). By applying a constant voltage across the composite, thermal energy is generated through Joule (voltage-induced) heating. This material is a good candidate for use in icephobic applications in the aerospace industry, power-line networks, and other fixed or mobile platforms. The authors claimed that delivering a power density of 0.5 W/cm^2 removed 14 g of ice from the blade surface of a helicopter at −20 °C.

Wang et al. [113] used both anti-icing and de-icing strategies to fabricate superhydrophobic films. They sprayed perfluorododecylated graphene nanoribbons (FDO-GNR) onto a substrate (Figure 1-10). These surfaces showed anti-icing properties down to −14 °C. By applying a voltage (~40 V) to the surface, they could generate heat and de-ice the surface at even lower temperatures. A low power density of 0.2 W/cm^2 maintained the surface of the coating at room temperature despite an ambient temperature of −32 °C. Wang et al. improved the de-icing performance of the coatings even further by adding a lubricating liquid to the films to create slippery surfaces.

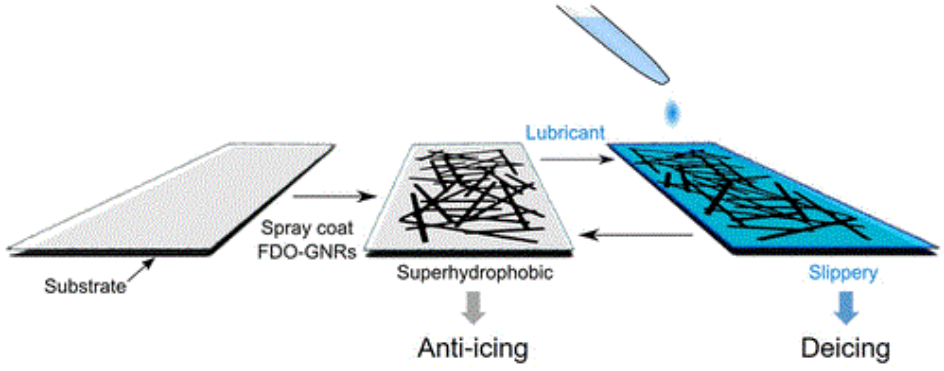

Figure 1-10. *Fabrication of the perfluorododecylated graphene nanoribbons (FDO-GNR), which involved the spraying of nanoribbons onto the substrate, and the addition of a lubricating liquid to the films [113].*

Graphene-based de-icing composites were designed using a microfluidic method. They coated glass-fiber roving with a conductive graphene-based ink [114]. The minimum electrical resistance of this coated roving was ∼1.7 Ω/cm. They then integrated the graphene-coated glass rovings with an epoxy resin using a vacuum resin infusion process to fabricate the glass–epoxy composites. The de-icing performance of developed coating was investigated by dipping the composite into an ice-filled bucket and applying 10 V. Through Joule heating, the temperature of the bucket containing the composites rose from −0.1 °C to 27.3 °C over five minutes, causing the ice to melt.

1.5.1.2 Magnetosensitive de-icing systems

The use of magnetic fields as an external stimulus for smart coatings has several benefits, including convenience, real-time response, and lower environmental impacts [115–118]. On magnetic responsive surfaces, the wettability and adhesive properties can be readily controlled to obtain the desired surface characteristics [119]. Irajizad et al. [120] fabricated magnetic slippery surfaces (MAGSS) having low interfacial energy and icephobicity. These surfaces demonstrated an ice formation temperature of −34 °C,

a low ice adhesion strength (~2 Pa), a high mobility of water and ice, self-healing characteristics, and stability under high-shear flows (Reynolds number $\leq 10^5$).

The application of a magnetothermal effect, which is related to Néel or Brownian relaxation, causes magnetic nanoparticles to generate heat [121,122]. This capacity of nanoparticles can be applied to treating hyperthermia and killing cancer cells [123]. The Joule effect is an effective approach for de-icing applications; however, there are drawbacks to its use, including a high cost and elevated energy consumption. Nonetheless, the heating capacity of magnetic nanoparticles under external magnetic fields could make them a good candidate for icephobic applications.

Cheng et al. [124] synthesized multifunctional magnetic hybrid coatings by mixing fluorinated copolymer-tethered epoxy groups with amino-modified Fe_3O_4 nanoparticles that were then crosslinked with diethylenetriamine (Figure 1-11). The magnetic heating capacity of the coatings showed a temperature increase from 24 °C to 44 °C within 25 seconds under experimental conditions.

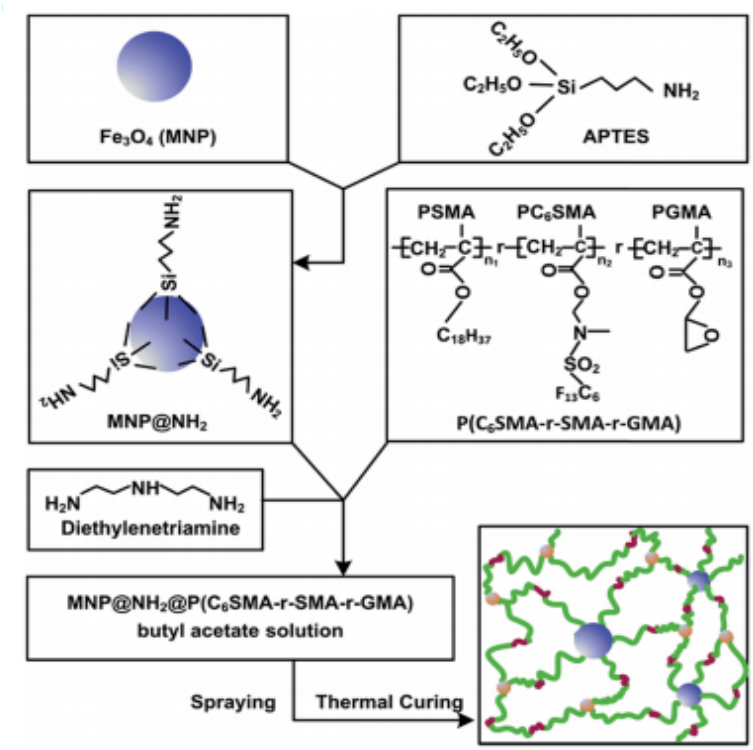

Figure 1-11. *Fabrication of multifunctional magnetic hybrid coatings, including a crosslinking process by mixing the fluorinated copolymer P(C6SMA-r-SMA-r-GMA), diethylenetriamine, and amino-modified Fe_3O_4 nanoparticles [124].*

1.5.2 Electromechanical (piezoelectric) de-icing systems

Electromechanical-based methods, particularly through the use of piezoelectric materials, have received much interest for their use in icephobic applications. Some of these materials, such as piezoelectric ceramics, are widely used as piezoelectric actuators. PZT (Pb $[Zr_xTi_{1-x}]$ O_3), quartz, lithium tetraborate (Li_2B4O_7), and barium titanate ($BaTiO_3$) are among the known piezoelectric materials [125]. Combining piezoelectric and icephobic properties can reduce ice adhesion strength. These materials convert electrical signals, applied as an electrical field, into displacement because of the expansion and contraction of the piezoelectric material. The opposite

behavior can be observed with these materials; deforming a piezoelectric material will generate an electrical charge [108].

As the piezoelectric material vibrates when an electric field is applied, its structure is highly stressed. These stresses can be modified according to the frequency of the applied electrical field, e.g., low (Hz) and high frequencies (kHz) [126]. The generated shear stresses on the surface can remove adhesive bonds between the ice and the surface [127]. In the aerospace industry, for instance, piezoelectric actuators along an aircraft's leading edge can be supplied with a current. These stimulated actuators produce ultrasonic waves, which travel through the aircraft skin and produce shear stresses. This stress causes any ice to be removed from the surface [36]. Such an approach offers a solution for reducing energy consumption in anti-icing applications.

The de-icing process of the electromechanical system is attributed to vibrations. These vibrations cause ice to shed in two ways. First, they can generate shear stresses greater than the ice adhesion strength at the interface, resulting in ice delamination. Second, the vibrations can create a tensile stress that is greater than that of ice, forming cracks within the ice [38].

Piezoelectric films and, in particular, electro-active polymers, such as polyvinylidene fluoride (PVDF), can be utilized for various de-icing purposes. Ferroelectric polymers, e.g., polymers of the group comprising PVF_2, serve as the piezoelectric materials used to fabricate de-icing optical and radio-optical windows [128]. Using polymeric piezoelectric materials provides greater benefits than use of ceramic piezoelectric materials, as the former allows very thin and flexible coatings, which can tolerate higher mechanical and electrical stresses than the ceramic material [14].

Pommier-Budinger et al. [126] combined piezoelectric systems with icephobic coatings. They obtained an analytical model of a structure, placing the actuators at fixed positions, to investigate the power and voltage required to remove accumulated ice from a surface. From this model, the authors evaluated the effect of frequency on tensile stress at the ice–structure interface on lead zirconate titanate (PZT) materials. Pommier-Budinger et al. also fabricated two icephobic coatings on aluminum substrates, namely an ethylene tetrafluoroethylene (ETFE) and a commercial silicone coating. They then measured ice adhesion strengths using a lap shear test setup. These coatings reduced the voltage and the PZT tensile stress and, consequently, power usage.

Hybrid systems, fabricated by combining a hydrophobic coating, heating elements, and piezoelectric actuators, have been applied to the surface of a small-scale airfoil [129]. The ultra-smooth surface, having a nanostructured hydrophobic morphology, consisted of a nanoporous aluminum oxide layer created using phosphoric sulfuric anodizing (PSA) followed by surface hydrophobizing. Piezoelectric multilayer actuators were used to shed ice in the unheated region of the surface. The analysis of the system performance, evaluated in a laboratory-scale icing wind tunnel, showed that this ultra-smooth surface shed ice from its surface and required 95% less power consumption than other electrothermal systems. The total power density was 2.74 kW/m^2, a much lower value than that observed for typical ice protection systems [129].

Huang et al. [36] found that the Young's modulus of the coating plays an important role in ice removal for electromechanical de-icing systems. A low Young's modulus generates very low shear stresses at the interface and, consequently, requires

relatively more power to reach the required shear stresses for ice delamination. They recommend using a coating having a Young's modulus of at least 1 GPa.

1.5.3 Self-healing icephobic coatings

Self-healing materials have received much attention due to their potential within a wide range of applications [130]. These materials can recover their original structures following mechanical, thermal, or other types of damage [131]. This capacity occurs intrinsically or as a response to a stimulus, such as heat or mechanical damage. These coatings have several advantages; for instance, self-healing coatings require less frequent monitoring or repair and may thus be more reliable, durable, and economical than conventional coatings [132]. Damage, particularly that initiated from inside the materials, is usually very difficult to detect; therefore, the use of self-healing coatings provides an ideal solution to counter this issue [133]. Such forms of intelligent coatings are inspired by naturally occurring biological phenomena [134]. For example, old and dead plant tissues can be replaced by new tissues, and after an animal breaks a bone, the body removes the surrounding debris, stabilizes the injury, and heals the wound [135]. In self-healing procedures, the self-healing reagents are commonly incorporated within microcapsules, which are then mixed into the polymer matrix. Once the coating is damaged by an external force, the microcapsules are broken, resulting in the release of the self-healing reagent, and the damaged area is then repaired [136,137]. Despite the considerable capacity of these coatings to recover their damaged characteristics, this self-healing ability is not unlimited, as the number of incorporated microcapsules or microcontainers is limited; once the healing agent is exhausted within the matrix, self-healing is no longer possible.

Self-healing properties used for anti-icing purposes could prolong the service life of coatings. Generally, there are two approaches for fabricating icephobic self-healing coatings. The first involves using lubricant-infused surfaces (see Section 4.5). The second is to benefit from low surface energy compounds that provide molecular mobility and form chemical bonds at the material interface [138,139].

Zhuo et al. [55] fabricated a mechanically durable icephobic coating by integrating an interpenetrating polymer network (IPN) into a re-healable elastomer. They used Fe-pyridine dicarboxamide-containing PDMS (Fe-Py-PDMS) as a matrix because of its low modulus and surface energy (Figure 1-12). The polymer chains are crosslinked by weak metal-ligand coordination bonds. This causes creep deformation and, therefore, increased ice adhesion strength. Introducing PDMS into the structure formed IPN and, consequently, produced self-healing properties and a low ice adhesion strength.

The reversibility of metal-ligand coordination bonds and the mobility of polymeric chains were the main causes of the observed self-healing behavior. The icephobic coating showed a very low ice adhesion strength (~9 kPa) at −18 °C, and it remained around 12.2 kPa after 50 repeated icing/de-icing tests [55]. The low modulus and unloading rigidity of IPNs formed cavities or voids at the ice–coating interface, thereby detaching the ice from the surface. Because the use of a covalently crosslinked network can increase creep resistance and suppress self-healing properties, this relationship between these two behaviors must be considered carefully [55].

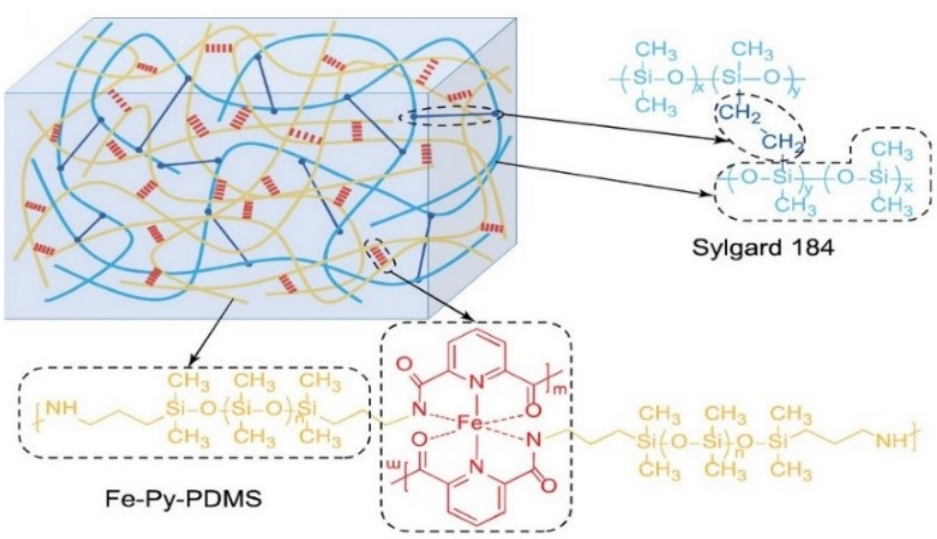

Figure 1-12. *Structure of a self-healing interpenetrating polymer network (IPN) [55].*

In another attempt, Zhuo et al. [140], using both experimental and atomistic simulations, designed an icephobic coating having very fast self-healing characteristics. The relationship between chain diffusion and bond site density was modeled in nanoscale mechanisms. The atomic mechanism was obtained for ultrafast healing, which highlighted the optimal balance between polymer chain flexibility and the concentration of hydrogen bonding sites. The authors fabricated the coating by combining PDMS chains, as flexible segments, and urea groups, as bonding sites. The self-healing properties arose because of the diffusion of asymmetric alicyclic segments and through controlling the concentration of hydrogen bonding sites by adjusting the molecular weight of the PDMS segments. Increasing the concentration of hydrogen bonding can enhance the re-formation of hydrogen bonds and consequently decrease the diffusion rate. The fabricated coating regained more than 80% of its original tensile strength 45 min after being damaged. It also demonstrated an ice adhesion strength of

around 50 kPa after 20 icing/de-icing cycles and similar values after the cutting/healing process. The coating possessed a capacity to heal nano- and micro-defects. The coating also preserved its integrity after repeated icing/de-icing tests and prevented ice interlocking during the repair process. Furthermore, this coating had a transparency of about 90%, values similar to those of glass. Thus, this coating could be a potential candidate for applications such as solar panels, sensors, and windows [140].

Superhydrophobic surfaces (SHSs) represent one of the most effective anti-icing approaches. These surfaces repel water droplets before they can freeze onto the solid surface [41]. SHSs can also be combined with other properties, including a self-healing capacity, to fabricate intelligent coatings. Given the durability issues for SHSs, recent studies have focused on overcoming these problems and improve SHS service time [141]. Both surface morphology and surface chemistry of such multifunctional SHSs influence mechanochemical durability. Robust multifunctional SHSs can be fabricated through a variety of techniques, e.g., using hierarchical micro/nanostructures [142]. Stabilizing the hierarchical structure promotes not only a greater adhesion between the coating and the substrate but also favors the presence of other properties, particularly self-healing and anti-icing capacities [143].

Qin et al. [144] fabricated a robust superhydrophobic surface that showed excellent recoverability and icephobic properties. They designed such a surface by integrating a hierarchical texture into an elastomeric network, crosslinked by dynamic pyrogallol-Fe coordination. The first step of the fabrication process involved obtaining PDMS-GA by grafting gallic acid onto amino-modified PDMS via an acylation process. The PDMS-GA was then converted into a conductor in the presence of acetylene black (to fabricate hierarchical textures), a conducting agent, and $FeCl_3$. The

pristine PDMS-GA was coated by super P (a conductive carbon black) and TiO_2 and then treated with hydrophobic 1H,1H,2H,2H-perfluorodecyltriethoxysilane (PFDS). The fabricated surface showed a much longer delay in ice formation (430 s) than a pristine PDMS-GA film (100 s). Furthermore, the superhydrophobic surface had a lower ice adhesion strength than that of the pristine surface. The surface could also fully restore its characteristics within a minute of being damaged; this self-repair occurred through the reconstruction of the multiscale structures via dynamic coordination.

The spray coating of a polyurethane (PU) aqueous mixture and a hexadecyl polysiloxane-modified SiO_2 (SiO_2@HD-POS) produced a superhydrophobic surface having self-healing and icephobic characteristics [145]. The coatings showed a CA of 164° and a sliding angle of 4°. Furthermore, the high durability and hierarchical macro-nanostructure of the surface, as well as the solid lubrication of the SiO_2@HD-POS nanoparticles, produced a coating with mechanical stability against abrasion. In addition to exhibiting acceptable static and dynamic icephobic characteristics, the coating could restore its performance after being chemically damaged by having the healing agent migrate to the damaged area.

Another mechanically robust superhydrophobic coating having self-healing and anti-icing properties was obtained by synthesizing a fluorinated polyurethane via two-step thiol click reactions; the superhydrophobic coating was produced by adding SiO_2 NNPs [146]. The fluorine content decreased downward from the surface to the substrate. Therefore, the high flexibility of the fluoroalkyl chains on the uppermost surface allowed the coating to express rapid self-healing. The coating was mechanically durable owing to the strong linkage between urethane and the substrate.

The fluorinated polyurethane-SiO_2 coating also showed a greater delay in icing than several previously developed coatings.

UV-responsive microcapsules were synthesized to fabricate self-repairing superhydrophobic coatings [147]. To prepare the microcapsules, they used titania (TiO_2) and silica (SiO_2) nanoparticles as Pickering emulsifiers (Figure 1-13). The photocatalytic property of the TiO_2 nanoparticles under UV light causes the polystyrene (PS) shell of the microcapsules to decompose. The hydrophobic fluoroalkyl silane molecules are thus released. No considerable modification of the surface topography was observed after 96 h of an accelerated weathering test. The observed release rate of the hydrophobic molecules was determined by the TiO_2/SiO_2 ratio [147].

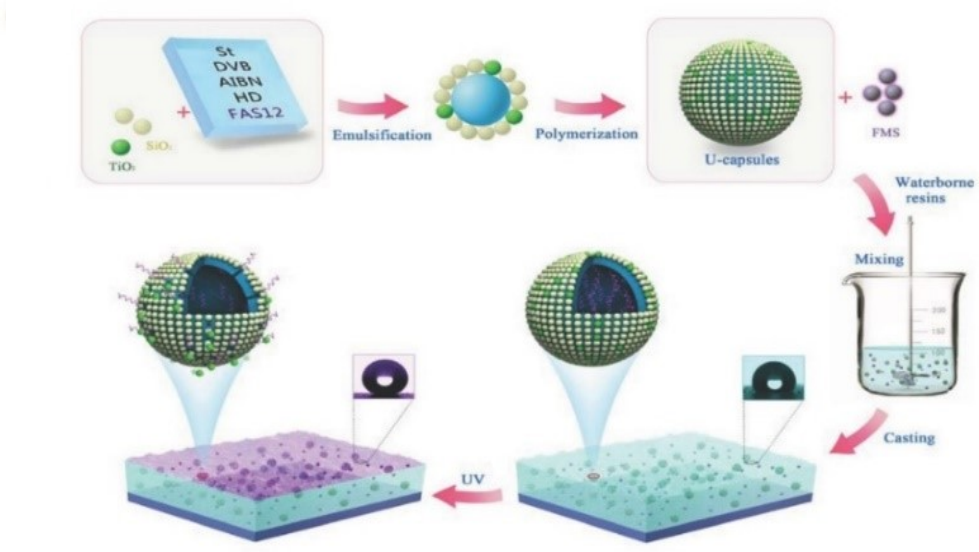

Figure 1-13. *The process used by Chen et al. to fabricate self-repairing superhydrophobic coatings [147].*

1.5.4 Self-lubricating coatings

The use of self-lubricating surfaces has been proposed as a practical solution for multiple applications [148], in particular for the fabrication of icephobic coatings [149], and oils have usually been the first choice as the lubricant. Various procedures have been developed to optimize surface performance. Among these procedures, post-infusing methods involve infusing the lubricating liquid into the porous matrices to obtain the final product. In contrast, pre-infused methods involve the lubricant being added to precursors to obtain the infused surface [149,150]. Some researchers have tried to take advantage of the near-ubiquitous presence of water in the environment and use it as a lubricating liquid for icephobic purposes. Undoubtedly, all these attempts aim to produce a surface characterized by superior icephobic performance and greater durability. We discuss two subcategories of self-lubricating surfaces, namely slippery coatings and aqueous lubricating coatings, in the following sections.

1.5.4.1 Slippery surfaces

Wong et al. [151] designed liquid-repellent surfaces and referred to them as slippery liquid-infused porous surfaces (SLIPS). Such surfaces consist of a lubricating layer trapped in a micro-nanoporous structure. The fabrication of SLIPS has a functionalized porous solid infiltrated by a low surface energy liquid; this produces a lubricating layer on the substrate. This approach has created liquid-infused surfaces on a variety of substrates [151,152]. Wong et al. identify three criteria for fabricating SLIPS. First, the lubricant should adhere stably to the substrate. Second, the substrate must have a greater tendency toward the liquid lubricant than toward the liquid being repelled. Third, there should be no miscibility between the lubricant and the liquids.

The Aizenberg group [153] developed icephobic surfaces on metallic substrates such as aluminum using SLIPS. On the fabricated surfaces, a very low contact angle hysteresis greatly reduced the size of the sliding droplets. Generally, cold, humid conditions create condensed water droplets that are pinned on the cold surface owing to surface heterogeneity. If condensation continues, the diameter of the sliding droplets will increase and reach a critical value. Critical droplet size refers to the droplet size below which droplets remain pinned to the surface. The fabricated surfaces remain frost-free under conditions in which conventional surfaces experience icing problems. Developed surfaces have demonstrated an ice adhesion strength of ~15 kPa at −10 °C; therefore, ice is readily eliminated even at a small tilt angle [153].

Several studies have fabricated SLIPS and evaluated their properties [154,155]. Nonetheless, the durability of these surfaces has always been a challenging issue. To improve the durability of SLIPS, researchers have applied various strategies, such as reducing the evaporation of the lubricating liquid and enhancing the compatibility of the lubricant and the substrate. Niemelä-Anttonen et al. [156] assessed the icephobic behavior of various SLIPS under repeated droplet freeze-thaw and ice accretion-detachment cycles. To simulate real conditions, they investigated the icephobicity of the surfaces in icing wind tunnels where mixed glaze ice was accreted onto the test surfaces. Their studies showed that impregnation of polymers with oils reduced ice adhesion strength and, in general, the PTFE-based SLIPS showed relatively lower ice adhesion than the PP-based ones. Ice accretion-detachment experiments, repeated four times, illustrated how the ice adhesion strength of PTFE-based SLIPS impregnated with perfluorinated oil increased only slightly after repeated cycles.

Yeong et al. [157] replicated microtextures from a laser-prepared substrate to an oil-infused elastomer and fabricated a superhydrophobic lubricated surface (Figure 1-14a). These microstructures and oil reduced ice adhesion strength to ~38 kPa at −10°C. Compared with a bare aluminum surface and a microstructured elastomer without oil infusion, this value represented a 95% and 30% decrease, respectively, in ice adhesion strength. The authors did not observe any considerable change in these adhesion values after a three-month aging at room temperature. The self-lubricating mechanism within the skin of frogs and earthworms provides a natural example of a durable slippery surface [158,159]. Inspired by the skin of a poison dart frog, Sun et al. [37] fabricated an anti-icing coating that released antifreeze liquid in response to surface icing (see Figure 1-14b). The coating was a bilayer consisting of a superhydrophobic epidermis and an underlying nanoporous nylon membrane dermis. To create this coating, the authors sprayed a superhydrophobic hierarchical polymeric shell onto a nylon membrane, and the dermis layer was infused with propylene glycol. The superhydrophobic layer acted as a barrier between the environment and the underlying layer and allowed the water droplets to roll off. Once ice accumulated on the surface, the coating released the antifreeze liquid as a response to this external stimulus (Figure 1-14c) [37]. Aside from delaying ice formation, the release of an antifreeze liquid reduced ice adhesion considerably, probably due to the presence of the lubricating layer between the ice and the surface. The antifreeze liquid could be replenished, as it becomes depleted through repeated icing and de-icing cycles [37].

Li et al. [160], inspired by epidermal glands, designed SLIPS having an icephobic self-releasing behavior for the lubricant. They placed lubricant capsules, consisting of hybrid surfactants, within a polydimethylsiloxane (PDMS) matrix. The

mechanical durability of this coating remained considerable even after 20 icing/de-icing cycles owing to its self-releasing property. Moreover, the coating was thermally durable, and the surfactant remained on the surface after keeping the material at 100°C for 60 h. The high thermal durability of the coating relates to the low diffusing rate of the lubricant because of encapsulation.

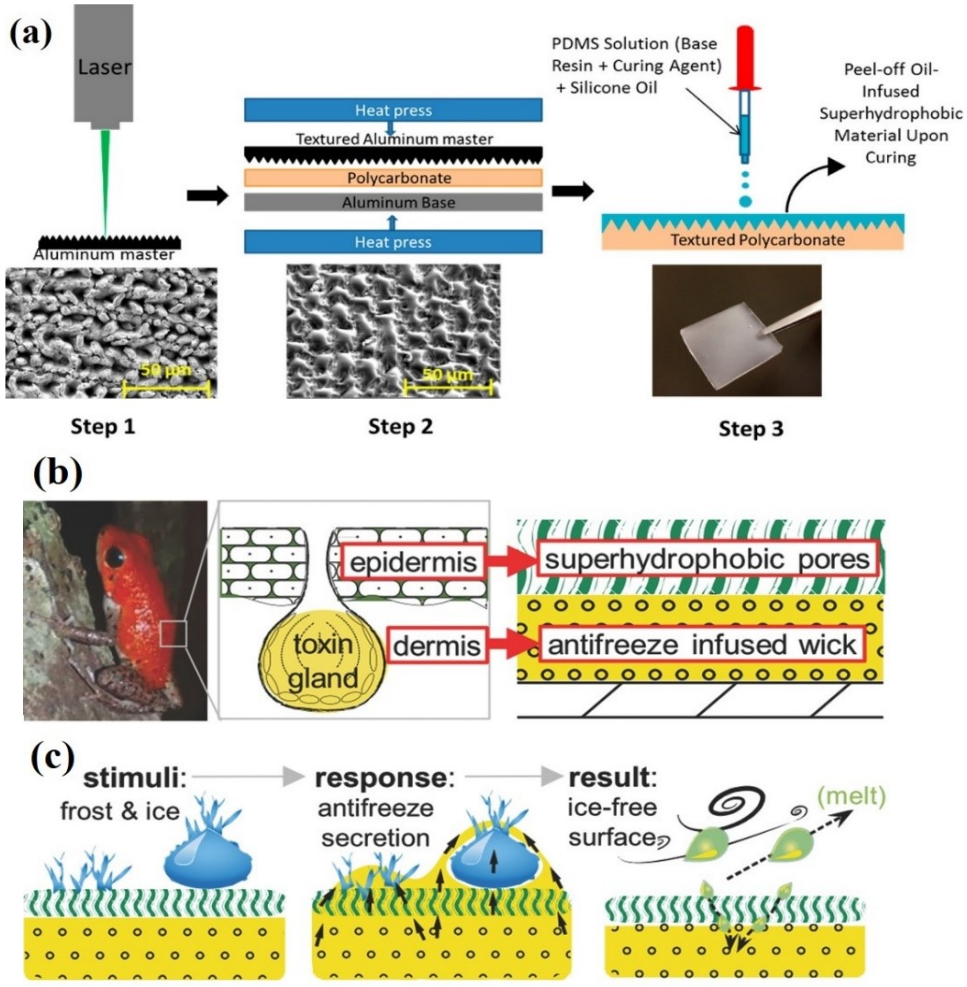

Figure 1-14. *(a) Steps for fabricating an oil-infused, microtextured elastomer [157]. Diagrams illustrating. (b) the stimuli-responsive anti-icing coating inspired by poison dart frog skin and (c) the release of an antifreeze liquid in response to contact with ice or frost, resulting in the melting of the ice [37].*

Coady et al. [161] investigated the icephobicity and durability of UV-cured silicone resins that were combined with silicone oil. The initial ice adhesion strength

for the coating was less than 10 kPa at −15 °C, and this ice adhesion remained less than 50 kPa for up to seven icing/de-icing cycles.

Another study fabricated lubricant-regenerable SLIPSs through a one-step procedure, the solvent evaporation-induced phase separation technique. This approach was inspired by amphibian skin. The residual stress of the fabricating process served as a driving force of the lubricant renderability by increasing the inner pressure of the polymer matrix relative to that of the atmospheric pressure; this stress caused the liquid paraffin inside the bulk material to move toward the surface and form a lubricant layer on this surface until the system achieved equilibrium. Removing the lubricant from the surface and, therefore, breaking the equilibrium, transferred the lubricant again from the bulk material to the surface to re-attain an equilibrium state. This lubricant-regenerable system preserved its icephobic performance, maintaining an ice adhesion strength less than 70 kPa at −18 °C after more than 15 icing/de-icing cycles. Both factors, namely the presence of the lubricant and the difference between the modulus of the ice and the polymer matrix, contributed to reducing ice adhesion strength [162].

The lubricant can be added either into a preformed matrix (post-infused method) or into the raw materials (pre-infused method). SLIPS are generally fabricated using the first method; nonetheless, this approach can cause a swelling deformation of the matrix. Therefore, the pre-infused method can be beneficial if, for example, greater control on the composition of the oil and polymer in a pre-infused method can avoid deformation [150].

A simple method developed to fabricate silicon oil pre-infused polydimethylsiloxane (PDMS) for icephobic applications [163]. By attaching vinyl and Si-H groups to the polydimethylsiloxane main chain, they increased the crosslink

density of the final product to improve its mechanical properties. They fabricated the coating by mixing two prepared parts, namely PDMS-H (PDMS containing 10 mol% Si-H groups) and PDMS-V (PDMS containing 1.5 mol% vinyl groups) with silicon oil, and they added modified silica particles to the mixture to enhance the nanoscale surface roughness. This coating demonstrated an ice adhesion strength of ~40 kPa at −10 °C.

Controlling the crosslink density of the coatings and enabling interfacial slippage generated a low ice adhesion strength of less than 5 kPa (at −10°C) on silicone oil pre-infused PDMS surfaces [56]. Interfacial slippage also significantly affected the ice adhesion strength of the elastomer having a low crosslink density. The fabricated coatings showed a good stability under various durability tests, including thermal cycling, severe mechanical abrasion, and 100 icing/de-icing cycles. Given that ice adhesion strength values remained below 10 kPa after these tests, these icephobic surfaces are considered to be extremely durable coatings [56].

Textured organogel coatings can limit oil depletion from slippery surfaces. These coatings have been fabricated using the pre-infused method and a diffraction grating (DG) film as a mold [164]. These coatings, known as self-lubricating gels (SLUGs), have been prepared by mixing polydimethylsiloxane infused with polymethylphenylsiloxane (PMPS) oil [164]. In response to a temperature lower than the critical synergetic temperature (CST), SLUGs release oil toward the surface. Below this temperature the oil is re-absorbed back (reverse-syneresis) into the bulk. Conversely, the synereted oil is reabsorbed (reverse syneresis) into the gel matrices when environmental temperatures are above the CST [164]. These SLUGs demonstrate considerable icephobic characteristics, and these coatings do not have issues related to oil depletion, as observed with SLIPS. Using SLUGs as coatings for solar panels

subjected to a cold climate could enhance the performance of the panels in colder regions [164].

A reversibly thermosecreting organogel was designed by incorporating a binary liquid mixture into an elastomer network [165]. Such a combination produces a phase-separating process as the temperature varies, leading to a reversibly changing lubricating regime from boundary lubrication to hydrodynamic lubrication. Therefore, the friction coefficient of the produced surface switched between 0.4 and 0.03. Below the critical phase separation temperature (T_{ps}) of the organogel, droplets appeared on the gel surface. These droplets gradually became larger as the temperature decreased. The fabricated surface produced a low ice adhesive strength of 1 kPa at −15 °C.

A self-lubricating coating was fabricated by grafting silicone oil having a low interfacial energy onto a rough metal–organic framework (MOF) coating [166]. Covering the ice nucleation sites on the surface with an organosilicone layer produced an ice adhesion strength of 9.4 kPa at −20 °C and a freezing temperature of condensed water of −36.0 °C. The synergistic effect of the porous micro-nanosurface structures and covalently bonded organosilicone enhanced the icephobic performance and long-term durability of the coating; the ice adhesion strength remained around 20 kPa for up to 20 icing/de-icing cycles.

1.5.4.2 Aqueous lubricating coatings

The slipperiness of ice surface has been the object of many studies for more than 160 years, and now, it is claimed that the presence of a very thin aqueous layer on the ice surface can result in such a slippery behavior even at sub zero temperatures [47,48]. This liquid-like layer is produced by pre-melting, and it has physical

characteristics between liquid water and ice. Fletcher proposed a theory that predicted the transition between ice and liquid-like layer happens between -6 and -3 ˚C [167]. Various techniques have been used to study this layer, such as optical spectroscopy, scattering, ellipsometry, scanning probe microscopy, and so on [48] that exhibits this layer usually is present at a temperature range between -35 and 0 ˚C [168], or even at -53 ˚C [169].

In ice skating, a thin aqueous layer is formed between the blade and the ice, enabling the movement of the skater across the frozen surface. Frictional heating, pressure melting, or both of these processes contribute to this phenomenon in which the ice structure is transformed into liquid water; this thin aqueous layer acts as a lubricant between the blade and the ice [170]. Some coatings have been developed on the basis of the same principles, whereby water has a role as a lubricating layer between surfaces, namely the ice and the coating [171]. The main advantage of these self-lubricating coatings over oil-infused coatings is that they do not have problems with oil depletion through leakage or evaporation.

Within many crystalline solids at temperatures slightly below the melting temperature (T_m), there is a disordered layer at the solid–vapor interface. The properties of this layer generally differ from those of bulk supercooled liquids at the same temperature; hence, this layer is commonly referred to as the “quasi-liquid layer” (QLL). In the case of the ice–air interface, the QLL plays a key role in certain phenomena, including the flow behavior of ice and snow, the adsorption of a substance onto ice, and the low friction between surfaces and ice [172]. The tribological characteristics of ice, which affect geological and glaciological processes, are thus determined by QLL dynamics. The thickness of the QLL can vary from a few to a few

hundred nanometers, depending on temperature and surface characteristics; for example, lower temperatures result in a thinner QLL [1,46]. Döppenschmidt et al. evaluated the impact of impurities on ice surface by study van der Waals and coulombic forces. Wettlaufer [173] evaluated the impact of impurities on ice surface by study van der Waals and coulombic forces. It was found that the slope of the layer thickness against temperature plot changed by decreasing temperature based on the strength of above-mentioned forces. Ikeda-Fukazawa [174] studied the formation mechanism of liquid-like layer on ice Ih (hexagonal ice crystal) using molecular dynamics calculations. Findings confirmed that the vibrational amplitude of superficial atoms was significantly dependent on the crystal orientation [174]. It was also found that the water/ice molecules are mostly bounded with the hydrophobic substrates via van der Waals forces that increasing thickness of the water layer at interface would result in weakening these interactions [175]. This unfrozen liquid-like water layer can be generated by grafting hygroscopic materials, resulting in producing hydrophilic surfaces [1,46,176]. Furthermore, QLL can effectively contribute to decreasing ice nucleation temperature due to reduced entropy at coating/ice interface [177]. This can be explained by effect of the interfacial water viscosity on regulating the ice nucleation [178]. To explain this phenomenon, the Eq. 1-2 is used in which the nucleation prefactor J_0 is correlated with the diffusion activation energy Δg as

$$J_0 \propto \left(\frac{\gamma_{SL}}{kT}\right)^{\frac{1}{2}} \exp\left(-\frac{\Delta g}{kT}\right), \qquad \text{Eq. 1-2}$$

Where T, γ_{SL}, and k are temperature, solid-liquid interfacial energy, and Boltzmann's constant, respectively. The parameter of Δg is associated to the transfer

of water molecules across the ice–water interface to add up to ice nucleation sites. On the other hand, Δg can be related to the viscosity μ, using the Eq. 1-3, as:

$$\mu = \left(\frac{h}{v_m}\right) exp\left(\frac{\Delta g}{kT}\right), \qquad \text{Eq. 1-3}$$

Where h and v_m are Planck's constant and molecular volume, respectively. Therefore, it can be written as Eq. 1-4:

$$J_0 \propto \left(\frac{\gamma_{SL}}{kT}\right)^{\frac{1}{2}} \left(\frac{h}{\mu v_m}\right), \qquad \text{Eq. 1-4}$$

Thus, it can be concluded that by increasing viscosity of the interfacial layer, the ice nucleation rate would decrease [178]. It was also claimed the on the hydrophilic coatings, the viscosity of the interfacial water layer is several times higher than that on hydrophobic coatings [179].

Hygroscopic polymers are materials that can absorb moisture and reach an equilibrium with the surrounding environment. This moisture level therefore varies with the water content of the surrounding atmosphere. This water is absorbed, penetrates the polymer, and then becomes bonded to the polymer by polar hydrogen bonds [180]. Hygroscopic polymers, including nylon, PET, TPU, and PC, possess a strong affinity for moisture, and water molecules can become bonded to the polymer chains. In contrast, non-hygroscopic polymers, such as PE, PP, and PVC, do not absorb moisture. Although these latter polymers can pick up surface moisture, this moisture can be easily removed, such as through using a hot-air dryer. The hygroscopic polymers will swell after absorbing water. From an anti-icing perspective, this means that as the air temperature drops, the absorbed water inside the micropores returns to the surface, in turn decreasing ice adhesion [181].

Generally, the concentration of components located near the surface influences the degree of icephobicity, and this effect can be described in terms of the structure of interfacial water [182]. Changes to the silanol density alter water structuring at the surface[183]. For instance, an increased silanol concentration at the surface affects the packing of water at the surface and enhances the ice-like behavior of the water. In the case of atactic polystyrene, as another example, the number of hydrogen bonds at the surface increases linearly with oxygen concentration [184]. Changing the near-surface concentration of the amphiphilic molecules can produce anti-icing hierarchies. Because of the surface conformations of ethylene glycol (EG) and its hydrogen bond–accepting characteristics, which result in various solvation shells at the interface and a reduced EG–EG complexation, this material offers much potential for anti-icing applications [182,185].

Micropore arrayed silicon wafers were designed via photolithography and then grafted crosslinked polyacrylic acid (PAA) within the wafers to fabricate an anti-icing coating (Figure 1-15a) [186]. This type of coating helps form a self-lubricating liquid water layer (SLWL) over itself. An external force, such as wind, can then easily remove the accumulated ice on the surface. They found that the ice adhesion strength was significantly lower for these wafers than for other superhydrophilic or superhydrophobic coatings. Furthermore, as water could be recovered from the environment, the coating is considerably durable and long-lasting.

Such a coating has a limited application because it cannot be used for a diverse range of substrates. To overcome this issue, they then synthesized polymers having backbones characterized by a high density of carboxyl to allow the structure to absorb a large quantity of water molecules. Polyurethane coatings can be also applied on

various substrates, and their chemical structures and functional groups permit an acceptable adhesion to the surface [169,187]. Each polyurethane chain contains two components, namely hydrophilic and hydrophobic components. Dimethylolpropionic acid, as a hydrophilic component, was covalently attached to the polymer chain. This anionomer was added to water to favor a polyurethane dispersion and then underwent a chain extension after the addition of isophorone diamine. Spherical particles form because water serves as a reaction medium, and, therefore, the hydrophilic components migrate toward the outside of the particles, whereas the hydrophobic components remain inside. Ice adhesion on developed coating was decreased because: firstly, surface roughness is decreased with the use of polyurethane by minimizing the mechanical entanglements between the ice and the coating. Secondly, the water absorbed by the hydrophilic components has a lower freezing point than that of bulk water. Within the matrix of hydrophilic coatings, water exists in two states, namely nonfreezable and freezable water [169]. Nonfreezable water creates well-oriented hydrogen bonds with hydrophobic groups of polymer chains in a locally favorable configuration. Freezable water also refers to the fraction of water that lies within macromolecular interstices and/or areas around attached water molecules. Consequently, the nonfreezable water contributes to the formation of a very thin aqueous layer between the ice and the coating surface. This thin aqueous layer acts as a lubricating layer. Using a greater amount of dimethylolpropionic acid (DMPA) as the hydrophilic component increases the amount of water absorption and consequently thickens the lubricating layer [169]. Increasing the thickness of this layer can shift the lubrication regime from a boundary to a mixed or even hydrodynamic regime, thereby leading to a significantly reduced ice adhesion strength [169]. Chen et al. [188] also

synthesized other durable anti-icing coatings, inspired by mussels, that consist of a hydrophobic conjugate of poly (acrylic acid) –dopamine. This method causes both freezable and nonfreezable water to remain in a liquid-like state under sub-zero temperatures. This nonfreezable water acts as a lubricant. The authors found this coating reduced ice adhesion strength to around 25 kPa. The coating remained stable over 40 icing/de-icing cycles and soaking tests.

Another method for reducing ice adhesion that has been inspired by natural processes is the use of ion-hosting superhydrophilic polyelectrolyte brushes. The presence of highly hydrated ions creates a QLL, which prevents ice nucleation [182]. Chernyy et al. [189] investigated the influence of polymer structure and ionic species on the icephobic properties of a hydroscopic polymer. Using initiated atom transfer radical polymerization (SI-ATRP), they fabricated various ionic and nonionic polymer brush coatings. The polyelectrolyte brushes included cationic [2-(methacryloyloxy) ethyl]-trimethylammonium chloride] and anionic [poly (3-sulfopropylmethacrylate) poly (sodium methacrylate)] brushes. Moreover, the ionizable groups of these brushes were exchanged with various ions, including H^+, Li^+, Na^+, K+, Ag^+, Ca^{2+}, La^{3+}, $C_{16}N^+$, F^-, Cl^-, BF_4^-, SO_4^{2-}, and $C1_2SO_3^-$. Ions such as Li^+ and Ca^{2+}, known as kosmotropes, are structure-making ions, and because of their high charge density, they disturb water hydrogen bonds (Figure 1-15b). Structure-breaking ions, such as K^+ and Cl^-, also called chaotropes, differ in their behavior from kosmotropes. When near water, kosmotropes, unlike chaotropes, remain hydrated. In addition, the hydrogen bonding of water molecules is readily broken when these molecules lie very close to kosmotropes. In contrast, chaotropes do not strongly coordinate water molecules [190]. Chaotropes, such as K^+, can slightly enhance the average water diffusion in the aqueous

salt solutions; therefore, they disturb the structuring of water, especially at moderate to high salt concentrations [191]. Therefore, the structure of QLL, and the tendency of water to crystallize within the brush–water interface are affected by the chemical nature of the polymer brush/counterions. Thus, the high tendency of ions to dissociate and to stay simultaneously within the brush layer increases the thickness of QLL under freezing temperatures. Figure 1-15b presents the change in ice adhesion strength of polymer brush layers [189]. Ice adhesion strength dropped 40% and 25% using Li^+ and Na^+, respectively, at −18 °C, whereas weak kosmotropes and chaotropes produced no significant change in ice adhesion. Polyelectrolyte coatings reduced ice adhesion by 20% to 80%, depending on the selected ion type [189].

Self-lubricating icephobic surfaces were also developed by blending amphiphilic copolymers within a polydimethylsiloxane (PDMS) matrix [68]. These coatings demonstrated ice adhesion strengths around 50 kPa, values lower than those observed for smooth hydrophobic surfaces. A small amount of PDMS-PEG copolymer in the coating can contribute positively to preserving the lubricating layer between the ice and the surface [24]. Given the strong hydrogen bonds between the PEG-PDMS copolymers and water molecules, this liquid-like layer, the QLL, remains unfrozen in sub-zero conditions (Figure 1-15c).

To sum up, the aqueous self-lubricating coatings can offer a low ice adhesion strength due to formation of non-frozen QLL under subzero temperature conditions. Such a layer usually exists between -53 to 0 ˚C, and depending on parameters like temperature, surface nature, and impurities its thickness varies between 0 and a few hundred nanometers. Some work has been done to fabricate the sustainable aqueous self-lubricating surfaces, but their durability and longevity still matters. It seems that

these coatings have the potential to be combined with other icephobic strategies, as a hybrid strategy to achieve the enhanced anti-icing characteristics [179].

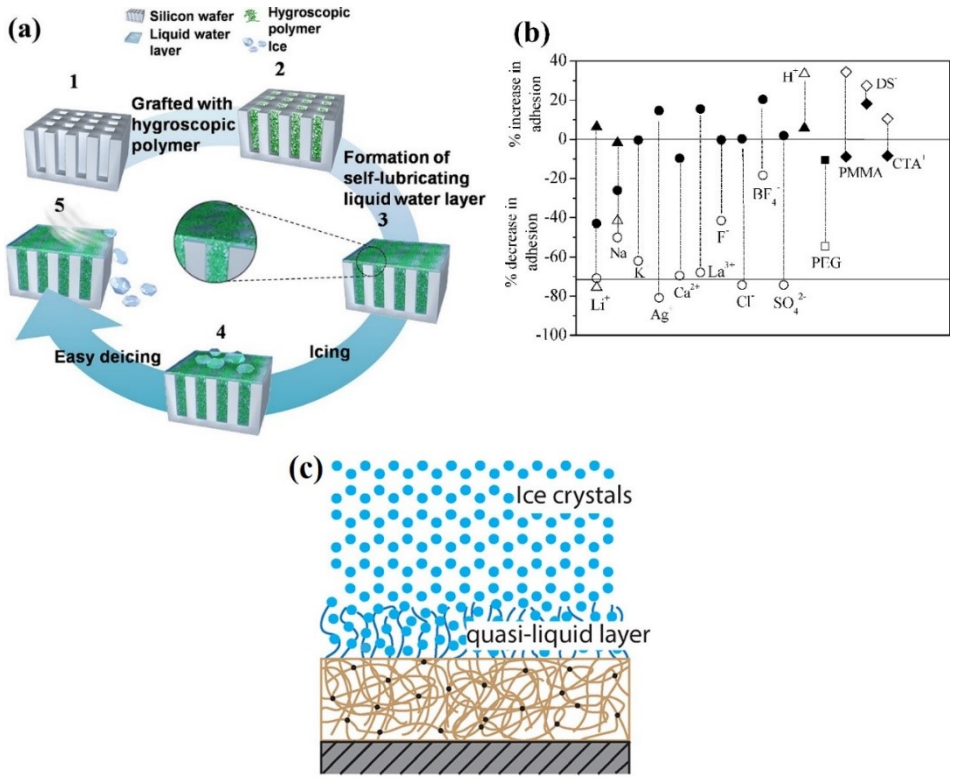

Figure 1-15. *(a) Fabrication of the self-lubricating surfaces: (1) creating micropore silicon wafer structures; (2) grafting the silicon wafer structures with hygroscopic polymers; (3) forming the self-lubricating liquid water layer on the surface; and (4 and 5) de-icing [186]. (b) Percentage change in ice adhesion strength for all ions incorporated in polyelectrolyte brushes. Filled and open symbols represent measurements at −18 °C and −10 °C, respectively [189]. (c) Schematic illustration of the formation of the quasi-liquid layer, produced through the strong hydrogen bonding between PEG-PDMS copolymers and water molecules, which reduces ice adhesion strength [68].*

1.5.5 Phase-change materials (PCMs)

Phase-change materials (PCMs) possess a high heat storage capacity, allowing them to store heat during a phase change process. This capacity, in particular during the melting–solidification transformation, has made PCMs attractive candidates for

many applications, including the air conditioning of buildings [192], spacecraft thermal control [193], thermoregulation functions of textiles [194], and cancer therapy [195]. PCMs, such as salt hydrates and alkane/aliphatic solutions, are sealed within organic or inorganic materials. Phenomena related to phase change, such as the release of latent heat, can be used in the above-mentioned applications [196].

1.5.5.1 Criteria of PCMs selection

Several criteria must be met for a PCM to be considered a good candidate. These criteria include having a desirable melting temperature, high latent heat, high thermal conductivity, reproducible phase change, durable properties, chemically stability and being cost-effective [197]. It should also possess small volume changes during phase transformation. An ideal PCM should have high nucleation rate to reduce super cooling. Furthermore, a high rate of crystal growth enhances the heat recovery from the energy storage system [198].

The thermal effusivity, I, is one of the essential factors to evaluate the thermal efficiency of a PCM. This parameter can be obtained using Eq. 1-5 [22].

$$I = \sqrt{\rho . C_p . k}\,, \qquad \text{Eq. 1-5}$$

Where ρ, C_p, and k are the density (kg/m^3) the mass specific heat capacity (kJ/kg.K), and the thermal conductivity (W/m.K) of the PCM, respectively. Accordingly, a PCM with a greater thermal effusivity presents a higher thermal release or storage in a shorter time. Furthermore, the temperature range of phase changing is another factor that should be considered, particularly for anti-icing applications. It is very important in selecting a PCM for such applications that the phase change procedure happens around 0 ˚C. For having a desirable releasing temperature range,

PCM should also have a minimized degree of supercooling that defined as difference between melting and crystallization temperature [199]. Adding of nucleation agent can be to a large extent effective to adjust the supercooling temperature [23].

The thermal properties of PCMs can be evaluated using different measurement techniques such as differential scanning calorimetry (DSC), differential thermal analysis (DTA), and T-history method. Using DSC method, various thermal characteristics can be studied like heat capacity, enthalpy, heat of fusion, heat storage capacity, and melting/solidification temperatures [200]. Same as DSC technique, DTA test can also be helpful to evaluate the thermal properties and the phase-change-related phenomena. In comparison with DSC and DTA methods, T-history method can be considered as a more precise technique to investigate thermal characteristics such as the melting point, supercooling degree, and thermal conductivity [200].

1.5.5.2 Classification of PCMs

In general, PCMs are grouped based on their phase change state, such as solid-gas PCMs, solid–solid PCMs, solid–liquid PCMs, and liquid–gas PCMs (Figure 1-16). Solid–liquid PCMs can be generally classified into three groups, namely organic components (e.g., paraffin, fatty acids), inorganic components (e.g., salty hydrates, metallics), and eutectics (e.g., organic–organic, inorganic–inorganic) [200].

As illustrated in Figure 1-16, Solid-liquid PCMs are divided into three different groups, namely organic, inorganic, and eutectic PCMs in terms of their chemical structures. The organic PCMs are also subcategorized as paraffins and non-paraffins (Fatty acids, alcohol, esters). The group of paraffins offers safe, stable, predictable, non-corrosive and cost-effective characteristics that make this group a potential

candidate for many energy storage applications. Non-paraffins exhibits various characteristics such as high latent heat, and low thermal conductivity [201,202].

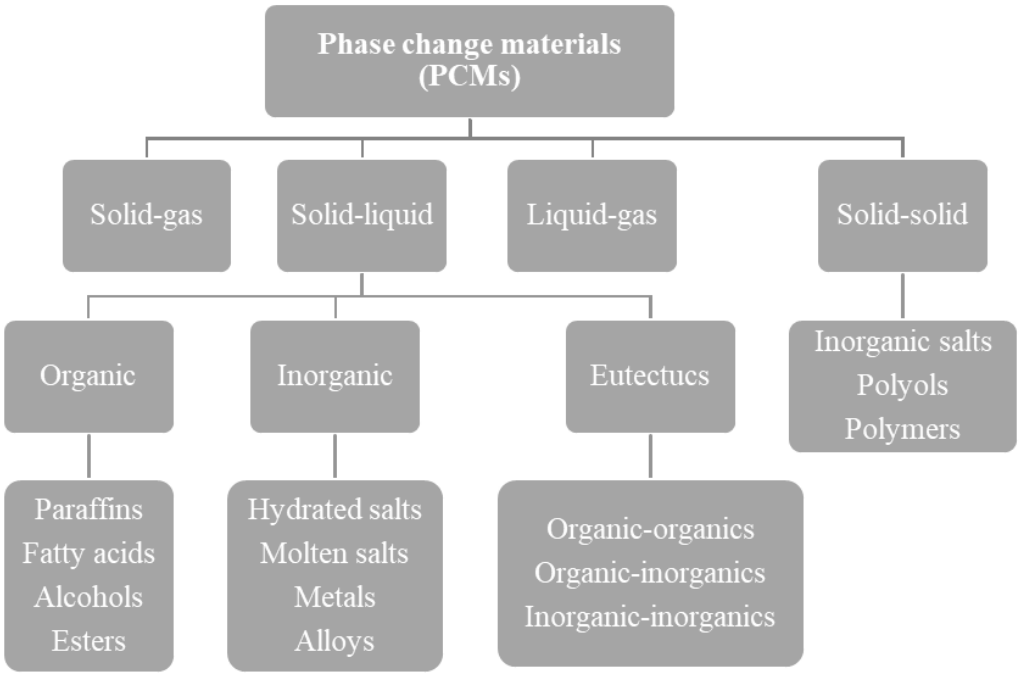

Figure 1-16. *Classifications of the phase change materials (PCMs) [203].*

Inorganic PCMs including salt and metal hydrates, are inexpensive, high thermal conductivity, and non-flammable, and have high latent heat. Despite advantages, they suffer from some drawbacks such as undercooling, and corrosion [201,202].

Eutectic PCMs can be obtained by combining inorganic and organic components and divided into three different groups of organic-organic, inorganic-inorganic, and organic-inorganic subcategories. Eutectics are considered as a potential candidate for many applications due to their wide range of phase change temperature, high heat capacity, and low degree of supercooling. However, they have some

downsides like low thermal conductivity [204]. Table 1-2 summarizes the advantages and disadvantages of different types of solid-liquid PCMs [204].

***Table 1-2**. The various tapes of the solid-liquid PCMs and their characteristics [204].*

	Organic material	Inorganic material	Eutectic material
Advantages	• Non-corrosive • Good chemical and • thermal stability • No supercooling • High heat of fusion • Low vapor pressure • Nontoxic	• Non-flammable • Inexpensive • High heat of fusion • Good thermal conductivity	• Wide range of phase change • temperature • Good chemical and • thermal stability • High heat capacity • No or little supercooling
Disadvantages	• Low thermal conductivity • Low phase change enthalpy • High changes in volumes during • Phase transition	• Corrosion • Phase decomposition • High supercooling effect • Loss of hydrate throughout the process • Insufficient thermal stability • Weight problem	• Leakage during the phase transition • Low thermal conductivity
Examples	• Paraffin • Fatty acids • Alcohol • Ester • Polyethylene glycol	• Salt hydrate • Metallic	• Organic-organic • Inorganic-inorganic • Organic-organic

Because of the phase change capacity of organic PCM such as paraffin, they have attracted substantial attentions. For example, the n-paraffin-swollen PDMS elastomers can alter water adhesion on a surface [205]. This n-paraffin-swollen organogel can switch back and forth between an air/liquid 1(water)/liquid 2 (paraffin))/solid (ALLS) system and an air/liquid (water)/solid (ALS) system owing to the thermoresponsive phase change of n-paraffin. At temperatures above the melting

temperature of n-paraffin, the coating surface has a low adhesion with the water droplet because the liquefied n-paraffin wets the elastomer surface and acts as a lubricant between the water droplet and the solid surface. Below this temperature, the n-paraffin solidifies and, therefore, surface roughness increases to produce a Wenzel state with high-adhesion toward water drops. Such a structure can readily switch between low-adhesion slippery and high-adhesion states without any need for conventional functionalizing [205].

1.5.5.3 Impregnation of PCMs within a matrix

Three different methods have been presented to impregnate PCMs within materials that include direct incorporation, immersion, and encapsulation [206]. Among these methods, encapsulation is most effective for a variety of applications. This procedure consists of enclosing a substance such as monomers, catalysts, curing agents and the PCMs into a shell to protect it from the surrounding materials. This protective shell (Figure 1-17) prevents problems such as material exchange with the environment and leakage-related issues [207]. Using encapsulating can handle materials such as PCMs and improve their processability. There are a various range of encapsulation techniques, including suspension polymerization, emulsion polymerization, in-situ polymerization, sol-gel process, layer-by-layer assembly and electrospraying [22].

Shell thickness is another factor that must be optimized to maximize the performance of the encapsulated PCM. Therefore, by defining the core-to-shell ratio, one can evaluate shell thickness. A lower ratio leads to a thicker shell and, consequently,

a weaker heat transfer from the PCM to the binder. Moreover, a high core-to-shell ratio can increase the probability of PCM leakage [22].

An appropriate binder must be selected and be compatible with the shell material to facilitate a heat transfer between components. The binder's thermal conductivity and thermal capacity should also be accurately determined, and the PCM content in the binder should be optimized according to the final application. Excessive PCM in the binder can affect the general mechanical properties of the coating [208].

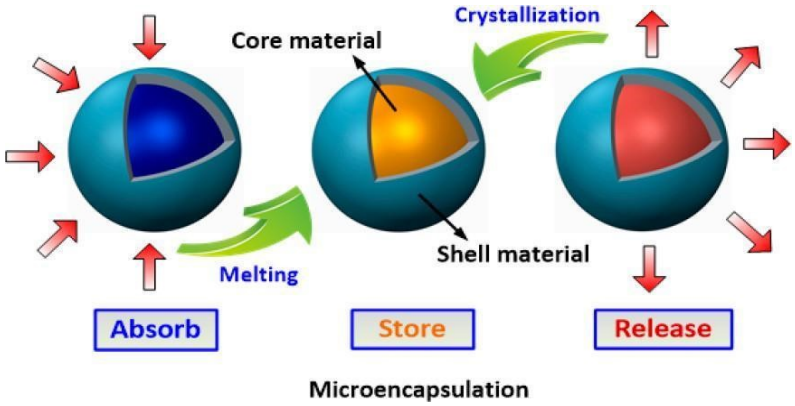

Figure 1-17. *Schematic showing the structure of PCM microcapsules and PCM release [207].*

In icephobic applications, the appropriate selection of PCMs is critical. The phase-change temperature range should correspond to the application temperature range. Moreover, shell materials and the encapsulation process must be carefully chosen. The fabrication procedure parameters, such as agitation speed, PCM concentration, viscosity, and temperature, significantly affect PCM size and their size distribution [22,209,210]. As the specific surface area is critical for heat transfer and heat exchange with the surroundings, smaller capsules provide a larger specific surface area than larger capsules and, therefore, improve transfer efficiency. Thus, smaller

capsules are preferred for improving the heat-transfer performance owing to their greater surface-area-to-volume ratio [209]. Macro-sized capsules also offer less thermal reliability and chemical stability than the smaller PCM capsules, namely micro- and nanoencapsulated PCMs [22,210].

1.5.5.4 Anti-icing mechanisms of PCMs

There are three possible mechanisms that can be used to interpret the anti-icing behavior of PCMs, namely producing a hydrophobic structure, the production of local strains, and the formation of the quasi-liquid layer (QLL) [22]. For first mechanism, embedding PCM capsules within the matrix can create micro- and submicro-scale structures in the surface that reduce the ice-surface contact area. It can result in trapping of air within the asperities, and producing a superhydrophobic surface (WCA >150°). Yuan et al. fabricated phase change microcapsules and incorporated them within a permanent room temperature vulcanized (PRTV) silicon rubber to obtain icephobic surfaces. They evaluated the wettability of the prepared coatings, and found that for the sample containing 34% PCM microcapsules, the contact angle was 164 ˚. So, besides the low surface energy, the coating had the micro-scale hierarchical topography, resulting in superhydrophobic characteristics. Therefore, the coating showed water repellant properties that enhanced anti-icing performance [23].

The second mechanism can be based on expansion/contraction of the surface, resulting in ice detachment. The decrease of temperature can lead to contraction of the surface. On the other hand, releasing latent heat of PCM, and absorption of the heat by their adjacent areas causes the local expansion. The overall contraction and localized expansion of the surface would produce a shear stress that can break surface-ice bonds,

and consequently, it results in ice detaching from the surface. The released latent heat in PCMs can be used for anti-icing purposes. Bhamidipati [211] fabricated an icephobic coating by incorporating silicone PCMs within hydrophobic silicone-based resins. The de-icing process of this PCM-incorporated coating consists of three steps. First, a change in the solid–solid phase occurs within a very small area near the surface across a narrow temperature range. Cold air causes the substrate to contract at the same time as PCMs are expended. Second, after ice formation on the surface, a portion of the latent heat of ice is transferred to the PCMs located near the surface. Finally, the absorption of the heat by PCMs changes the solid–solid phase, resulting in high local shearing at the ice–coating interface because of a volume change of the coating. The actual local lateral displacement, which was around one-tenth the diameter of the PCM particles, breaks the bands between the ice and the surface and, therefore, removes the ice from the surface [211].

In the third mechanism, a portion of this heat energy that reaches the coating/ice interface, can melt the ice and form a quasi-liquid layer. This layer can act as a lubricant, resulting in producing a mixed lubrication regime and therefore, reducing ice adhesion strength. It is noteworthy that after this phase-transmission temperature range, the liquid-like layer can be reduced, and the lubricating regime would return back to boundary regime [212,213]; because PCM would not release more heat. PCMs such as hexadecane and octadecane have been encapsulated within inorganic microcapsules using a sol-gel process and then incorporated into different wind-driven power generator elements, including blades, nacelles, and generators [214]. Combining a sol-gel process and emulsion techniques can produce capsules 30 nm to 30 μm in diameter and having controlled shapes. The synthesized capsules can then be incorporated into

either coatings or the materials composing the power generator elements. As temperature decreases and approaches the crystallization temperature of the PCMs, the release of latent heat maintains temperature within the range of the PCM phase-changing temperature. During functionality tests, the incorporated PCMs showed a 20 to 30 min delay in ice formation, the specific delay time depending on PCM type and concentration [214].

Encapsulated PCMs have also been incorporated into room-temperature vulcanized (RTV) silicone rubber coating and fluorosilicone (FS) copolymers, considered as low-energy surface materials [215]. The copolymers not only protected microcapsules from breaking but they also prevented the leakage of PCM. By increasing PCM content in the coating, surface roughness increased. Greater surface roughness increased the water contact angles of the coating. Zhu et al. [215] nonetheless found no proportional relationship between the contact angle and surface roughness; although roughness can affect the contact angle. The presence of hydrophilic polar groups, such as -OH and $-NH_2$ in the urea-formaldehyde microcapsules on the coating, caused hydrogen bonds to form with water molecules and, accordingly, altered the contact angle. Furthermore, the content of PCMs affected the icing delay time of water droplets on the coating; increasing the PCM content prolonged the freezing process. This delay is related to the release of latent heat as temperatures decreased. Comparing both copolymers, the authors concluded that because of the composition of RTV, RTV/PCM coatings produced lower ice shear strengths than FS/PCM coatings. The low T_g of PDMS reduced ice shear strength and made the RTV/PCM more flexible.

1.5.6 Other types of smart icephobic coatings

Some smart coating–based studies have relied on other stimuli such as pH and light. Yin et al. [216] fabricated a photothermal responsive film for icephobic purposes. Their fabrication progress comprised four steps (Figure 1-18a). First, they prepared a compact template by assembling polystyrene microspheres. A silicone precursor with Fe_3O_4 nanoparticles was then poured onto the template. They then removed the template to produce an inverse porous film having uniformly distributed nanoparticles. They finished their fabrication process with a fluorinated treatment of the template using perfluorosilane and then infiltrated the template with perfluoro polyether lubricants. Fe_3O_4 nanoparticles dispersed within the film responded to a near-infrared (NIR) laser by changing the laser's optical energy into heat. The thermogenic capacity of the nanoparticles produced the icephobic properties of the film under various high humidity and freezing rain conditions. NIR lasers can penetrate various materials; therefore, this icephobic strategy has great potential to expand from an experimental to an industrial scale for mass production [216].

TiO_2 was used to fabricate dual stimuli-responsive superhydrophobic coatings having photocatalysis properties and pH-sensitive microcapsules [217]. The fluoroalkyl silane–loaded microcapsules that their average diameter increased to 420 nm under acidization condition, were fabricated using mini-emulsion polymerization. The obtained microcapsules were mixed with TiO_2 nanoparticles, modified nanosilica (FMS), and waterborne resin to fabricate a self-healing waterborne superhydrophobic coating (Figure 1-18b). The coating was then applied to various substrates and cured by UV light. The coatings showed acceptable superhydrophobicity and self-cleaning properties, and they possessed a self-healing capacity under UV irradiation after

mechanical damage. Nonetheless, the superhydrophobic performance was reduced after 10 icing/de-icing cycles. This degradation of performance could reflect the loss of the hydrophobic substance at the surface; after stimulation by UV light, the coating regained its superhydrophobicity.

Multifunctional superhydrophobic coatings can be fabricated by crosslinking a fluorinated copolymer, amino-functionalized magnetite particles (MNP@NH_2), and a polyamine compound [124]. When photothermal effects of the coating were investigated (Figure 1-18c and Figure 1-18d), the magnetic particles adsorbed light energy and converted optical energy into thermal energy to enhance the thermogenic de-icing characteristics of the coating.

A hybrid coating was synthesized by combining an amphiphilic copolymer with amino-functionalized magnetic Fe_3O_4 nanoparticles, followed by infiltration with polyols [48]. The photothermal properties of the magnetic particles generated heat under light irradiation. The presence of magnetic particles allowed the coating to melt the ice and improve the active thermal de-icing properties (Figure 1-18d).

Shape-memory materials are another group of smart materials that have responsive-recovering capabilities. Materials in this category have a reversible shape-changing behavior and can return to their original shape. Shape-memory materials revert to their preformed shape after deforming because of external stimuli, such as electric and magnetic fields, light, and temperature [219]. Various materials, including metals, alloys, and polymers, can be used to create a shape-memory effect. However, there are a greater number of advantages when using polymers; for instance, the properties of polymers can be readily tailored. In addition, the material and processing costs of polymers are lower than those for alloys and metals [220].

Shape-memory polymers (SMPs) are relatively well studied because of their distinguishing characteristics. In addition to the above-mentioned advantages of shape-memory polymers, they are also much lighter than the others. Furthermore, they show a higher recoverable strain relative to the shape-memory alloys [220,221]. One of the most important features of SMPs is their memory of various surface morphologies without any required external forcing. This smart behavior allows the contact and roll-off angles to be reversibly controllable and permits multiple novel functions, such as a continuously tunable wettability (Figure 1-18f) [222].

Most studied SMPs having a controllable surface wetting property are intrinsically thermoresponsive. Two structural factors are required for this capacity: 1) a switching unit for temporary shape fixing and recovery and 2) a crosslinking network for setting the permanent shape [223]. An epoxy-based SMP surface demonstrated variable wettability for a tilted state and a recovered state [224]. The surface, covered by an array of micropillars, recovered its original state through heating at a temperature above that of the glass transition temperature of the polymer. Because of the Wenzel wetting state owing to the wide spacing between pillars, the water droplet on the deformed SMP pillars was prevented from rolling off the surface. On the pillars having their original shape, the droplet could slide over the surface at a finite roll-off angle because of the Cassie–Baxter wetting state. Thus, thermal actuation of the surface having deformed micropillars (and, therefore, a lower contact angle) returns the surface to its initial structure and original hydrophobic characteristics [225]. These materials show enormous potential for use as smart icephobic coatings [226].

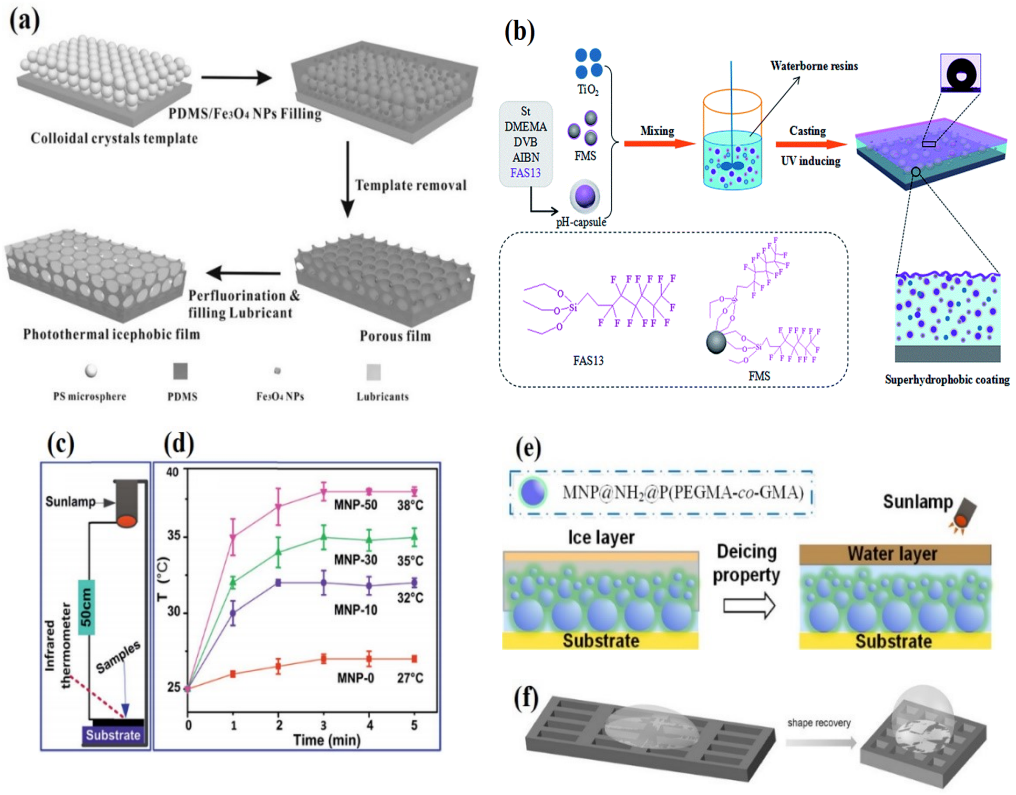

Figure 1-18. *(a) The four-step fabrication of a photothermal responsive film by Yin et al. [216]; (b) schematic showing the steps for fabricating dual stimuli-responsive self-repairing superhydrophobic coatings [217]; (c) schematic showing the photothermal setup, including a sun lamp and an infrared thermometer; (d) the change in surface temperature over time in relation to the heating of the samples [124]; (e) the de-icing of the coating owing to the photothermal properties of the functionalized magnetic Fe_3O_4 nanoparticles [218]; (f) the shape recovery of shape-memory polymers (SMP), resulting in the continuous change of the contact angle [222].*

1.6 Combining smart anti-icing strategies

Table summarizes the general advantages and disadvantages of smart icephobic coatings. There is no doubt that each smart icephobic coating has its downsides, and obtaining a desirable ice adhesion strength based on each category would very likely face some limitations. Therefore, it can be beneficial to combine some strategies

together in order to eliminating the drawbacks associated to each individual strategy [227]. In fact, the synergic effects of multiple icephobic strategies can lead to fabricate a coating with better anti-icing performance in comparison with each one. For instance, an intelligent icephobic surface was produced by Liu et al. [228] by integrating a superhydrophobic copper mesh and an intelligent polyvinyl alcohol (PVA)–based organogel. The self-secreting organogel, as an antifreezing agent, prevented the frosting of the surface at sub-zero temperatures. Moreover, the fabricated surfaces showed a renewability of the organogel—using a heat-cooling treatment without losing their self-secreting capability. An ice adhesion strength of 8 Pa was achieved at −20 °C for these surfaces [228]. In the other study, He et al. fabricated an icephobic coating by combining two strategies, namely the aqueous self-lubricating coating and macro-crack initiators at ice-coating interface. The former strategy was produced by grafting poly (acrylic acid) onto PDMS matrix, and the later one was based on introducing macro-hollow structures into the coatings. They showed using the synergistic effect of these two strategies, an ice adhesion reduction of about 51% (compared to pure PDMS) was obtained that provides a promising approach towards the fabricating smart anti-icing coatings [229]. Wang et al. also fabricated a robust icephobic surface by combining multiple techniques, namely using low modulus elastomers and superhydrophilicity. Such a surface repelled water and ice at -20 ˚C, and high humidity 90%. The icephobic mechanism of the prepared surfaces was based on the synergetic effect of the matrix flexibility and micro-nanostructure. In fact, the condensed droplets were repelled and suspended by ZnO nano-hairs and PDMS microstructure, respectively [230]. Therefore, combining different anti-icing methods can be an effective approach to achieve enhanced anti-icing characteristics due to their synergistic effect [175,231].

Using this approach, one can minimize the disadvantages of each individual strategy and break the theoretical limits of icephobic coatings.

Table 1-3. *A summery of smart icephobic strategies.*

Strategy	Advantages	Disadvantages
Thermoresponsive coatings	• Convenience • Real-time response • Lower environmental impacts	• Limited applications
Electromechanical (piezoelectric) de-icing systems	• Efficient • High de-icing performance • Potential to be used in particular applications such as aircrafts	• Need an external energy resource • Probability of Energy dissipation
Self-healing icephobic coatings	• Reducing the frequent inspection • Suitable for remote areas	• Need for total replacement of the coating after finishing healing agent
Slippery surfaces	• Desirable anti-icing performance • Very low ice adhesion	• Oil depletion
Aqueous lubricating coatings	• No oil depletion • Low ice adhesion • - No environmental impacts	• Studies are still in their primary stages
Phase-change materials (PCMs)	• No need for an external energy resource • High energy storage capability	• Material leakage

1.7 Conclusion

Demands for innovative coatings to mitigate ice accumulation and ice adhesion have guided academic and industrial sectors toward developing smart icephobic coatings because of the multiple advantages of these coatings for solving icing-related issues. In this chapter, we investigated and classified various smart icephobic coatings in terms of their stimuli response.

Although most research in smart icephobic coatings remains in its initial stages, investment in this area is expected to expand greatly over the next few years. Some icephobic coatings, such as self-lubricating coatings, have shown marked progress in their development and may soon offer the possibility of large-scale production. The fabrication of smart icephobic coatings using phase change materials (PCM), for instance, requires more investigation for being commercialized. The lack of a comprehensive series of test method to investigate the icephobic performance is also another issue to present a coating with desirable anti-icing properties. Furthermore, the synergistic effect of combing two or more strategies can be considered as a promising approach to obtain more desirable anti-icing characteristics and avoid limits for each individual icephobic technique. The range of research activities presented in this chapter illustrates the potential of smart icephobic coatings to fulfill market requirements. Increased demand for such coatings will also favor the development of cheaper and more environmentally safe products.

Chapter 2: Icephobic properties of aqueous self-lubricating coatings containing PEG-PDMS copolymers

Mohammadreza Shamshiri*, Reza Jafari, Gelareh Momen

Department of Applied Sciences, University of Quebec in Chicoutimi (UQAC), 555, boul. de l'Université, Chicoutimi, Quebec, G7H 2B1, Canada

*Corresponding author: E-mail address: mohammadreza.shamshiri1@uqac.ca.

2.1 Abstract

Icephobic coatings offer an effective solution for protecting infrastructures subjected to harsh cold-weather environments. Aqueous self-lubricating coatings, derived from the principles of ice skate sliding over ice, provide a cost-effective anti-icing method. Here, we fabricate aqueous self-lubricating coatings by adding polydimethylsiloxane-poly (ethylene glycol) (PEG-PDMS) copolymers to a PDMS matrix. We analyzed the wettability, morphology, and topography of the fabricated coatings using a goniometer, scanning electron microscopy (SEM), and atomic force microscopy (AFM), respectively. Differential scanning calorimetry (DSC), push-off and centrifugal tests detailed the icephobic characteristics of the coating surfaces. Blending PEG-PDMS into the elastomeric matrix enhanced the effective contact area between the water droplet and the coating; the formation of hydrogen bonds between water molecules and the hydrophilic functional groups of the coating produced this

effect, and water molecules spread readily over the surface. Increased concentrations of these functional groups increased the freezing-delay time and reduced ice adhesion strength, likely owing to the formation of a quasi-liquid-like layer. Nonetheless, the immiscibility of the PEG-PDMS copolymer within the PDMS matrix can negatively affect wettability and the icephobic characteristics of the coatings. An optimized copolymer content of 5% produced a durable icephobic aqueous self-lubricating coating.

Keywords: Icephobicity, wettability, PEG-PDMS copolymer, aqueous self-lubricating coatings, smart coatings, ice adhesion

2.2 Introduction

Preventing ice formation and ice accumulation on exposed surfaces is an important issue for enhancing the safety, energy generation efficiency, and operational performance of exposed infrastructures [1–13]. Ice nuclei are generated within a water droplet at either the free or solid interface, termed homogeneous and heterogeneous nucleation, respectively [41,42,45].

Various methods have been developed to reduce icing-related risks [1,49]. In recent decades, lubricated surfaces have served as icephobic coatings; oil has been traditionally employed as the lubricant [56,83,120,149,165,228,232]. Post-infusing methods, where lubricating liquid is added to a porous matrix, and pre-infused methods, where the lubricant is added to a precursor, are the most common procedures for fabricating lubricated surfaces [150]. Drawing on the principles associated with ice

skating, researchers have tried to use the presence of water on wetted surfaces to fabricate aqueous self-lubricating icephobic coatings. As a skate blade passes over the ice, a very thin aqueous layer forms between the skate blade and the ice and serves as a lubricant to facilitate the slippage of the skater's blade across the ice surface. Such a lubricating layer can be created by frictional heating, pressure melting, or both to cause the uppermost layer of ice to transform into liquid water [170,171]. Aqueous self-lubricating coatings hold certain advantages over oil-infused coatings. Aqueous coatings involve water, a naturally occurring lubricant, and such coatings also avoid issues related to oil depletion through oil leakage or evaporation [148]. Moreover, aqueous self-lubricating coatings can be quite durable and long-lasting because water can be easily recovered from the surrounding environment [186].

Just below the melting point of ice, a disordered liquid-like layer, often labeled the "quasi-liquid layer" (QLL), exists at the solid–vapor interface. This layer differs in its properties from those of bulk supercooled liquids subjected to the same thermal conditions. The presence of the QLL at the ice–air interface plays a key role in such phenomena as the adsorption of dust onto the ice surface and the low friction between surfaces and ice [172]. The tribological characteristics of ice in glaciological processes are also affected by the dynamics of the QLL. The QLL varies in thickness from a few nm to a few hundred nm, depending mainly on temperature and surface chemistry; for instance, lower temperatures lead to a thinner QLL [1,46].

The QLL can be generated on the surface of coatings by grafting hygroscopic materials to thereby create hydrophilic surfaces [1,46,176]. The non-freezable water can be created by well-oriented hydrogen bonds between water molecules and

hydrophilic groups on polymer chains. This non-freezable water thus forms a very thin liquid-like layer between the ice and the surface that acts as a lubricating layer [169,186].

Generally, the concentration of the hydrophilic components present at the surface determines the degree of hydrophilicity and change to the structure of the interfacial water [182]; for example, variations in the concentration of silanol on a surface alter the packing of surficial water molecules and enhances more ice-like water [183,184].

Amphiphilic molecules can also be used to create anti-icing hierarchies; for example, the surface conformation and hydrogen-bond generating characteristics of ethylene glycol (EG) result in various solvation shells at the coating–water interface and a reduced EG–EG complexation; coatings containing EG show potential for use in anti-icing applications [182,185]. Aqueous self-lubricating coatings can be developed using polymeric matrices containing amphiphilic copolymers such as PDMS-PEG copolymers. The strong hydrogen bonding between the PEG-PDMS copolymers and water molecules helps preserve the QLL, even under subzero conditions. This liquid-like layer can act as a lubricant between the ice and the surface [68].

Aqueous self-lubricating coatings also hold an advantage over other icephobic surfaces through their “smart” functioning. This capacity allows the coatings to sense humidity within the surrounding environment and attract water to the surface. This response to the humidity stimulus helps form and maintain QLL on the surface, which

acts as a lubricant in icephobic applications [186]. The coating returns to its original state when the stimulus is removed.

In this study, we fabricate aqueous self-lubricating coatings by blending PEG-PDMS copolymers in a silicone elastomer. We varied copolymer content of the coatings and applied the prepared coatings to aluminum substrates through spin-coating. The wettability of the samples was then studied over time. We investigated the compatibility of the copolymer in the matrix via scanning electron microscopy and atomic force microscopy. We also evaluated the effect of copolymer type and copolymer percentage on nucleation temperature, freezing delay time, and ice adhesion strength.

2.3 Experimental protocols

2.3.1 Fabricating the anti-icing coating

We used Sylgard 184 silicone elastomer (polydimethylsiloxane (PDMS)) as a base and its curing agent, both obtained from Dow Corning. CMS-221 ((carbinol functional) methylsiloxane dimethylsiloxane copolymer) and DBE-224 (dimethylsiloxane-(25-30% ethylene oxide) block copolymer), as polydimethylsiloxane (PDMS)-poly (ethylene glycol) (PEG) copolymers, were purchased from Gelest Inc. These copolymers were selected based on their capability for producing hydrogen bonding between their hydrophilic groups and water molecules [68]. The molecular weight of copolymer CMS-221 is 4,000 g/mol; the molecular weight of DBE-224 is 10,000 g/mol. The molecular structure of these copolymers is shown in Figure 2-1.

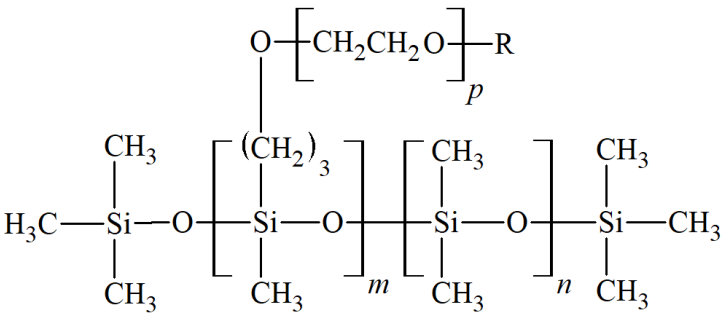

Figure 2-1. *The molecular structure of the PEG-PDMS copolymers, where R is equal to hydroxyl (-OH) group for CMS-221 and methoxy (-OMe) group for DBE-224.*

The curing agent was added to the base at a standard ratio (10%) and stirred thoroughly in a clean beaker for 30 min. During the mixing, we blended various percentages (1, 2.5, 5, 7.5, and 10 wt. %) of each copolymer into the PDMS precursor of the respective samples. To adjust mixture viscosity, we added 40−60 wt.% of chloroform (Sigma-Aldrich) as a solvent to obtain the same film thickness for all samples. The viscosities of the coatings were in the range of 200-300 mPa.s, obtained by a Brookfield viscometer (Brookfield Engineering Laboratories, USA). After 10 min of stirring, each mixture was degassed 10–15 min using a vacuum to remove air bubbles. Prior to applying coatings, we polished the aluminum substrates using P320, P800, and P1200 SiC papers to obtain smoother surfaces and better coating adhesion. The polishing was followed by ultrasonic cleaning with ethanol.

We applied the prepared mixtures, and a reference mixture lacking the copolymer, onto the treated substrates using a spin-coater run at 1500 rpm for 1 min. The coated samples were placed in an oven at 90 °C for 24 h to fully cure the coatings. We labeled the samples on the basis of the type and content of copolymer; for example, sample 221-5% contained copolymer CMS-221 at 5 wt.%. Coating thickness averaged

approximately 20 ± 1µm as measured using a micrometer. Samples 224-7.5% and 224-10% required 72 h for curing to minimize the tackiness of these samples.

2.3.2 Surface characterization

The contact angle measurement was carried out using a Kruss™ DSA100 goniometer (Krüss GmbH, Germany) at 25 ± 0.5 °C. We placed a 4 µL water droplet on the samples and measured the contact angle over time. We used a scanning electron microscope (JSM-6480 LV SEM, JEOL Japan) to observe the morphology of the coating. The acceleration voltage used in SEM imaging was 20 kV. Surface roughness of the samples was evaluated using a MultiMode-8 AFM (Bruker, USA) with scanning in the ScanAsyst mode using PeakForce Tapping. We scanned the surfaces over 10 µm × 10 µm and 500 nm × 500 nm areas. The larger scanning area provided the general information and representation of the surfaces (global topography, defects, and contamination), whereas the 500 nm × 500 nm images focused on details of the coating (porosity, structure, etc.). It should be noted that the 500 nm × 500 nm images were obtained from five different areas across the sample to ensure greater representativeness of the obtained measurements.

2.3.3 Icephobic properties

We ran differential scanning calorimetry (DSC) using a DSC Q200 (TA Instruments, USA) to investigate the effect of the coating on ice nucleation. For each sample, we placed a 5 mg deionized water droplet into a Tzero aluminum pan, each pan covered by a very thin layer of a coating. We then sealed the pan with a lid. The

measuring process involved the cooling of the prepared samples, from 30 to −40 °C at a 5 K/min rate.

Freezing delay times were measured using a Kruss machine equipped with a cold chamber and a Peltier stage able to cool to −20 °C. For each sample, the measurement was repeated three time to ensure their accuracy. Humidity within the cold chamber can be varied; however, we used anhydrous calcium sulfate desiccants to minimize the effect of condensation on the measurements.

We used push-off and centrifugal tests to measure the ice adhesion strength of the samples at −10 °C (Figure 2-2). In the push-off test, deionized water was poured into a 1-cm diameter cylindrical column placed on the sample. This sample was kept in a cold chamber at −10.0 ± 0.2 °C overnight to obtain an ice cylinder.

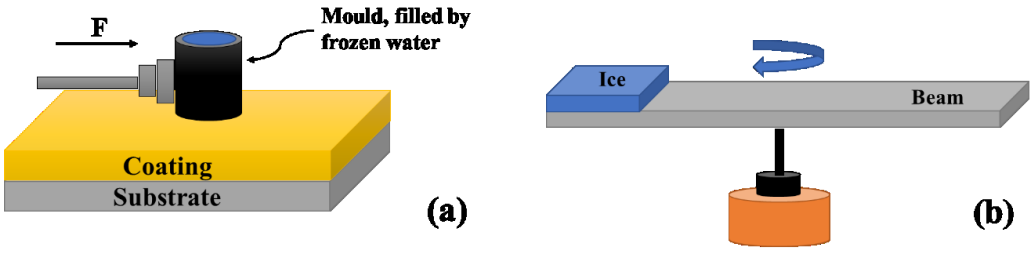

Figure 2-2. *Schematic of (a) the push-off test and (b) the centrifugal test.*

We used a push-off test apparatus (Figure 2-2a). We placed the sample on the holder and then used vacuuming to fix the sample onto the holder. The probe of the force meter approached the cylindrical column at 0.05 mm·s^{-1} and applied force until the frozen cylinder detached from the sample surface. We obtained the ice adhesion

strength by dividing the maximum measured force at ice detachment by the cross-sectional area of the ice–surface interface. We replicated the same process for each of the samples for three times. We evaluated the durability of the surfaces when subjected to multiple icing/de-icing cycles by repeating the push-off test seven times with the same procedure.

Unlike the push-off test, in which we used non-impact bulk ice, the centrifugal test involved glaze ice deposited by spraying supercooled water microdroplets onto the surfaces at −10 °C to produce an ice layer averaging 7 ± 1 mm thick. We bonded the sample to a beam and placed the beam on the centrifuge apparatus (Figure 2-2b). The ice adhesion force represents the centrifugal force required to detach the deposited ice, calculated using Eq. 2-1.

$$F = mr\omega^2, \qquad \text{Eq. 2-1}$$

where m, r, and ω are the detached ice mass, the beam radius at the center of ice mass, and angular velocity at which detachment occurs, respectively. Ice adhesion shear stress was obtained by dividing the centrifugal force by the iced area at acceleration rate of 300 rpm/sec. The test was repeated three times for each coating.

2.3.4 Mechanical properties

To evaluate sample hardness, we prepared free films of samples, 6.0 ± 0.1 mm thick. A Max-Hand 2000 Shore A durometer (Rex Gauge, USA) was used to measure sample hardness. For each sample, we measured hardness at seven points on the film at −10 °C using a similar load at each point. Furthermore, the adhesion strength of the

coatings to the Al substrate was evaluated based on ASTM D3359 method B (2022). In this test method, the coating adhesion was rated based on evaluating grid area for removal of the coating by a special cutter. The adhesion of the coatings to the substrate was rated based on the scale provided in the standards that ranges from 0B for the poorest and 5B for the best. The measurement was repeated on 3 different points of each sample at −10 °C.

2.4 Results and discussion

2.4.1 Surface characterization

2.4.1.1 wettability

The near-surface concentration of an embedded copolymer plays a key role in determining the structure of interfacial water. Thus, the percentage of copolymer in coatings will affect surface wettability, evidenced by a change in water contact angle over time. We observed that increasing the PEG-PDMS copolymer percentage generally decreased the water contact angle (Figure 2-3). For samples containing copolymer CMS-221 in particular, increased copolymer concentrations enhanced the hydrophilicity of the surface owing to the formation of more hydrogen bonds between water molecules and the hydrophilic groups of the coatings. We also observed that increased copolymer content in the coating caused the contact angle to decrease at a faster rate, especially for samples containing 7.5% and 10% copolymer. For these latter samples, the contact angle drops markedly within the first 30 seconds. As well, the water droplets on the 7.5% and 10% CMS-221 copolymer samples spread more widely with changes in copolymer content. For instance, the contact angles of the samples

containing 7.5% and 10% begin (t = 0 s) at approximately 105° and reach approximately 61° and 54.2° at t = 330 s, respectively. This change relates to both the enhanced hydrophilicity of surfaces as copolymer content increased and the miscibility of copolymer CMS-221 in PDMS.

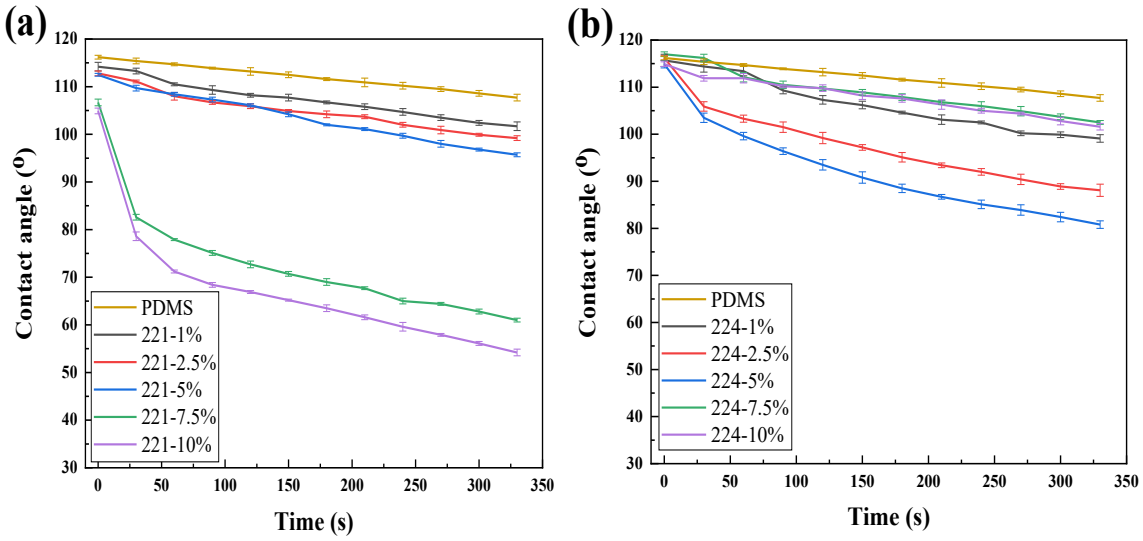

Figure 2-3. *Water contact angle of samples containing copolymer (a) CMS-221 and (b) DBE-224 over time.*

Samples containing 1%, 2.5%, and 5% copolymer DBE-224 displayed a similar trend as the copolymer CMS-221 samples; an increasing copolymer content produced lower contact angles. In contrast to the copolymer CMS-221, however, copolymer DBE-224 samples having a copolymer concentration above 5% exhibited a lower rate of decrease in contact angle. Among the copolymer DBE-224 samples, the 5% copolymer sample

displayed the greatest decrease in contact angle over 330 s, and, therefore, the maximum water droplet spreading over the surface of the prepared samples.

SEM imagery provided insight into the surface topography of the samples (Figure 2-4). The presence of some staining in the SEM image, obtained from the surface of sample 224-10% (Figure 2-4e), confirmed that miscibility between the DBE-224 copolymer and the PDMS matrix was reduced by an increase in the percentage of copolymer. There also appeared to be less compatibility between copolymer DBE-224 and PDMS relative to that between copolymer CMS-221 and PDMS. Indeed, both copolymers contain the same main polymeric chain, although they differ in terms of the functional groups that they hold: hydroxyl (-OH) groups for CMS-221 and methoxy (-OMe) groups for DBE-224. The presence of different functional groups causes the copolymers to differ in their molecular structures. This structural difference may be the main factor responsible for phase separation between the PDMS and copolymer DBE-224; the sample surfaces shift from homogeneous to heterogenous surfaces by increasing the copolymer percentage. Therefore, immiscibility and phase separation produce a heterogenous surface area. For such a surface, the Cassie Eq. 2-2 can be used to evaluate the apparent contact angle.

$$\cos\theta_C = x_1.\cos\theta_1 + x_2.\cos\theta_2, \qquad \text{Eq. 2-2}$$

where x_1 and x_2 are the ratios of the contact area of each component to total projected area, and θ_1 and θ_2 are the Young contact angles related to each chemistry [233]. As observed in Figure 2-3, for heterogenous surfaces, such as sample 224-10%, the apparent contact angles approach that of the reference (PDMS). From equation (2-

2), the apparent contact angle of such surfaces is most similar to the contact angle of the component having the higher contact ratio (x_1 or x_2). In our samples, this component is the main matrix, PDMS.

2.4.2 Surface morphology and surface topography

We observed no evidence of immiscibility in samples containing the CMS-221 copolymer (Figure 2-4g and Figure 2-4i); however, topographical images and corresponding roughness parameters (Figure 2-4h, Figure 2-4j, and Table 2-1) confirm that adding either copolymer into the elastomeric matrix alters the surface topography and roughness parameters relative to those of the reference. As most polymer blends are immiscible, it should be rare for the polymers to mix at a molecular scale [234]. The immiscibility of copolymers and PDMS matrix in our samples appears as phase separation at the molecular scale and, consequently, increases roughness. For samples containing DBE-224 copolymer, however, this phenomenon is detectable at a larger scale; samples containing the DBE-224 copolymer exhibited a saturation of copolymer content in the mixture at lower concentrations than the CMS-221 copolymer samples. Therefore, for sample 224-10%, surface roughness parameters could not be obtained within a 5 μm × 5 μm area owing to the great height of the asperities. As noted above, the curing of this sample required more time than the other samples, thereby affecting and intensifying phase separation.

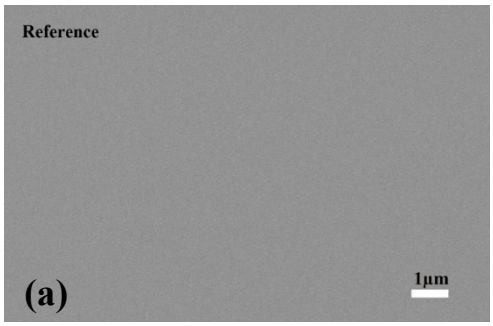
Reference
1μm
(a)

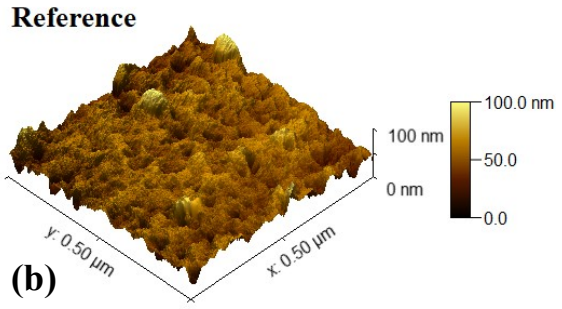
Reference
100.0 nm
50.0
0.0
100 nm
0 nm
y: 0.50 μm
x: 0.50 μm
(b)

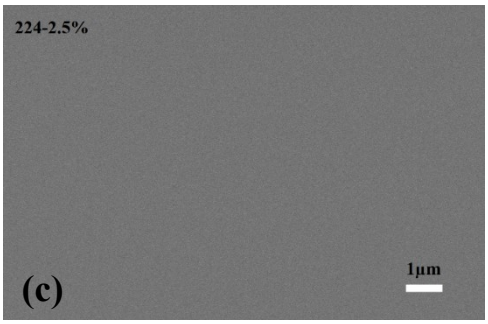
224-2.5%
1μm
(c)

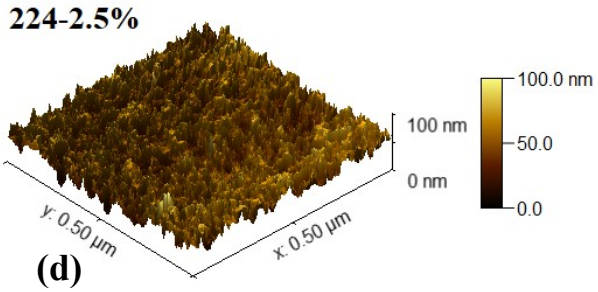
224-2.5%
100.0 nm
50.0
0.0
100 nm
0 nm
y: 0.50 μm
x: 0.50 μm
(d)

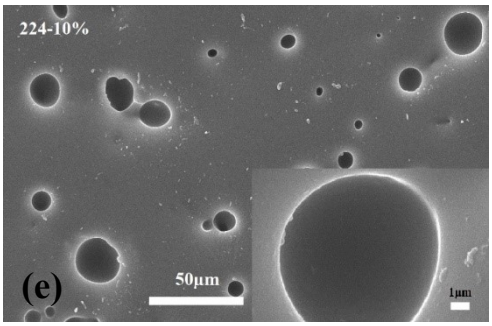
224-10%
50μm
1μm
(e)

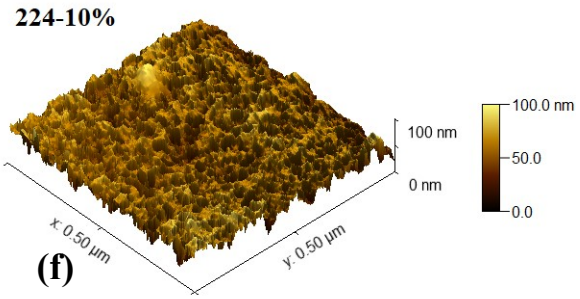
224-10%
100.0 nm
50.0
0.0
100 nm
0 nm
x: 0.50 μm
y: 0.50 μm
(f)

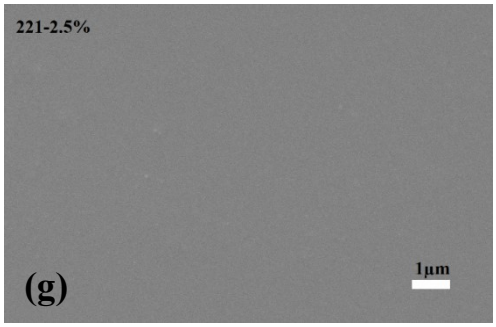
221-2.5%
1μm
(g)

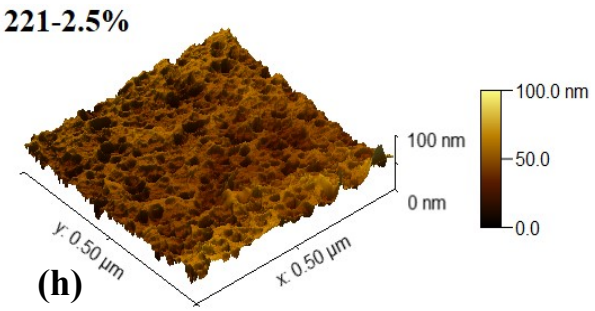
221-2.5%
100.0 nm
50.0
0.0
100 nm
0 nm
y: 0.50 μm
x: 0.50 μm
(h)

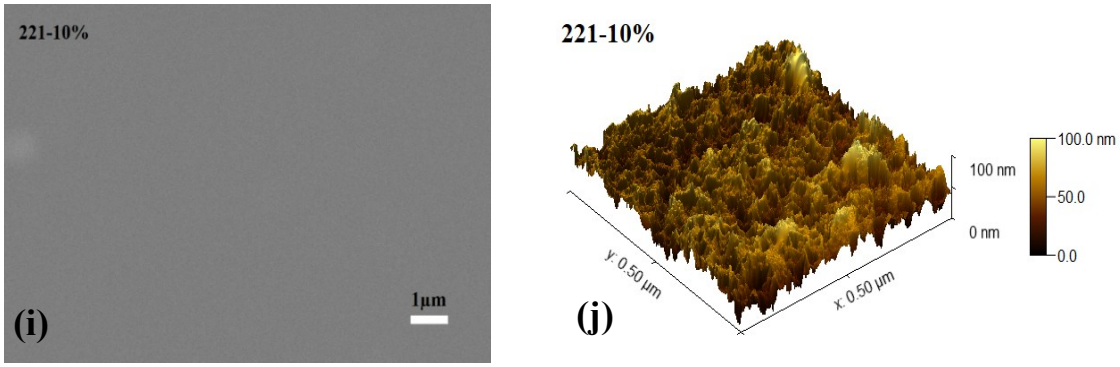

Figure 2-4. *The micrographs of (a) reference (PDMS), (c) 224-2.5%, (e) 224-10%, (g) 221-2.5%, and (i) 221-10% along with their corresponding surface topography ((b), (d), (f), (h), and (j), respectively), obtained by AFM.*

Table 2-1*. Surface roughness parameters of the fabricated surfaces.*

Roughness parameters	**Reference**	**221-2.5%**	**221-10%**	**224-2.5%**	**224-10%**
RMS roughness (S_q) (nm)	6.81 ± 0.81	9.45 ± 2.08	14.87 ± 2.96	18.2 ± 1.13	7.76 ± 1.4

2.4.3 Icephobic characteristics

Differential scanning calorimetry served to measure the delay in ice nucleation on the surface of samples in contact with the water droplet (Figure 2-5). We observed that, in general, adding PEG-PDMS copolymers to PDMS reduced the ice nucleation temperature.

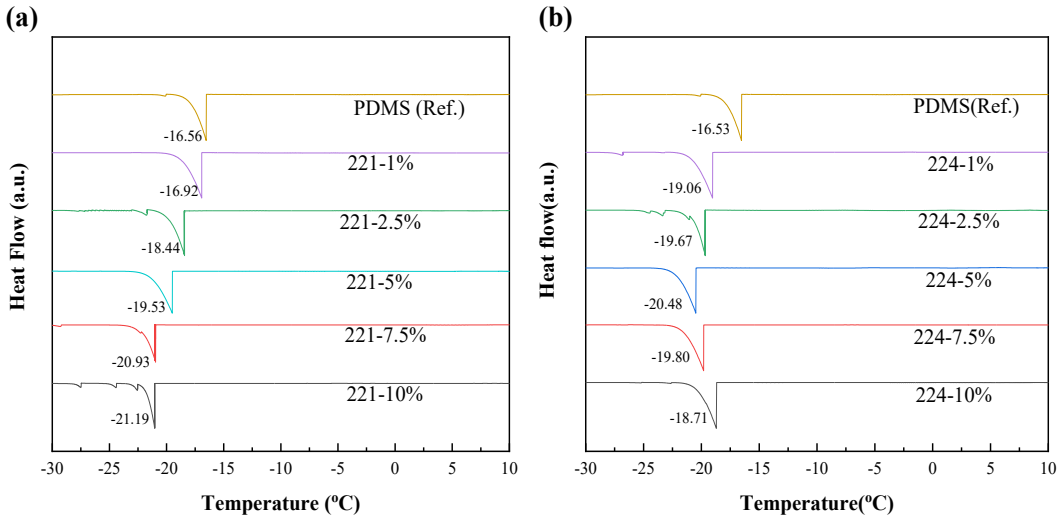

Figure 2-5. *Delayed ice nucleation on the surface of samples containing copolymer (a) CMS-221 and (b) DBE-224, as evaluated by differential scanning calorimetry (DSC).*

Hydrogen bonds between the surface and water molecules are promoted owing to the presence of the hydrophilic groups in the coatings; their presence forms the quasi-liquid-like layer at the ice–surface interface, and the creation of such a layer delays ice nucleation. This phenomenon can be explained using Eq. 2-3, in which the ice nucleation rate J is described as:

$$J \propto \frac{K_B T}{h} exp\left(-\frac{\Delta G_f^*}{k_B T} - \frac{\Delta g_{act}}{k_B T}\right), \qquad \text{Eq. 2-3}$$

In this equation, Δg_{act}, ΔG_f^*, and T are the activation energy barrier, the Gibbs free energy, and temperature, respectively. K_B (Boltzmann constant) and h (Planck's constant) are the constants. Δg_{act} is a critical factor linked to the transfer of water molecules across the ice–water interface. In the other words, Δg_{act} is an energy barrier associated with the self-diffusion of water molecules to add up to an ice embryo. The formation of hydrogen bonds between water molecules and hydrophilic groups

increases viscosity; this change decreases the mobility of water molecules at the interface. The hydrogen bonds increase Δg_{act} and consequently, decrease the ice nucleation rate, *J*. The formed QLL thus has a higher viscosity at lower temperatures, which slows the transformation of water molecules from a liquid to solid phase [49].

Figure 2-6 presents the ice nucleation and complete freezing times for all samples as well as the form of frozen droplet. The ice nucleation rate *J* is inversely proportional to the freezing-delay time. Accordingly, we would expect that our results in Figure 2-6 agree with those obtained using DSC measurements. We observed a clear prolonging of the freezing-delay time (Figure 2-6) when PEG-PDMS copolymers were added to PDMS. For samples containing copolymer CMS-221, adding more copolymer to the matrix increased the freezing time, whereas freezing time for samples containing copolymer DBE-224 peaked at 5%, followed by a reduced freezing time.

Furthermore, the ice nucleation time for samples containing copolymer CMS-221 increased with greater copolymer content; however, the difference between complete freezing and ice nucleation ($\Delta t_{nucleation \rightarrow freezing}$) did not follow the same trend. The $\Delta t_{nucleation \rightarrow freezing}$ values corresponding to 221-1%, 221-2.5%, 221-5%, 221-7.5%, and 221-10% were 7.9 ± 0.1 s, 8.2 ± 0.2 s, 10.8 ± 0.4 s, 9.3 ± 0.3 s, and 7.3 ± 0.2 s, respectively (Figure 2-6). From Figure 2-3, for samples containing copolymer CMS-221, those having a higher copolymer content produced larger water contact angles after 330 s, increasing the contact area. This was particularly the case for copolymer at percentages ≥7.5%. According to Fourier's law (Eq. 2-4), the heat flow rate (*q*) is proportional to the interfacial area between water droplet and the coating (*A* in Equation 3).

$$\frac{q}{dt} = -KA\frac{dT}{dx} \ , \qquad \text{Eq. 2-4}$$

It is obvious, therefore, that samples having a larger contact area with the water droplet possess a higher heat flow rate and, consequently, samples 221-7.5% and 221-10% experienced lower $\Delta t_{nucleation \rightarrow freezing}$ values than the other samples containing the same copolymer. For samples containing copolymer DBE-224, $\Delta t_{nucleation \rightarrow freezing}$ values for 224-1%, 224-2.5%, 224-5%, 224-7.5%, and 224-10% were 10.5 ± 0.3s, 11.4 ± 0.4s, 12.2 ± 0.2 s, 8.8 ± 0.6 s, and 12.8 ± 0.5 s, respectively. Unlike samples containing copolymer CMS-221, the $\Delta t_{nucleation \rightarrow freezing}$ values of the DBE-224 samples presented no clear trend.

The presence of the quasi-liquid-like layer delays ice nucleation and reduces ice adhesion strength between ice and coatings. The liquid-like layer decreases the effective contact area between the two surfaces and, therefore, lowers ice adhesion strength [235]. To evaluate this characteristic, we applied two different methods, namely the push-off adhesion and the centrifugal adhesion tests. We selected both methods after assessing the difference in the types of ice normally used to study ice adhesion. Although using glaze ice in the centrifugal test can produce harsher icing conditions than those of the push-off test, which uses non-impact bulk ice, all plots followed, to a large extent, the same trends (Figure 2-7). Adding PEG-PDMS copolymers into PDMS decreased ice adhesion and, therefore, produced self-lubricating properties [68]. The presence of PEG-PDMS in such a coating forms strong hydrogen bonds with water molecules. These hydrogen-bonded water molecules

remain unfrozen at subzero temperatures, thereby reducing the adhesion strength between the ice and the coating's surface.

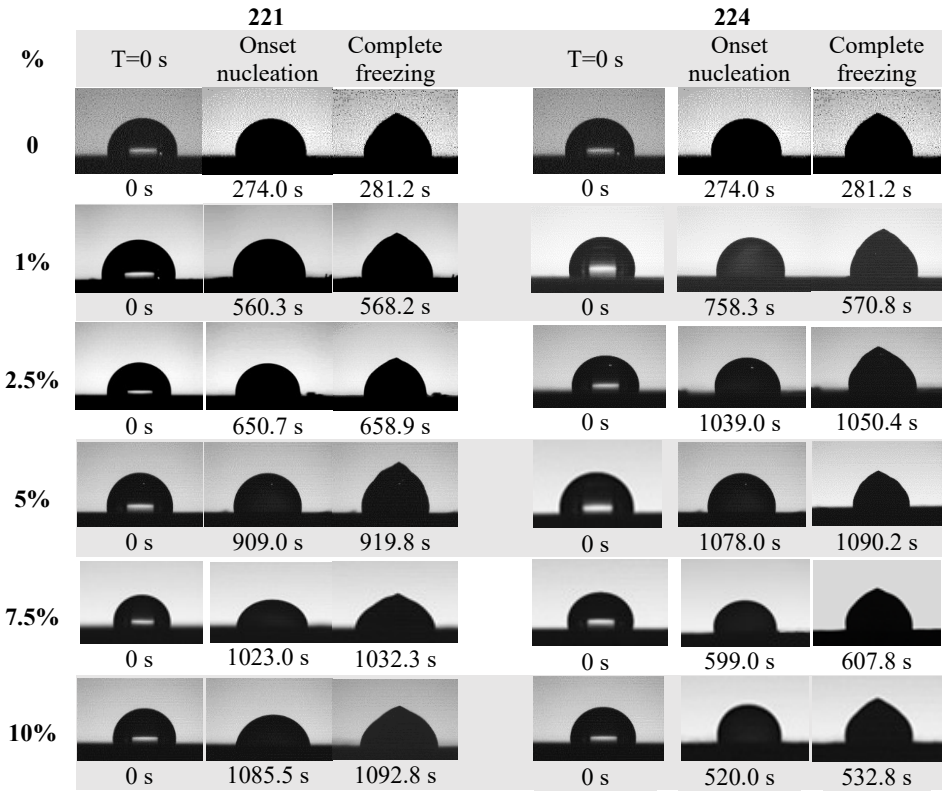

Figure 2-6. *Ice nucleation time on the surface of the copolymer samples*

For samples containing copolymer CMS-221, increasing the copolymer content reduced ice adhesion from 90.3 to 39.1 kPa and 134 to 99.5 kPa in push-off and centrifugal tests, respectively (see Figure 2-7). Ice adhesion strengths of samples containing copolymer DBE-224, however, decreased until the 5% (from 62.1 to 53.2 kPa) and 2.5% (from 124.5 to 85.5 kPa) copolymer samples in the push-off and centrifugal tests, respectively; at greater concentrations of DBE-224, we observed an increasing trend in ice adhesion strength. We note that the rate of reduction of ice

adhesion strength for the push-off test, from 1% to 5% copolymer, was greater than that observed for copolymer DBE-224, very likely due to low molecular weight and a low non-siloxane structure. Furthermore, a lower ice adhesion was obtained using copolymer DBE-224 at these concentrations.

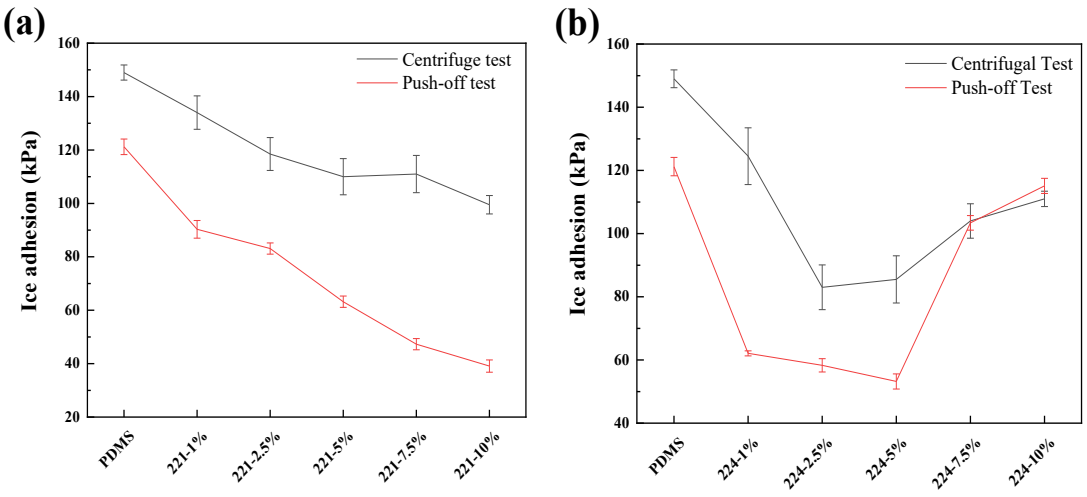

Figure 2-7. *Ice adhesion strength of samples containing copolymer (a) CMS-221 and (b) DBE-224, obtained using push-off and centrifuge tests.*

For samples containing DBE-224, the sudden rise in ice adhesion strength relates to the immiscibility of the copolymer and the matrix, which enhances the probability of mechanical interlocking between the ice and surface. The presence of the PEG-PDMS copolymer can promote the formation of hydrogen bonds at the ice–surface interface, but it cannot ensure lower ice adhesion strength. The immiscibility between copolymer and matrix causes phase separation, resulting in increased surface roughness and, therefore, heightened ice adhesion strength.

2.4.4 Durability

We combined use of seven icing/de-icing cycles and the push-off test to assess coating durability. Adding copolymer CMS-221 to PDMS reduced ice adhesion strength (Figure 2-8), and values for ice adhesion strength of samples containing 1%, 2.5%, and 5% copolymer CMS-221 did not vary considerably over the seven cycles (Figure 2-8a). Although samples with 7.5% and 10% copolymer CMS-221 presented the lowest ice adhesion strengths, these samples experienced a relatively lower durability. This reduced durability may reflect the poorer mechanical properties of the samples as copolymer content increases.

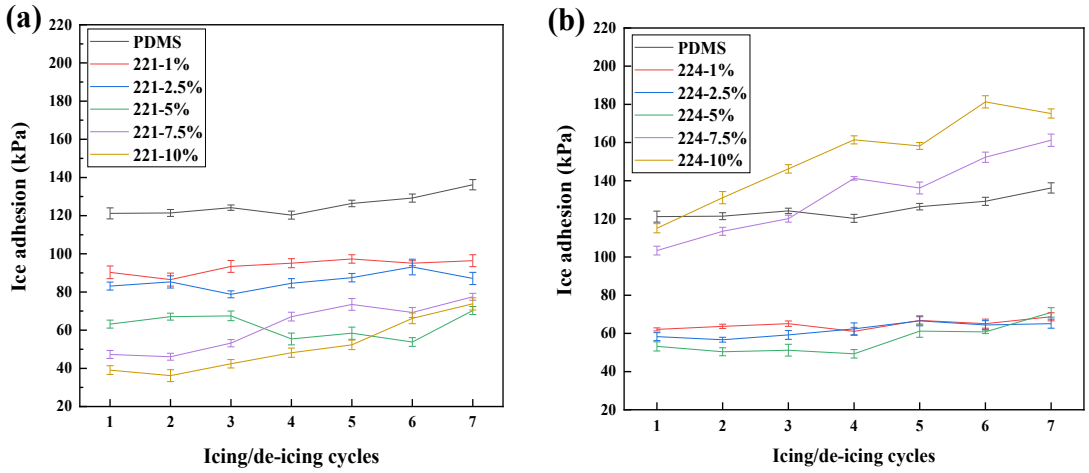

Figure 2-8. *Ice adhesion strength in samples containing (a) CMS-221 and (b) DBE-224 over seven icing/de-icing cycles. Ice adhesion strength was determined using a push-off test.*

2.4.5 Mechanical characterization

As a measure of resistance against local surface deformation, hardness provides a quick observation of the probable effect of copolymer content in the PDMS matrix on mechanical properties [236]. Hardness values of samples containing copolymer CMS-221 decreased from approximately 62.5 to 44.4 Shore A (Figure 2-9), whereas the hardness of the sample containing 10% copolymer DBE-224 was approximately half that of samples containing only 1% copolymer DBE-224. Indeed, the decrease in hardness values as copolymer DBE-224 content increased was more marked than when the content of copolymer CMS-221 was increased. Although differences between the mechanical properties of ice and the surface can favor a lowering of ice adhesion strength, an excessive reduction in hardness can lead to mechanical failure and, therefore, a reduced durability of the surface. It is noteworthy that since the coatings just physically adhered to the Al substrates, so generally, the coating adhesion strength for all samples were relatively low. Moreover, the evaluation of coating adhesion to the Al substrate for samples containing copolymer CMS-221 showed the same levels, except sample 221-10% (Table 2-2); while for samples containing copolymer DBE-224, there was a decrease in coating adhesion to the substrate from the sample with 5% copolymer content and more.

For samples containing copolymer DBE-224, we observed generally lower ice adhesion strength than the reference coating. Ice adhesion strengths for samples having 1%, 2.5%, and 5% copolymer DBE-224 differed minimally. Ice adhesion values for these samples were less than 72 kPa over seven icing/de-icing cycles (Figure 2-8b). Samples containing 7.5% and 10% copolymer DBE-224, on the other hand, were not

durable, and their ice adhesion strengths increased from about 103 and 115 kPa to around 161 and 175 kPa, respectively. The phase separation between PDMS and copolymer DBE-224 intensifies as copolymer content in the PDMS matrix increases, leading to the poorer mechanical properties of these coatings.

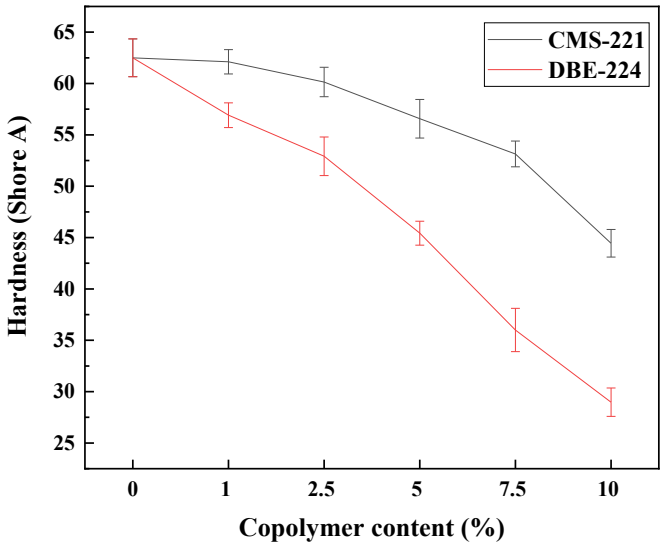

Figure 2-9. *Hardness values of the fabricated samples in relation to copolymer type and content, measured at −10 °C.*

Table 2-2. *Evaluation of coating adhesion to the Al substrate at −10 °C.*

Sample	**Reference**	**221-1%**	**221-2.5%**	**221-5%**	**221-7.5%**	**221-10%**	**224-1%**	**224-2.5%**	**224-5%**	**224-7.5%**	**224-10%**
Coating adhesion	3B	3B	3B	3B	3B	2B	3B	3B	2B	2B	2B

2.5 Conclusion

We fabricated aqueous self-lubricating coatings by blending separately two types of PEG-PDMS copolymer into a PDMS matrix and evaluated how copolymer content affected wettability and icephobic characteristics of the coatings. Increasing the PEG-PDMS copolymer content tended to decrease contact angle and, therefore, enhanced surface wettability. Both the functional group type of the copolymer and the copolymer content in the matrix affected surface wettability. Samples containing copolymer DBE-224 experienced greater phase separation with an increase in copolymer amounts. Nonetheless, altering copolymer percentage also produced positive effects on the icephobic characteristics of the fabricated coatings. Increased PEG-PDMS content enhanced the hydrogen-bond formation between the coatings and water molecules and modified the liquid-like layer. Water molecules therefore must pass through a more viscous barrier layer and add to ice embryos developing on the surface; therefore, freezing-delay times are lengthened. The miscibility of the copolymer in the elastomer matrix affects the freezing-delay time; as copolymer content increased, samples containing copolymer CMS-221 experienced a greater freezing-delay time than samples containing copolymer DBE-224.

We used push-off and centrifugal tests to evaluate the effect of PEG-PDMS content on ice adhesion strength. In general, increased copolymer content reduced ice adhesion strength; however, samples containing DBE-224 presented this trend only at lower copolymer contents. Excessive copolymer in the coating saturates the coating with copolymer and increases surface roughness. Ice adhesion strength therefore increased owing to a probable mechanical interlocking effect. Nonetheless, an increase

in copolymer content can, to an extent, increase wettability and the icephobic characteristics of the coating. When considering coating durability and coating mechanical properties, an optimized copolymer content of around 5% is ideal for achieving an appropriate aqueous self-lubricating coating.

Acknowledgments

The authors acknowledge all support from the Natural Sciences and Engineering Research Council of Canada (NSERC), Hydro-Québec, and PRIMA Quebec. The authors would like to thank Caroline Blackburn at the Anti-icing Materials International Laboratory (AMIL), UQAC, for helping to carry out the centrifuge test. The authors would also like to thank Caroline Potvin at the département des sciences fondamentales, UQAC, for helping to perform DSC test.

Chapter 3: An intelligent icephobic coating based on encapsulated phase change materials (PCM)

Mohammadreza Shamshiri[1,*], Reza Jafari[1], and Gelareh Momen[1]

[1] Department of Applied Sciences, University of Quebec in Chicoutimi (UQAC), 555, boul. de l'Université, Chicoutimi, Quebec, G7H 2B1, Canada

*Corresponding author: mohammadreza.shamshiri1@uqac.ca.

3.1 Abstract

The phase change materials (PCMs) have attracted great interest for applications as smart icephobic coatings because of their capability to restore and release energy. PCMs release a large amount of energy in the form of latent heat upon freezing, which is a stimuli-response behavior for anti-icing applications. Such materials embedded within coatings can be applied to exposed infrastructures to protect them against icing. Here, we encapsulated a mixture of PCMs in a urea–formaldehyde (UF) shell by in situ polymerization and then incorporated the microcapsules into a polydimethylsiloxane (PDMS) coating. Microcapsules 5 to 15 μm in diameter having a shell thickness of about 200 nm were fabricated. Investigating the chemical composition of the fabricated microcapsules confirmed that PCM material was successfully encapsulated within the UF shell. Moreover, the differential scanning calorimetry (DSC) analysis showed that the PCM preserved its phase-change characteristics when encapsulated and embedded within the matrix. Increasing the

abundance of microcapsules within the coating lowered the ice nucleation temperature, verified by DSC, and increased the freezing-delay time because of PCM latent heat release. We utilized a custom-made apparatus, called micro-push-off set-up that allowed us to measure ice adhesion at the exact moment that the water droplet was completely frozen. Therefore, it was observed that the presence of the PCM microcapsules reduced ice adhesion strength, through either possible mechanism of the formation of quasi-liquid layer (QLL) or thermal expansion differences. Furthermore, lower ice adhesion resulted in reduced ice accumulation on the PCM-containing coatings, verified by the static accumulation test (SAT).

Keywords: Icephobicity, phase change materials (PCMs), latent heat, smart coatings, ice adhesion, ice accumulation

3.2 Introduction

Smart (intelligent) coatings exhibit great potential in high-tech applications because of their stimuli-response behavior. These coatings can sense their surrounding environment and respond to environmental changes in a predictable manner. Smart coatings can be stimulated by changes in pressure, temperature, light, among other stimuli. When the stimulus is removed, a smart coating ideally returns to its original state [19–21].

Therefore, from the above-mentioned definition, an intelligent icephobic coating senses environmental stimuli (or a stimulus) and responds in a manner to reduce ice accumulation or delay ice formation [21]. A smart icephobic coating should therefore meet the following criteria: (1) interactions between the surface and water

droplets should be reduced, limiting water accumulation on the surface; (2) the surface must inhibit or delay ice nucleation; and (3) the icephobic coating should weaken ice–surface bonds [1,39,49,50,237,238].

Smart icephobic coatings have been classified in regard to the type of stimuli, including thermoresponsive coatings [124], self-healing icephobic coatings [140,144], self-lubricating coatings [149,160,165,239], and PCM-impregnated coatings [211,214].

Phase change materials (PCMs) have a great ability for storing and releasing heat during a phase change [202], making these materials potential candidates for applications including construction and buildings [192], solar energy storage [196], spacecraft [193], textiles [194], medical treatments [195], and anti-icing surfaces. Wang et al. [240] used the concept of phase transition property of lubricants to fabricate an anti-icing surface by infusing peanut oil in porous PDMS matrix. The solidification of the oil before water freezing stabilized it in porous structure, resulting in enhanced icephobic characteristics. Latent heat release is the most important property of PCMs to affect ice nucleation and ice adhesion. For these materials, a change in temperature and then phase can be considered as the stimulus; latent heat release is the response [21,22,241]. Chatterjee *et al.* [242] infused phase-switching liquids within textured surfaces that illustrated a longer freezing delay as a result of the released latent heat. Moreover, solidification of the lubricant can change the surface morphology, resulting in surface miscibility on water. They also [243] designed PCM-based coatings in which releasing latent heat from PCM can effectively contribute in the self-lubricating mechanism of the surfaces, and therefore, their anti-icing properties.

A desirable melting temperature, high latent heat, high thermal conductivity, reproducible phase change, durable properties, and cost effectiveness are among the criteria of an acceptable PCM [197]. PCMs can be generally subcategorized into organic components (e.g., paraffin), inorganic components (e.g., salty hydrates), and eutectics (e.g., organic–organic, inorganic–inorganic) [200].

Three methods are generally used to incorporate PCMs into material matrices: direct incorporation, immersion, and encapsulation [206]. Encapsulation is the most effective because it avoids issues such as material exchange with the environment and PCM leakage. Furthermore, the PCM is enclosed within a shell to protect it from the surrounding materials [207].

The phase change temperature range is a critical factor for selecting a PCM in icephobic applications because it must match that of the application temperature range. Moreover, the shell material must be selected carefully. The procedure parameters of the encapsulation, such as agitation speed and process temperature, can affect microcapsule size and their size distribution [22]. Smaller capsules improve heat transfer performance because of their higher surface-area-to-volume ratio [209]. Moreover, the larger capsules have lower thermal reliability and chemical stability [22,210].

The core-to-shell ratio also affects the thermal and mechanical performance of the encapsulated PCMs. A lower core-to-shell ratio increases shell thickness, weakening the heat transfer between the PCM and its surrounding environment, whereas a higher ratio would heighten the possibility of PCM leakage [22]. The

compatibility of the material shell with the binder must also be considered, as this can affect the heat transfer between components [208].

Bhamidipati [244] incorporated silicone PCMs within hydrophobic silicone-based resins and detailed a three-step mechanism for the functioning of the produced icephobic coatings. First, cooling below 0 °C contracts the base. Then, the freezing of supercooled water on the surface causes part of the water's latent energy to be transferred to the uppermost PCMs on the surface. This energy transfer caused these PCMs to expand. Finally, the contraction of the base matrix and, at the same time, expansion of the near-surface PCMs produces strong localized shearing at the ice–coating interface, which causes bonds between the ice and surface to break.

Goitandia et al. [245] mixed encapsulated PCMs, such as hexadecane and octadecane, within an inorganic shell by combining a sol-gel process and emulsion techniques. As the temperature decreased, PCMs underwent crystallization and released latent heat. This heat maintained the temperature within the PCM phase-changing temperature range and delayed ice formation. Zhu et al. [215] fabricated icephobic coatings by incorporating encapsulated PCMs within room-temperature vulcanized (RTV) silicone rubber coating and fluorosilicone (FS) copolymers. The copolymers protect the microcapsules against breaking and prevent the leakage of PCM. The latent heat release from the encapsulated PCMs extended the icing delay time of deionized water droplets on the surface, and a greater amount of PCMs prolonged the freezing process.

Most of the previous studies of using potential of PCMs for icephobic applications focused on directly impregnating these materials into a matrix, but the study on encapsulated PCMs before embedding them is limited. As mentioned before, encapsulation not only can prevent PCM leakage, but also it promotes the possibility of using these materials in a various range of material matrices. Furthermore, the icephobic performance of the fabricated coatings must be assessed from different aspects, such as ice nucleation temperatures, freezing times, and ice accumulation that is rear in the existing research works. So, herein, we encapsulated a mixture of PCMs by in situ polymerization and embedded the fabricated microcapsules within a silicone elastomer. We characterized the fabricated PCM microcapsules using scanning electron microscopy (SEM) and Fourier-transform infrared spectroscopy (FTIR). Then, we fabricated a series of coatings of varying PCM microcapsule content and applied the prepared coatings to aluminum substrates using a film applicator. The wettability and roughness of the samples were then assessed. The latent heat-releasing capability of the encapsulated PCM, embedded within the coating, was assessed using differential scanning calorimetry (DSC). We then evaluated the effect of PCM microcapsule abundance (%) in the coating matrix on ice nucleation temperature and freezing-delay time. Surfaces were compared in terms of surface ice accumulation and surface temperature changes using a static accumulation test (SAT) and IR camera, respectively. Finally, the ice adhesion strength of the samples was determined using a specially designed apparatus, and we evaluated the effect of ice adhesion on ice accumulation.

3.3 Experimental protocols

3.3.1 Materials

We purchased n-dodecane, n-tetradecane, n-hexatriacontane, urea, resorcinol, and ammonium chloride from Alfa Aesar (USA). Ethylene maleic anhydride (EMA) was purchased from Sigma-Aldrich. Sylgard 184 silicone elastomer (Polydimethylsiloxane (PDMS)), serving as a base and a curing agent, was received from Dow Corning.

3.3.2 Encapsulation of PCM

The PCM was encapsulated using in situ polymerization in an emulsion medium. A mixture of n-dodecane and n-tetradecane (ratio of 3:7) was prepared to obtain a PCM mixture having a melting point at 0 °C. It is noteworthy that the phase change temperatures corresponding to n-dodecane and n-tetradecane are about -9 and 6 °C, respectively. Therefore, it was expected that the combination of these PCMs could have a great potential for icephobic applications. We added 3 wt.% n-hexatriacontane to the mixture as an anti-supercooling agent [215], and the mixture was sonicated for 1 min. It is noteworthy that in liquid-to-solid phase transformation, the liquid supercooling degree, $\Delta T_s = T_{m,o} - T_{f,o}$, is defined as the difference between onset temperature on the heating (endothermic) curve, $T_{m,o}$, and onset temperature on the freezing (exothermic) curve, $T_{f,o}$ [23,49,199]. Reducing the size of microcapsules below 100 μm can result in increased supercooling degree [23,199]. Therefore, the solidification temperature of PCM mixture would exceed the glaze ice temperature

range (between 0 and -10 ˚C) [246]. Accordingly, we added n-hexatriacontane which acted as nucleating agent to decrease supercooling degree of PCM mixture.

The encapsulation process is adapted from the procedure presented by Brown et al. [247]. Figure 3-1 illustrates the formation reaction of Poly (urea-formaldehyde) scheme. We dissolved 1.25 g of EMA copolymer in 250 mL deionized water at 25 °C. the copolymer acted as an emulsifier to to form an oil-in-water emulsion. Then, 5 g urea, and 0.5 g resorcinol (as shell forming components), as well as 0.5 g ammonium chloride (as a catalyst), were added to the EMA aqueous solution, and the pH of the solution was adjusted to 3.5 using an aqueous solution of sodium hydroxide. The sonicated PCM mixture was added to the solution and homogenized using a Fisher homogenizer. The prepared mixture was then transferred into a three-necked reactor and stirred at 500 rpm (Figure 3-2a). As the system's temperature reached 60 °C, we added 12.67 g of the aqueous solution of formaldehyde to the emulsion (as another shell forming component) [247] by droplets using a variable pump. After 4 h of agitation, the microcapsule suspension was cooled to ambient temperature and then filtered to obtain the microcapsules. The microcapsules were then washed with deionized water and air-dried for 24 to 48 h. The encapsulation yield was obtained by dividing the mass of the dried product ($M_{capsules}$) by the total mass values of the encapsulation ingredients (M_{shell}+M_{core}), as presented in Eq. 3-1.

$$Encapsulation\ yield\ (\%) = \frac{M_{capsules}}{M_{shell}+M_{core}} \times 100 \qquad \text{Eq. 3-1}$$

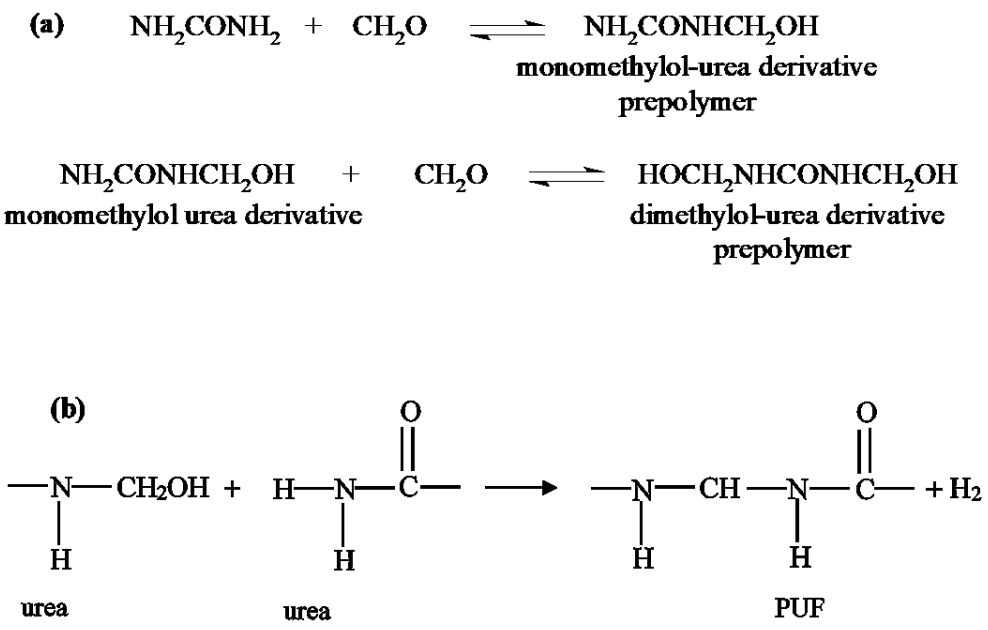

Figure 3-1. *Formation reaction of Poly (urea-formaldehyde) scheme a) addition reaction b) condensation reaction.*

3.3.3 Preparation of the elastomeric coatings

Polydimethylsiloxane (PDMS), as a member of polysiloxane family, is viscoelastic, chemically stable, non-toxic, and highly tunable for the polymeric processing. Furthermore, PDMS is a hydrophobic material due to its low surface energy, that can result in a low ice adhesion strength [248]. Besides, it can show icephobic characteristics via another mechanism, called deformation incompatibility (DI). The silicone materials have a Young's modulus lower than 10 MPa; while for ice, this value varies between 0.3 and 3.6 GPa. Under stress, this considerable difference between their modulus leads to DI, and consequently ice detachment from the surface

[248,249]. Therefore, these characteristics make PDMS a suitable candidate for fabricating the icephobic surfaces.

The curing agent was added to the base resin at a standard ratio (1:10) and mixed thoroughly in a clean beaker for 30 min. During the mixing process, different percentages (10, 20, and 30 wt.%) of PCM microcapsules, dispersed in a suitable amount of hexane, were blended into the PDMS precursor. After 10 min of stirring, each mixture was degassed using a vacuum for 10 to 15 min to remove air bubbles. Aluminum plates were prepared as substrates for the coating. They were polished using 800 and 1200 SiC papers to improve the adhesion of the coating to the substrate. The polished substrates were then cleaned ultrasonically with ethanol. The prepared mixture and reference mixture lacking microcapsules were applied to the treated substrates by a film applicator (ZEHNTNER testing instrument, Switzerland). The coated samples were placed in the oven at 90 °C for 24 h to obtain fully cured coatings. The samples were labelled according to their microcapsule content as 10-PCM, 20-PCM, and 30-PCM, i.e., sample 10-PCM contained 10 wt.% PCM microcapsules. The average coating thickness was around 100 ± 5 μm, measured via a coating thickness gauge. Furthermore, the free-film of each coating with a thickness of 1mm was prepared and broken in the liquid nitrogen to evaluate the homogeneity of dispersed microcapsules throughout the matrix.

3.3.4 Characterization

3.3.4.1 Chemical structure

The chemical composition of the fabricated microcapsules, the core, and the extracted shell material was evaluated using a FTIR spectrometer (Agilent, Cary 630, USA) in the attenuated total reflection (diamond ATR) mode within an infrared range of 400–4000 cm^{-1}. The evaluation was repeated 2 times per each sample with the resolution of 4 cm^{-1}.

3.3.4.2 Morphology and size distribution

The microcapsules' morphology, size distribution, and shell thickness were investigated using a scanning electron microscope (JSM-6480 LV SEM, JEOL Japan). The SEM images were scanned in ImageJ software to obtain the particle size distribution. The acceleration voltage used in SEM imaging was 20 kV.

3.3.4.3 Surface characterization

The water contact angle was measured using a Kruss™ DSA100 goniometer (Krüss GmbH, Germany) at 25 °C. The measurement was carried out by placing a 4 µL water droplet onto the samples. We then used a confocal laser scanning microscope (Profil3D Filmetrics, USA) to determine the surface roughness of the samples. The measurements were carried out using WLI mode, covering roughness down to 0.05 µm. PSI mode was used to measure roughness at 0.001 µm precision for the reference sample. It is worth mentioning that the surface parameters were obtained from three

different areas across the sample to ensure greater representativeness of the obtained measurements.

3.3.4.4 Icephobic properties

The effect of PCM microcapsule content on ice nucleation temperature was assessed using differential scanning calorimetry (DSC), performed using a DSC Q200 (TA Instruments). Accordingly, a precise 5 mg deionized water droplet was placed into a DSC Tzero aluminum pan, coated with a thin layer of each coating (thickness around 200-250 μm), and then sealed. The measurement began by first cooling the prepared sample from 40 to −40 °C at a 5 K/min rate. We used a similar DSC procedure, although without the placing of a water droplet, to assess the phase change capability of PCM microcapsules embedded within the elastomeric coating.

The freezing delaying time of the samples was examined at −20 °C using a Kruss machine equipped with a Peltier plate within a cold chamber. The freezing time (freezing onset) is expressed as the time at which a water droplet deposited on the sample starts freezing. As such, the 4-μL water droplet was placed on the stage at -20 °C, and monitored by a camera. With time, the transparent water droplet became non-transparent, and consequently, the frozen state occurred. The corresponding time of this change was reported as the freezing delay. We also, minimized the influence of humidity and condensation on the measurements by placing anhydrous calcium sulfate desiccants in the chamber. The relative humidity was around 50% ± 3%. We also, repeated the measurement at three different points on the samples prepared in the session 2.1.

The static accumulation test (SAT) aimed to measure the amount of ice accumulated on tilted samples. For this purpose, the coatings were applied to 3 cm × 15 cm substrates via a film applicator (ZEHNTNER testing instrument). For each coating formulation, four samples were prepared to ensure the accuracy of the obtained results. The average coating thickness for all samples was about 100 ± 5 μm. The substrates were then placed onto a specially designed stand that can accommodate samples at different angles, including 0°, 45° and 80° to compare the accumulation of ice on the samples. The horizontal position (0°) was used to estimate precipitation intensity. The entire setup was kept in the cold chamber at an air temperature of −5 °C for half an hour, and the relative humidity of around 84% ± 2%. The icing conditions included 15 min of precipitation (supercooled water droplets with an average diameter of 327 μm), followed by an additional 45 min of cold temperatures to ensure icing. The samples were weighed before and after the procedure to obtain the amount of ice accumulated. Moreover, sample temperature was monitored during the precipitation and icing processes using an Optris PIX infrared camera.

We measured the ice adhesion strength of the samples by a "micro-push-off" method developed by our research group (Figure 3-2b). Conventional methods for measuring ice adhesion [22][245] do not provide helpful information about ice adhesion strength of samples varying in PCM microcapsule content. These standard methods involve measurements after a standard time for all samples; however, this is not appropriate for evaluating the effect of latent heat release from PCM microcapsules on ice adhesion. In our setup, a camera attached to the micro-push-off apparatus provided real-time monitoring of the water droplet, and we measured ice adhesion at

the exact moment that the water droplet was completely frozen. Very likely, at the moment of complete freezing, the adhesion strength between the surface and frozen droplet can continue to be affected by the release of latent heat from the PCM microcapsules. The sample was placed on a cooling plate within a small cold chamber, adjusted to a target temperature of −10.0 ± 0.1 °C. Then, a 10 µL deionized water droplet was placed onto the sample and the freezing process was filmed. Once the water droplet froze completely, the probe of the force meter approached the frozen droplet at 0.5 mm/s until the frozen droplet detached from the surface, and a maximum force was recorded. We determined ice adhesion strength by dividing the maximum measured force at ice detachment by the contact area of the frozen water droplet–surface interface. We assessed the durability of the samples when subjected to subsequent icing/de-icing events by repeating the micro-push-off test ten times with the same procedure.

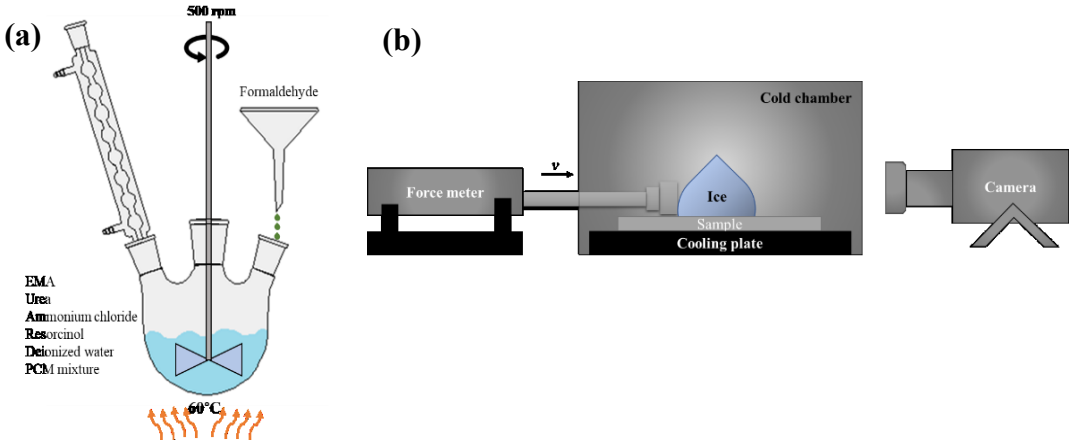

Figure 3-2. *(a) Schematic illustration of the experimental setup used for the encapsulating PCM within an UF shell, and (b) illustration the micro-push-off apparatus used for the ice adhesion measurements.*

3.4 Results and discussion

3.4.1 Characterization of microcapsules

Using the encapsulation process described in Figure 3-2a, we fabricated UF microcapsules filled with PCM having the desired size distribution. These microcapsules were embedded within an elastomeric matrix.

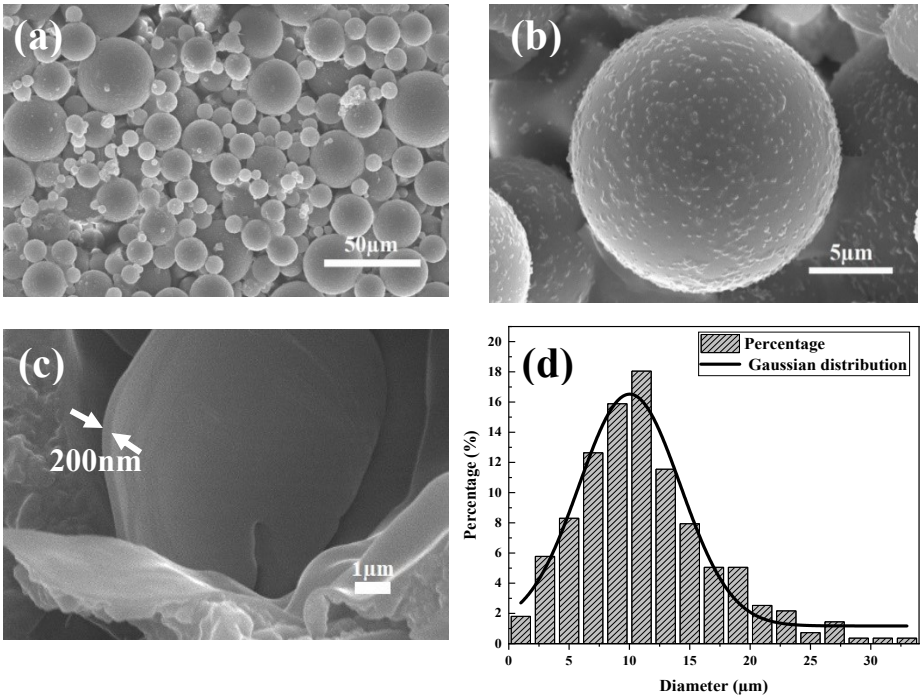

Figure 3-3. *SEM images illustrating (a) PCM microcapsules, (b) the surface of a PCM microcapsule, and (c) the shell thickness along with (d) the size distribution of the fabricated microcapsules.*

The ratio of the mass of obtained microcapsules to the total mass of PCM and shell components, known as the yield of encapsulation, was ~67%. The use of an EMA emulsifier [251] caused the microcapsules to be spherical (Figure 3-3a and Figure

3-3b), and the microcapsules had a shell thickness of approximately 200 nm (Figure 3-3c). About 70% of the microcapsules had a diameter between 5 and 15 μm, and the size distribution followed a relatively broad Gaussian curve. Particle size and size distribution were optimized by changing parameters such as agitation speed, polymerization time and temperature to improve the dispersion of the microcapsules within the matrix. The chemical structure of the microcapsules, their shell, and the core (Figure 3-4) were investigated by FTIR to confirm that PCM encapsulation had occurred correctly.

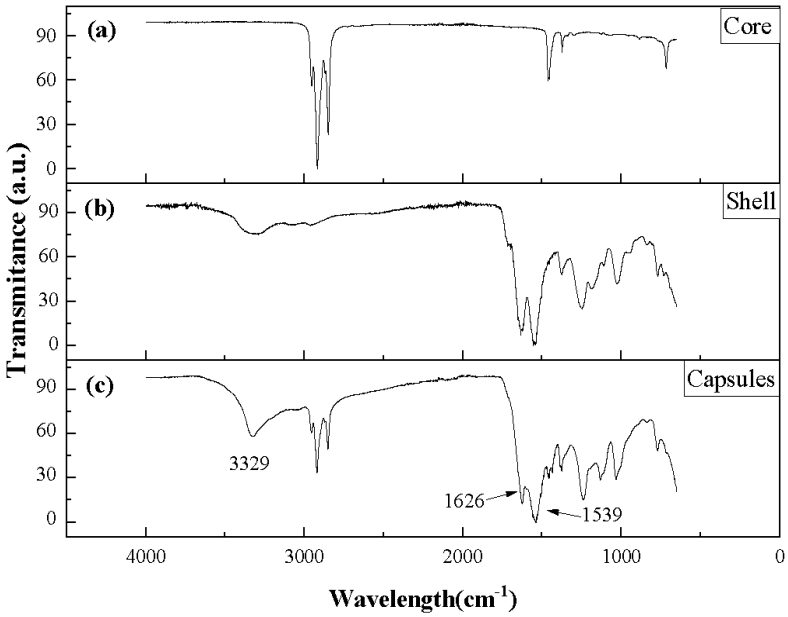

Figure 3-4. *FTIR spectrum of the (a) shell material, (b) PCM-filled microcapsules, and (c) core material.*

Peaks corresponding to the formation of poly(urea–formaldehyde) appeared at 3329 cm^{-1} (O–H and N–H stretching), 1626 cm^{-1} (C=O stretching), and 1539 cm^{-1} (N–

H bending). Furthermore, the FTIR spectrum of the microcapsules contains the observed peaks in each spectrum of the shell and core material (Figure 3-4c), indicating that PCM material was successfully encapsulated within the UF shell.

3.4.2 Surface characterization

The cross-sectional SEM images from the prepared samples (Figure 3-5) confirmed that the PCM microcapsules had dispersed homogeneously throughout the elastomeric matrix, without any considerable agglomerations or detectable defects.

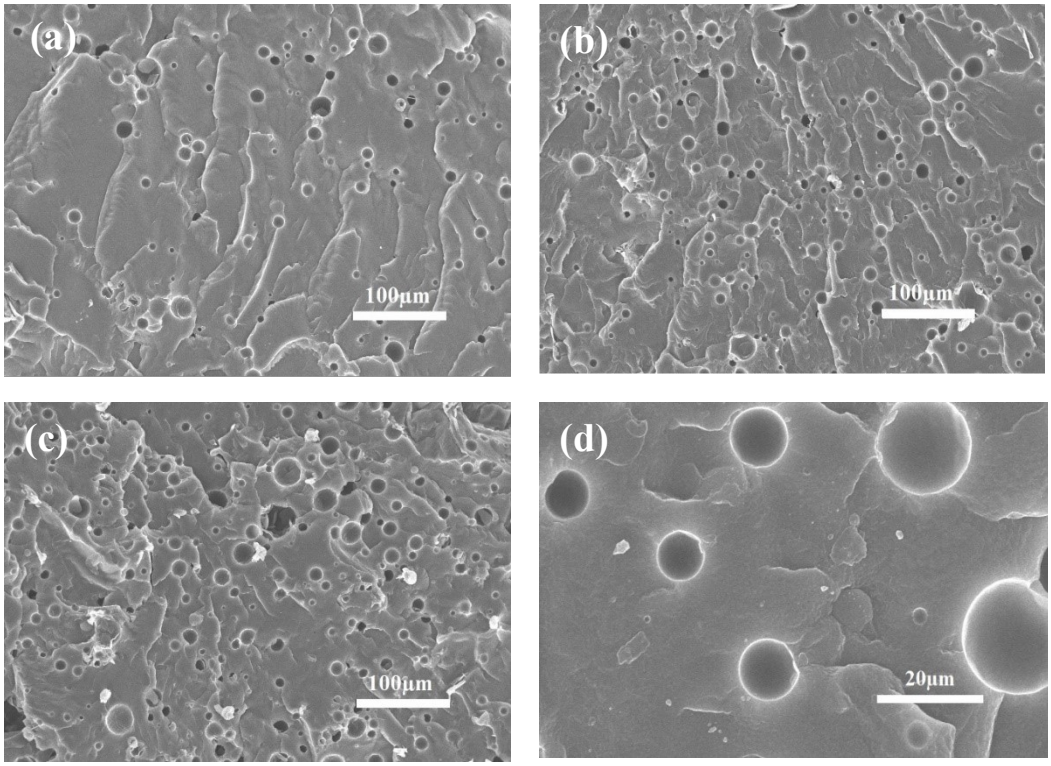

Figure 3-5. *The cross-sectional micrographs of samples (a) PCM-10, (b) PCM-20, and (c) PCM-30 at 400x magnification. (d) PCM-30 at 1000x magnification.*

Furthermore, the microcapsules were closely bound to the PDMS matrix (Figure 3-5d). The surface asperities of the microcapsules promote mechanical interlocking, resulting in adhesion between microcapsules and the matrix (see Figure

3-5b). Therefore, the PDMS matrix can protect microcapsules against mechanical stress, thereby preventing PCM leakage.

The coating topography was also altered because of the presence of microcapsules on the sample surface (Figure 3-6). Moreover, increasing the abundance of microcapsules within the matrix heightened surface roughness; surface roughness passed from 0.32 to 1.14 µm as microcapsule content within the elastomeric matrix increased (Table 3-1).

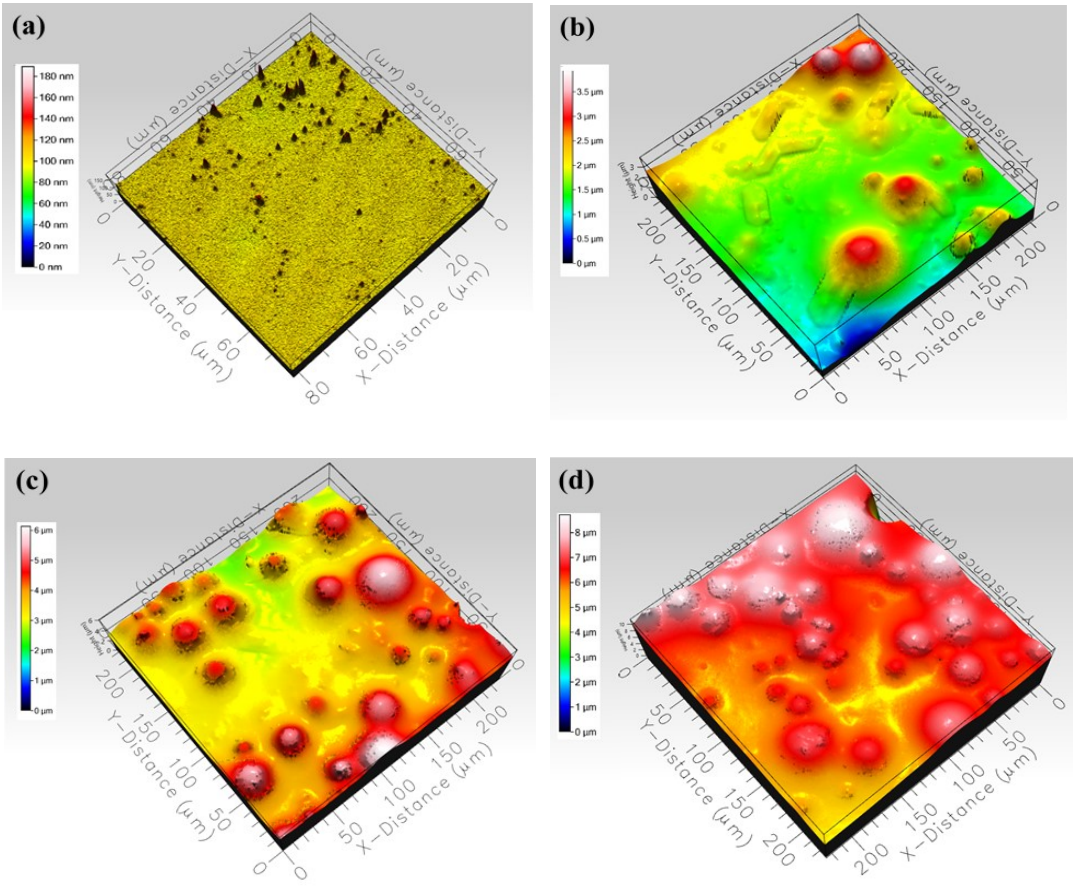

Figure 3-6. *A series of 3D topographical maps of the (a) reference samples and samples containing (b) 10%, (c) 20%, and (d) 30 wt.% PCM microcapsules.*

Table 3-1. *Surface roughness values of the fabricated surfaces*

Roughness parameters	Reference (PSI mode)	PCM-10	PCM-20	PCM-30
RMS roughness (S_q)	3.7 ± 0.5 nm	0.32 ± 0.06 µm	0.73 ± 0.19 µm	1.14 ± 0.26 µm

We measured the water contact angle to evaluate the effect of impregnated microcapsules on the coating wettability. The contact angles of all the samples did not change considerably relative to that of the reference (Figure 3-7a). The observed change from 110° for the reference sample to 120° for PCM-10 can be attributed to the increased surface roughness due to the incorporated microcapsules. However, increasing the microcapsule content further led to the contact angle decreasing to about 111° for PCM-30; this decrease likely relates to the presence of hydrophilic groups such as OH and NH in the structure of embedded microcapsules (Figure 4). These hydrophilic groups can favor the formation of hydrogen bonds between the coating and the water droplet, resulting in a further spreading of the water droplet over the surface.

3.4.3 Icephobic characterization

3.4.3.1 Ice nucleation temperature and ice nucleation time

We used differential scanning calorimetry (DSC) to determine the capability of encapsulated PCMs to release latent heat (Figure 3-7b). Much similarity was observed between the DSC curves of the PCM microcapsules and PCM-20 in terms of the starting and ending phase-change temperatures in both endothermic and exothermic processes. For the reference sample, no peak was observed across the same temperature range. Therefore, the PCM preserved its phase-change characteristics as temperatures decreased both when encapsulated and embedded within the coating matrix.

The released latent heat would likely affect the ice nucleation temperature and freezing time. Thus, we added a certain amount of deionized water to the DSC aluminum pan, coated with a thin layer of each coating, to evaluate this effect on ice nucleation temperature. DSC measurements confirmed that adding PCM microcapsules to the elastomeric coating produced a desirable effect on ice nucleation temperature, and the increase of PCM microcapsules content in the coating decreased the ice nucleation temperature (Figure 3-8a).

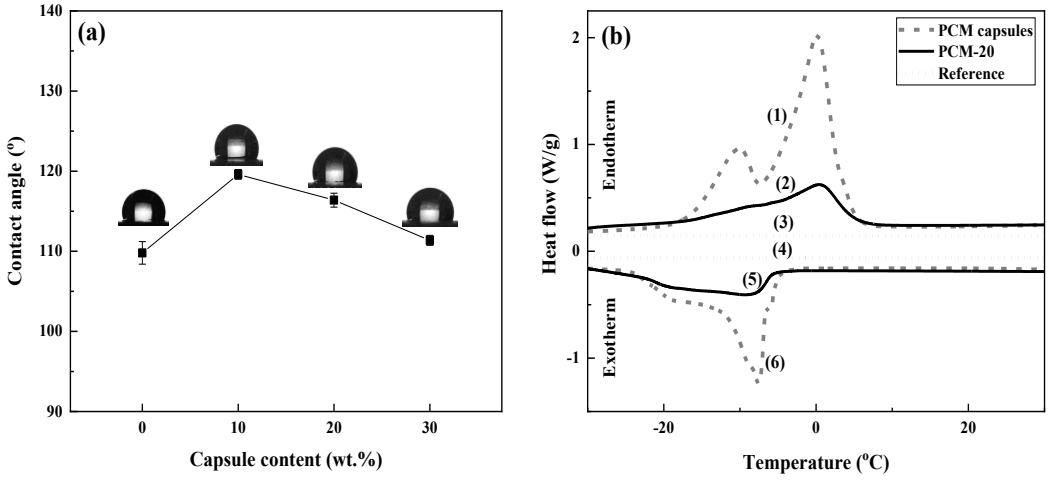

Figure 3-7. *(a) Contact angle of the samples containing various PCM microcapsule contents. (b) The evaluation of the phase change capability of PCM microcapsules, sample PCM-20, and the reference sample. The curves (1), (2), and (3) are endothermic processes, whereas curves (4), (5), and (6) are exothermic processes. The corresponding enthalpy (ΔH_m) of PCM microcapsules and PCM-20 were 111.2 and 19.2 J/g, respectively.*

In fact, change in temperature can significantly affect the ice nucleation rate so that an increase of 1 °C in supercooling degree can result in heightened ice nucleation rate even in 2-3 orders of magnitude [49]. When we compared ice nucleation times of a water droplet (volume) on the samples at −20 °C, we noted a clear increase in the

freezing-delay time because of the PCM microcapsules embedded within the coating (Figure 3-8b). Furthermore, adding a greater number of microcapsules to the coating increased the time to complete freezing from 181.2 s (reference) to 1194.6 s (PCM-30).

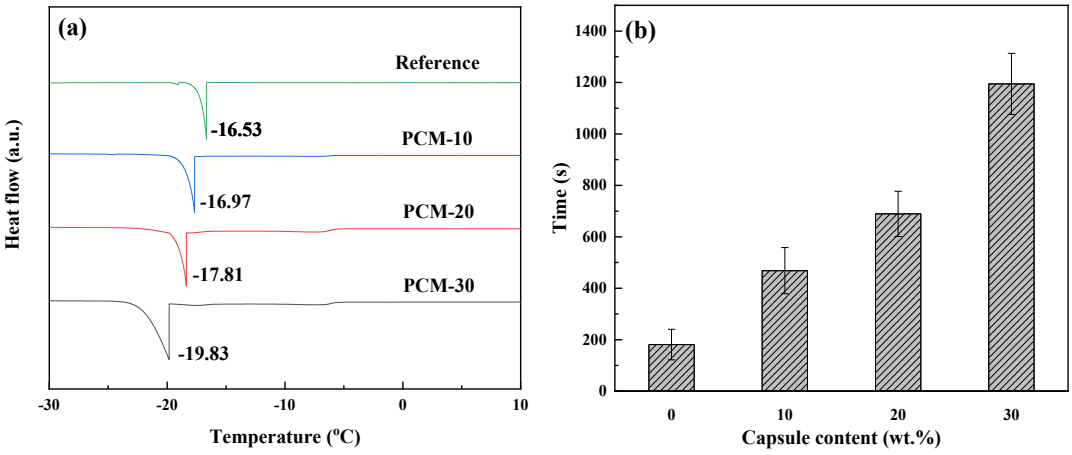

Figure 3-8. *(a) Delayed ice nucleation temperature on the surface of samples containing different PCM microcapsule contents, as evaluated by differential scanning calorimetry (DSC). (b) Comparison of the ice nucleation time for PCM-containing coatings at three microcapsule concentrations and the PDMS coating without microcapsules, as a reference.*

3.4.3.2 Ice accumulation

The amount of ice accumulated on samples at different angles (0°, 45°, and 80°) was determined using the SAT method. Figure 3-9a shows the schematic diagram of a freezing droplet on an inclined plane along with applied gravity force and its components.

Accordingly, the force that can detach the droplet from the surface is the tangential component of the gravity force ($F_{\parallel}$), obtained by Equation 2.

$$F_{\parallel} = W \cdot sin\alpha, \qquad \text{Equation 2}$$

where W is the weight of the droplet, and α is the angle corresponding to the inclined plane. For α = 0°, sinα is equal to zero, and, consequently, there is no force to cause ice to detach. Therefore, the accumulated ice mass for all samples is highest at 0° (Figure 3-9b). Furthermore, sin 80° is greater than sin 45°; thus, a greater force is applied to the droplet at 80°, resulting in less ice accumulation on all samples at 80° than at 45°.

All graphs followed a similar trend for each inclination angle (Figure 3-9b), with the mass of accumulated ice highest in the reference sample, followed by the 10% and then 20% PCM samples. Ice accumulation on the reference sample at 0° was significantly higher than the accumulation on the PCM-containing samples. However, the latter showed no significant differences in their accumulated ice mass. The 30% PCM sample increased in ice mass relative to the 20% sample at all angles.

Temperature variations of the fabricated samples during SAT were monitored by IR thermography (Figure 3-9c). During the 15 min of precipitation, the sample color did not change considerably. However, after stopping the precipitation and continuing the icing conditions (at −5 °C), the reference sample color gradually became green (Figure 3-9d). Nonetheless, the color of PCM-containing samples showed less change than that of the reference sample, especially for the 20% and 30% PCM samples. The color (temperature) of PCM-20 changed least among all samples. The tracing of sample temperatures (Figure 3-9d) confirmed that the surface temperature of the PCM-containing samples microcapsules decreased gradually over time; therefore, the rate of change in temperature decreased as PCM content increased. For the reference sample, the surface temperature markedly dropped as temperatures approached 0°.

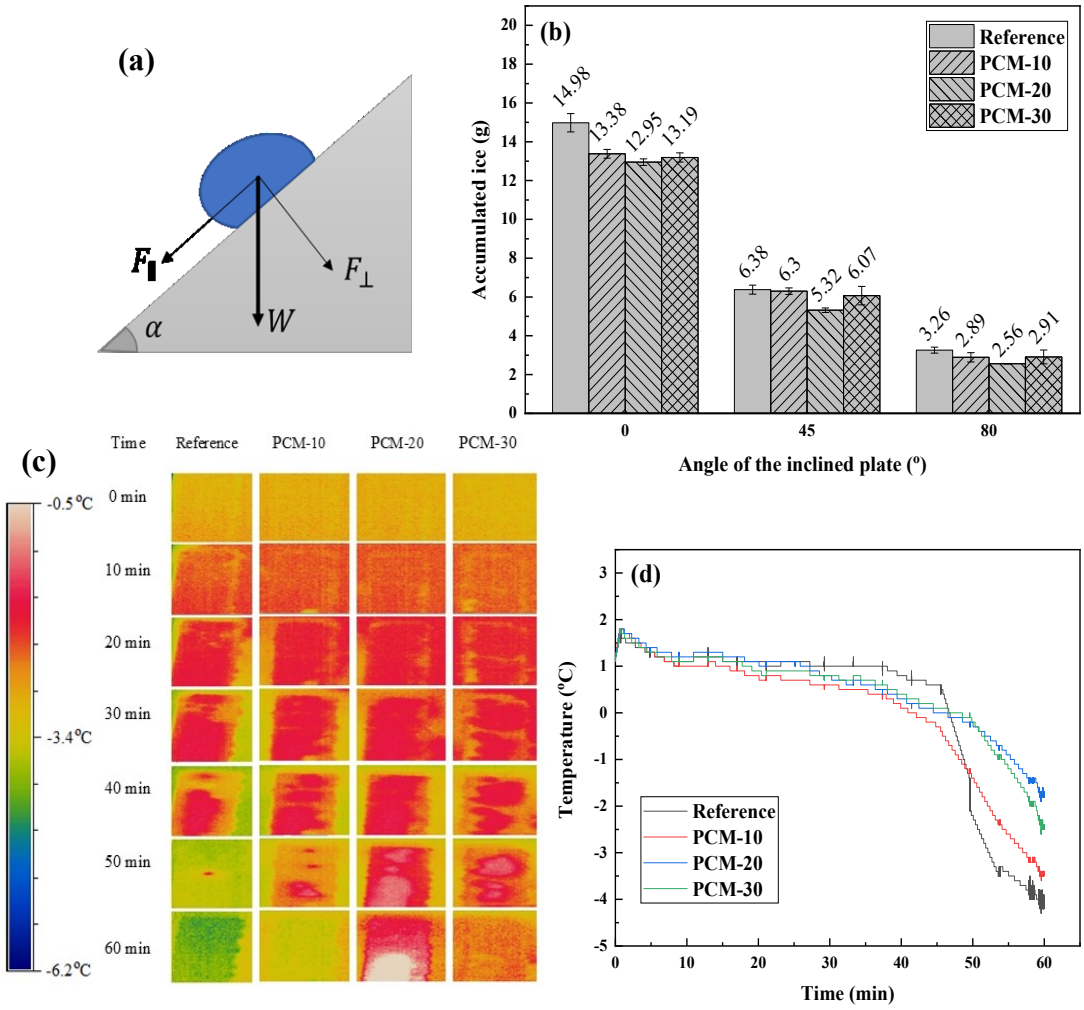

Figure 3-9. *(a) Diagram illustrating a water droplet on an incline with the applied gravity force and its components. (b) The amount of accumulated ice on each sample at inclines of 0°, 45°, and 80°, as measured by SAT. (c) IR thermography of the samples at the angle of 0˚ during precipitation and icing; (d) temperature of the samples over time.*

The more limited response of the PCM-containing samples near 0° relates to the release of latent heat by the PCM in the coatings. Furthermore, the sample temperature containing 20% PCM microcapsules was higher than that of the 30% PCM

samples. Slightly more ice surface covered the sample containing 30% PCM microcapsules (13.19 g) than the 20% PCM samples (12.95 g); this pattern related likely to the higher temperature of the 20% PCM samples.

3.4.3.3 Ice adhesion measurements

The adhesion strength between the surface and the ice affects ice accumulation. We applied the micro-push-off adhesion test to evaluate the effect of embedding PCM microcapsules on ice adhesion strength and, therefore, ice accumulation. Incorporating PCM microcapsules within coatings, generally reduced ice adhesion strength immediately following freezing. The average ice adhesion strength of samples containing PCM microcapsules decreased until 20% composition from about 379 to 116 kPa (Figure 3-10). Furthermore, it is worth mentioning that for the sample containing 30% PCM microcapsules, the sudden rise in ice adhesion strength relates to the increasing surface roughness, which enhanced the probability of mechanical interlocking between the ice and the surface. These results agreed with the amount of ice accumulated on the surfaces at different angles (see Figure 3-9b). The decreasing ice adhesion from the reference sample to the 20% PCM sample also led to a similar decreasing trend for ice accumulation in the corresponding samples. The 30% PCM samples produced an increase of ice accumulated on the surface linked to a heightened ice adhesion strength relative to the 20% PCM-containing sample. Furthermore, the use of ten icing/de-icing cycles and the micro-push-off test were combined to evaluate coating durability. As seen in Figure 3-10a, values for ice adhesion strength of samples containing 10%, and 20% PCM microcapsules did not vary significantly over the ten cycles. Although sample with 30% microcapsules experienced a relatively lower

durability. This reduced durability can be attributed to the poorer mechanical properties of the coatings as microcapsule content increases. The water contact angle of the fabricated coatings was measured after the 10th cycle of icing/de-icing ((Figure 3-10b). Accordingly, the coatings presented no considerable change after multiple icing/de-icing cycles.

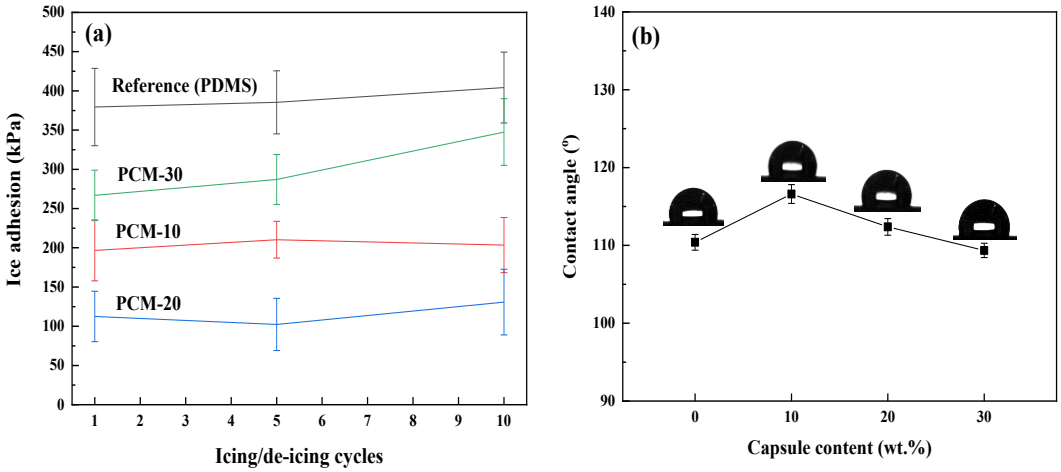

Figure 3-10. *(a) The ice adhesion strength of the reference sample and samples containing PCM microcapsules over ten icing/de-icing cycles. The ice adhesion strengths of bare copper, steel, and glass in first cycle were measured as 921±98, 680 ± 86, and 721±101 kPa, respectively. (b) The variation of water contact angle of the prepared samples after ten icing/de-icing cycles.*

As temperature decreases, the PCM microcapsules undergo phase transformation and release a considerable amount of latent heat is released. This release decreases the ice adhesion strength by two possible mechanisms: the formation of the quasi-liquid layer (QLL) and the production of local strains on the sample. In the first mechanism, a portion of this heat energy reaches the coating–ice interface and melts the ice to form a quasi-liquid layer. This layer acts as a lubricant to produce a mixed lubrication regime and, therefore, reduce ice adhesion strength. It is noteworthy that

beyond this phase-change temperature range, the liquid-like layer is reduced, and the lubricating regime switches to a boundary regime [212,213] because the PCM does not release any more heat. The second mechanism involves the expansion and contraction of the surface, resulting in ice detachment. Lower temperatures lead to surface contraction, whereas the release of latent heat from the PCM and absorption of the heat by the surrounding matrix causes local expansion. The surficial contraction and localized expansion can lead to stress-localization function [252] that produces a shear stress, and consequently, breaks the surface–ice bonds to favor ice detachment from the surface.

3.5 Conclusions

We encapsulated a mixture of PCMs using an in-situ polymerization of urea–formaldehyde (UF) and embedded the fabricated microcapsules within a PDMS matrix. Our encapsulation method produced spherical microcapsules having a relatively broad size distribution; around 70% of microcapsules varied between 5 and 15 μm in diameter. FTIR confirmed that the PCM mixture was successfully encapsulated within the UF shell. Cross-sectional micrographs of embedded microcapsules within the PDMS matrix showed that they were very well dispersed throughout the coating and bound closely with the elastomeric coating. DSC tests showed that the microcapsules preserved their ability to release latent heat while embedded within the matrix. Based on DSC analysis also, the presence of these PCM microcapsules affected ice nucleation temperature due to PCM latent heat release. Increased microcapsule content lengthened freezing-delay times because of the greater amounts of heat released by the embedded PCMs. The quantity of accumulated ice on surfaces inclined at various angles on PCM-

containing samples was lower than that on the reference surfaces. IR thermography confirmed that this reduced ice accumulation in the PCM-containing samples occurred because of the higher surface temperature of these samples related to the latent heat released by the PCM. The lowest ice accumulation was observed for samples containing 20% PCM. In general, greater microcapsule content led to higher released latent heat, and therefore, reduced ice adhesion strength; however, for the sample containing 30% microcapsules, an increased ice adhesion is most likely related to a higher surface roughness favoring greater mechanical interlocking, matching the patterns observed with ice accumulation. In general, decreased ice adhesion due to latent heat release can be justified by either of possible mechanism of the formation of quasi liquid layer (QLL) or thermal expansion differences. PCM microcapsules thus provides anti-icing mechanism that can be impregnated in various matrixes. It is noteworthy that the time period for latent heat release was limited, and as temperature stabilizes, the presence of microcapsules may increase adhesion strength as a result of increased surface roughness.

Acknowledgments

The authors acknowledge all support from the Natural Sciences and Engineering Research Council of Canada (NSERC), Hydro-Québec, and PRIMA Quebec. The authors would like to thank Ms Caroline Blackburn and Dr Jean-Denis Brassard at the Anti-icing Materials International Laboratory (AMIL), UQAC, for helping carry out the centrifuge and SAT tests.

Chapter 4: A novel hybrid anti-icing surface combining an aqueous self-lubricating coating and phase-change materials

Mohammadreza Shamshiri[1, *], Reza Jafari[1], and Gelareh Momen[1]

[1] Department of Applied Sciences, University of Quebec in Chicoutimi (UQAC), 555, boul. de l'Université, Chicoutimi, Quebec, G7H 2B1, Canada

[*]Corresponding author: mohammadreza.shamshiri1@uqac.ca.

4.1 Abstract

The ability of phase change materials (PCMs) to absorb and release large amounts of latent heat has led to great interest in their use in anti-icing applications. Combining PCMs and other passive icephobic strategies such as self-lubricating coatings could enhance anti-icing performance. Here, we fabricate an icephobic coating by impregnating an elastomeric matrix containing PEG-PDMS copolymers with PCM microcapsules. We encapsulate a selected mixture of n-dodecane and n-tetradecane within urea–formaldehyde shells using in-situ polymerization. Various concentrations of microcapsules are then added into the self-lubricated PDMS coating and 2.5 wt.% of hydroxyl-terminated PEG-PDMS copolymer. Differential scanning calorimetry confirms that the PCM-embedded coating has colder ice nucleation temperatures than the self-lubricating coatings lacking microcapsules. The release of latent heat by the PCMs likely preserves the liquid-like layer for a more extended time and delays ice nucleation. The presence of PCM microcapsules can positively affect

self-lubricating characteristics of the matrix containing the PEG-PDMS copolymer to further reducing ice adhesion. The presence of a liquid-like layer lowers ice adhesion strength and decreases ice accumulation on surfaces. These particular properties are further enhanced by the incorporated PCM microcapsules and their ability to release latent heat. Finally, we confirm the durability of the fabricated coatings after multiple icing/de-icing cycles. Such PCM-impregnated coatings therefore offer potential uses for diverse icephobic applications.

Keywords: Ice accumulation, ice adhesion, icephobicity, phase change materials (PCMs), quasi liquid-like layer, smart icephobic coatings, synergistic effect

4.2 Introduction

Ice formation and accumulation on exposed infrastructure and equipment in cold-weather areas can have serious safety and operational consequences [5,9,10,34,175,253]. For instance, ice accretion on wind turbines produces a load imbalance on the blades that can disrupt turbine operation and decrease their energy production [8]. For transmission lines, icing can mechanically damage power network equipment, resulting in massive economic losses [2,74]. Moreover, the various forms of ice-related phenomena, including freezing rain, dry and wet snow, and frost formation, complicate our understanding of surface icing [254]. Ice nucleation, a critical step in icing processes, is affected by a wide range of variables, including humidity, temperature, cooling rate, and contamination; thus, investigating these variables and their effect on ice formation is essential [255].

The use of coatings is an efficient strategy to combat icing on exposed surfaces. These coatings work by delaying ice formation and/or reducing ice adhesion. Progress in coating science has led to novel icephobic surfaces such as superhydrophobic coatings [75,256] and slippery liquid-infused porous surfaces (SLIPS) [257,258]. However, these coatings suffer from some drawbacks, including durability and oil depletion, which must be addressed to enhance the anti-icing performance of these surfaces and their application in the context of harsh environmental conditions. Recently introduced smart (intelligent) icephobic coatings aim to minimize the disadvantages of passive strategies, such as oil depletion, and prolong the service life of these coatings [150,254]. Smart coatings sense environmental stimuli, e.g., shifts in pH, temperature, and humidity. Smart icephobic surfaces react to the environmental change and, as a consequence, reduce ice formation and accumulation [254]. Smart icephobic coatings can be categorized into several groups, including thermoresponsive coatings [124], self-healing icephobic coatings [149,160,165], aqueous self-lubricating coatings [149,160,165,259], and coatings containing phase change materials (PCMs) [211,214].

Aqueous self-lubricating coatings represent an anti-icing strategy in which a thin water layer acts as a lubricant; therefore, these surfaces avoid problems such as oil depletion [170,171,186]. The icephobic characteristics of these coatings derive from the presence of a liquid-like layer, known as a “quasi liquid layer” (QLL) at the ice–surface interface [46,169,172,176,182–186]. Such layers can be fabricated using hygroscopic materials that readily absorb water from the surrounding environment. Embedding hydrophilic components within the primary matrix is another means of producing QLL. Interactions such as hydrogen bonding between water molecules and

hydrophilic groups in the coating produce an unfrozen layer at the interface that facilitates ice slippage. Blending PEG-PDMS copolymers as amphiphilic components with polymeric matrices has also been used to fabricate aqueous self-lubricating coatings with acceptable anti-icing properties [68]. The presence of these copolymers produces a viscous lubricating layer at the ice–surface interface. Chen et al. [68] used solid-state nuclear magnetic resonance (NMR) spectroscopy to verify the presence of such a QLL on an elastomeric matrix containing PEG-PDMS copolymers in contact with water. They confirmed that a polydimethylsiloxane (PDMS) matrix containing PEG-PDMS copolymers did not follow the empirical correlation between the ice adhesion strength (τ_{ice}) and the practical work of water adhesion, proposed by Meuler et al. [66,68]. Furthermore, the fabricated surfaces showed a higher contact angle hysteresis (>30°) than other icephobic surfaces such as SLIPS [68,149]. The QLL can endure subzero conditions and reduce ice adhesion strength by maintaining a lubricating layer between ice and the surface [24,68].

PCMs have received much interest because of their extraordinary energy conservation and storage. During their phase change, PCMs release a large amount of energy as latent heat, which can be used in a range of applications, including building [192], solar energy [260], automotive [261], and anti-icing applications [23]. A useful PCM must meet certain criteria, including a suitable melting point, a low supercooling temperature degree, and high thermal conductivity, to be considered a suitable candidate for icephobic applications [22,241,254]. Combining various forms of PCM can achieve these criteria. PCMs can be added directly into a matrix or encapsulated before being incorporated into the matrix [206,242,243]. The encapsulation of PCMs prevents their direct contact with the matrix and avoids material exchange between the

PCM and matrix. The encapsulated materials can also be handled as solids, favoring greater control of the PCM properties. Moreover, encapsulation prohibits PCM leakage and therefore prolongs the service life of PCMs [207,215].

Combining two or more icephobic strategies should produce a more effective anti-icing surface than use of a single strategy [227,262]. For such a hybrid approach to be successful, the performance of each method should be complementary using synergistic effect, not negatively affecting or canceling out the performance of the other. Moreover, previous studies focused on using either self-lubricating coatings or phase-change materials (PCM) for icephobic applications remain limited [24,25].

Here, we fabricate an icephobic coating by incorporating PCM microcapsules into an elastomeric matrix containing a PEG-PDMS copolymer. We prepare a mixture of two PCMs, n-dodecane and n-tetradecane with an optimized ratio of 2:8, and successfully encapsulate this mixture within a UF shell. As part of a coupled anti-icing strategy involving the self-lubricating property of the matrix and latent heat release of PCMs, microcapsules are then incorporated within a PDMS matrix containing 2.5 wt.% PEG-PDMS copolymer. According to our previous work [24], blending these amphiphilic copolymers with the elastomeric matrix enhanced the icephobic performance of the coating due to formation of the QLL. Differential scanning calorimetry (DSC) is used to confirm that PCMs preserve their ability to release latent heat and delay ice nucleation. Moreover, the release of latent heat by PCMs further reduces an already relatively low ice adhesion strength related to the presence of a QLL. The fabricated samples also demonstrate their durability by maintaining their ice adhesion strength after 10 icing/de-icing cycles.

4.3 Experimental protocols

4.3.1 Materials

SYLGARD™ 184 silicone elastomer (polydimethylsiloxane (PDMS)) was generously provided as a kit (the base and cross-linker) by Dow Corning. The PEG-PDMS copolymer of CMS-221 ((carbinol functional) methylsiloxane dimethylsiloxane copolymer) was used as received from Gelest Inc. PCMs (n-dodecane, n-tetradecane, n-hexatriacontane), urea, resorcinol, hexane, and ammonium chloride were obtained from Alfa Aesar. Ethylene maleic anhydride (EMA, average M_w of 100,000–500,000) was purchased from Sigma-Aldrich.

4.3.2 Selection and encapsulation of PCM

We prepared mixtures of n-dodecane and n-tetradecane at different ratios (2:8, 3:7, 4:6), and 3 wt.% n-hexatriacontane was added as a nucleating agent to decrease supercooling degree of PCM mixture [23,215]. The selected combination was encapsulated via in situ polymerization of oil-in-water emulsion [247]. The encapsulation process is adapted from the procedure presented by Brown et al. [247]. We added 1.25 g of EMA emulsifier to 100 mL deionized water in a beaker. The water–emulsifier mixture was stirred constantly for 2 h using the magnetic stirrer until a transparent solution was achieved. The solution was further diluted by adding 150 mL deionized water. We then added 5 g urea to the solution, followed by 0.5 g ammonium chloride and 0.5 g resorcinol, all the while continuing to stir the mixture. The pH of the solution was adjusted to 3.5 by adding a few drops of aqueous sodium hydroxide. The PCM mixture was sonicated for 3 min, added to the prepared solution, and then homogenized (Fisher homogenizer) for a few minutes. The prepared mixture was

stirred using an overhead mixer, and the solution temperature was raised to 60 °C by placing the mixture in a water bath. We then introduced 12.67 g of 37% formaldehyde solution dropwise into the emulsion. The temperature was kept at 60 °C for 4 h. The emulsion was then allowed to cool to ambient temperature. The microcapsules were collected, washed with deionized water to remove unreacted chemicals, and then air-dried overnight.

4.3.3 Preparation of the elastomeric coatings

The base and curing agent SYLGARD™ 184 were mixed at a 10:1 ratio. We then blended 2.5 wt.% of CMS-221 into the mixture while the mixture was magnetically stirred. Afterward, 5, 10, and 15 wt.% of fabricated PCM microcapsules were dispersed separately in hexane and added to a PDMS precursor containing PEG-PDMS. We applied the prepared coatings to polished aluminum substrates using a ZEHNTNER film applicator. The coatings were then fully cured at 90 °C overnight. We labeled the samples on the basis of the content of the microcapsules as PP0, PP5, PP10, and PP15; for example, sample PP10 contained 10 wt.% microcapsules. The final thickness of the cured coatings was approximately 100 ± 5 μm. We also prepared five free films for each sample (10 cm × 1.5 cm × 400–500 μm) to evaluate their mechanical properties.

4.3.4 Characterization

4.3.4.1 Surface characterization

Sample wettability was evaluated by measuring the static water contact angle at 25 °C. We assessed the contact angle via the sessile drop method using a Kruss™ DSA100 goniometer. Furthermore, we determined contact angle hysteresis through the

difference between the advancing and receding contact angles of a water droplet moving over the samples. We repeated the measurements of contact angle and contact angle hysteresis at five points on each prepared sample.

We used scanning electron microscopy (SEM; JSM-6480 LV SEM, JEOL Japan) to observe the produced microcapsules and coating morphology. Scanning quality was enhanced by applying a very thin layer of gold on the samples. The surface topography of the samples was investigated using atomic force microscopy (AFM) (Bruker, Multimode8) and an optical profiler (Profil3D Filmetrics, USA). The former evaluated the effect of blending PEG-PDMS with the elastomeric matrix on surface roughness, whereas the second assessed the influence of the incorporated PCM microcapsules on surface roughness. AFM (ScanAsyst mode using PeakForce Tapping) provides more accurate measurements at the nanoscale than does profilometry. At a microscale, profilometry (WLI mode) presented a greater ability to obtain topographical maps than AFM because of the presence of the microcapsules. The topography of microcapsule-embedded surfaces was assessed using profilometry.

4.3.4.2 Chemical characterization

A Cary 630 Fourier transform infrared (FTIR) spectrometer (Agilent, USA) in diamond ATR (attenuated total reflection) mode was used to evaluate the performance of the encapsulation by investigating the chemical composition of the produced microcapsules, the PCM core, and the shell material.

4.3.4.3 Thermophysical characterization

The thermophysical properties of the PCM mixtures and microcapsulated PCMs, including melting and solidifying temperatures and the capacity of PCMs to release latent heat, were assessed via differential scanning calorimetry (DSC) using a DSC Q250 (TA Instruments). For this analysis, we placed 5 mg of either the PCM mixture or the sealed microcapsules into the DSC and then cooled the sample from 40 °C to −40 °C, followed by a heating to 40 °C at 5 °C·min^{-1}.

4.3.4.4 Icephobic properties

The freezing delay times were obtained in a cold chamber equipped with the Peltier cooling stage. We reported the unset and complete freezing times of the water droplet at 20 °C.

We also used DSC to evaluate the ice nucleation temperature of the samples. The measuring process consisted placing 5 mg deionized water into a DSC pan covered with the coatings and then sealed, and ice nucleation temperatures were obtained by cooling the pan from 40 to −40 °C at 5 °C·min^{-1}.

We obtained the ice adhesion strength of the coatings using a micro-push-off adhesion test (Figure 4-1). For samples containing PCM microcapsules, conventional methods such as the push-off test [24,250] are not ideal because values recorded after a given time (e.g., 24 h) would not provide any meaningful results about the effect of latent heat release on ice adhesion. Therefore, we used a micro-push-off test that provided real-time monitoring of the samples and allowed us to obtain ice adhesion at the exact moment complete freezing occurred and when ice adhesion could still be affected by the released latent heat. The measuring procedure of the apparatus was very

similar to that of the push-off test. Instead of using the usual cylindrical mold, we placed a 10 µL deionized water droplet onto the sample. Once the droplet froze, we recorded the maximum force at ice attachment. As with the conventional method, ice adhesion was obtained by dividing the maximum force by the ice–surface interfacial area. Ice adhesion on each of the coatings was examined three times. We also investigated the durability of the samples subjected to subsequent icing/de-icing events by repeating the micro-push-off test 10 times with the same procedure.

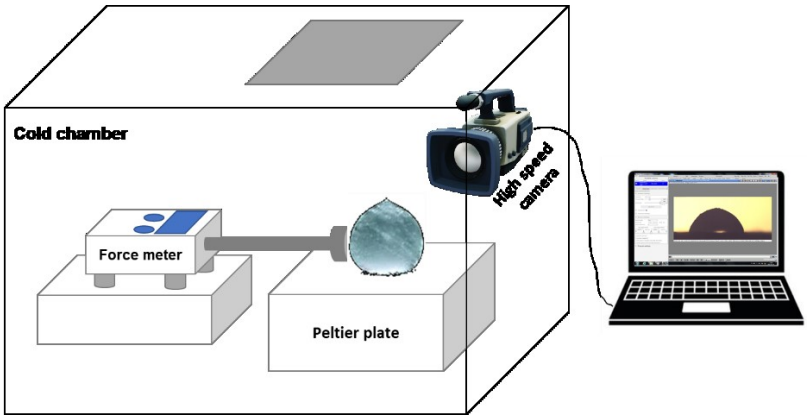

Figure 4-1. *Illustration the micro-push-off apparatus used for the ice adhesion measurements.*

Finally, we used the static accumulation test (SAT) to evaluate the capacity of the samples to reduce the amount of ice accumulation. Samples were placed on the holders fixed at three angles (0°, 45°, and 80°). After 2 h at −5 °C, we exposed the samples to 15 min of precipitation of supercooled water droplets (diameter 300–400 µm). The samples were kept at −5 °C for 45 min to ensure icing. The amount of ice accumulated on each sample was equal to the difference between the mass of the sample before and after the total icing conditions. For each coating formulation, four samples were prepared to ensure greater representativeness of the obtained measurements.

4.3.4.5 Mechanical characterization

The tensile test was carried out at room temperature using a TA.XTPlus 100 machine equipped with a *5 kg* load cell. The free films used for the measurements had length of 10 ± 0.5 mm, width of 1 ± 0.1 mm, and thickness of 2 mm. For each coating, five free films were prepared and tested at a speed of 50 mm/min.

4.4 Results and discussion

4.4.1 Blending the PEG-PDMS copolymer within the PDMS matrix

Generally, polymers are immiscibly blended; therefore, it is almost impossible to mix them at a molecular level [234]. The AFM topographical maps of a sample containing 2.5% CMS-221 and the reference PDMS demonstrate that surface roughness (S_q) increased from 6.81 ± 0.81 nm for the reference to 9.45 ± 2.08 nm for the sample containing CMS-221 (Figure 4-2). This difference likely stems from a phase separation between the PDMS and PEG-PDMS copolymer at the molecular scale. However, this situation did not cause any serious issues, such as heterogeneity, at a larger scale. Furthermore, DSC confirmed that adding 2.5% of CMS-221 copolymer to PDMS decreased the ice nucleation temperature from −16.53 to −18.44 °C; this shift can be attributed to hydrogen bonds formed between water molecules and hydrophilic groups at the surface. This hydrogen bonding produces an unfrozen layer that slows the transfer of water molecules to create ice nuclei because of an increased viscosity at the water–surface interface. Furthermore, this QLL prolongs ice nucleation. For example, the sample containing 2.5% PEG-PDMS copolymer froze completely after around 845 s, whereas the reference PDMS froze after approximately 240 s at 20 °C.

The presence of this unfrozen layer on the surface also reduced ice adhesion strength from around 350 kPa to approximately 96 kPa, as measured by the micro-push-off test. Such a layer acts as a lubricant to facilitate ice slippage on the surface, consequently decreasing ice adhesion.

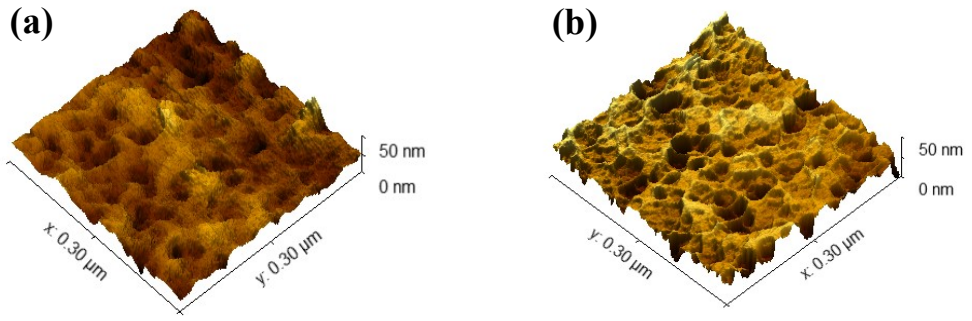

Figure 4-2. *Topographical maps of (a) the reference and (b) sample containing the 2.5% PEG-PDMS copolymer. Images were obtained by atomic force microscopy (AFM).*

4.4.2 Selecting the PCM combination

Freezing rain and drizzle can produce glaze ice [254], which is difficult to remove from an exposed surface because of the high adhesion of glaze [28]. Glaze ice represents one of the harshest icing conditions [263], occurring particularly between 0 and −10 °C [246]. Therefore, we prepared a range of PCM combinations to obtain an optimized solidification temperature range for preventing glazing conditions. The endothermic graphs of n-dodecane and n-tetradecane peaked at approximately −9 and 6 °C, respectively (Figure 4-3). Adding more n-dodecane to n-tetradecane led to a shift in the maximum peak temperature toward the lower temperatures. Therefore, given the supercooling of the PCM, we could expect a more desirable temperature range for

releasing latent heat during the exothermic process. As the PCM mixtures cooled, they started to release their latent heat below 0 °C (Figure 4-3b). Increasing the content of n-dodecane in the PCM mixture shifted the phase-changing temperature range. Although all combinations could serve anti-icing purposes, we selected the 2:8 ratio (n-dodecane: n-tetradecane) as the onset temperature on this ratio's freezing curve was approximately 0 °C. Therefore, this combination can release latent heat over the temperature range that glaze ice could be very likely produced. It was also noteworthy that adding 3 wt.% n-hexatriacontane to each mixture reduced the degree of supercooling. Encapsulation can enhance supercooling [23,215], thus, the presence of 3 wt.% n-hexatriacontane can control this temperature shift within a more desirable range.

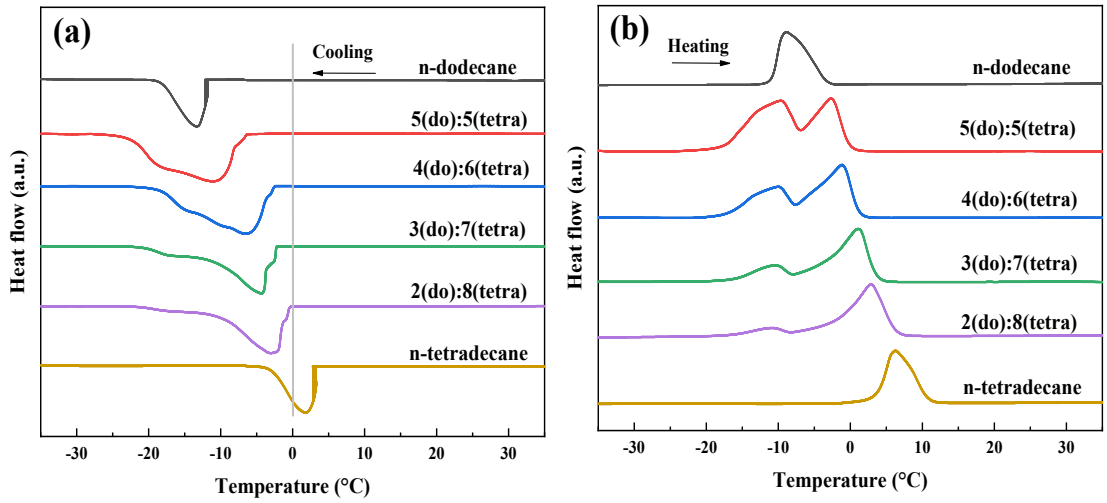

Figure 4-3. *Differential scanning calorimetry thermograms of the different combinations of n-dodecane and n-tetradecane during exothermic (a) and endothermic (b) processes.*

4.4.3 Encapsulation of the PCM mixture

The mixture of n-dodecane and n-tetradecane (selected ratio of 2:8) was encapsulated within a poly urea–formaldehyde (PUF) shell. SEM micrographs show that microcapsules were spherical when using EMA as an emulsifier (Figure 4-4a) [251].

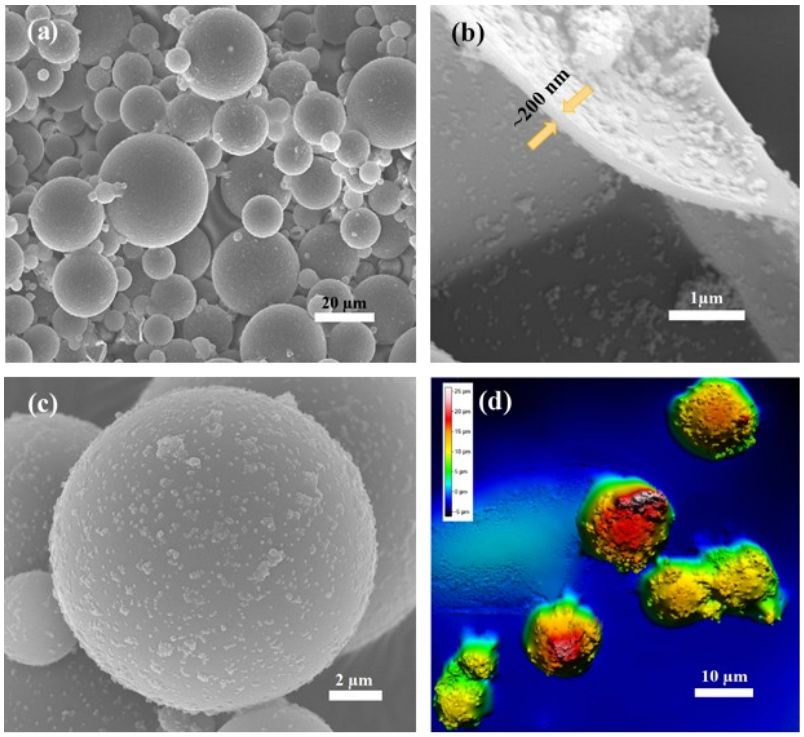

Figure 4-4. *SEM images illustrating (a) spherical microcapsules, (b) poly urea–formaldehyde (PUF) shell thickness, (c) a PCM microcapsule surface, and (d) a topographical map of microcapsules obtained by profilometry.*

Microcapsule shell thickness was approximately 200 nm (Figure 4-4b), and the encapsulation yield (ratio of the mass of the dried product to the total mass values of

the encapsulation ingredients) was approximately 70%. Moreover, SEM image (Figure 4-4c) and 3D topographical (Figure 4-4d) images of the microcapsules confirmed qualitatively that the microcapsules had surface asperities, which enhance bonding between the microcapsules and the matrix. Furthermore, the particle size distribution of the microcapsules was relatively wide; their particle size ranged generally from 5 to 25 µm (Figure 4-5a).

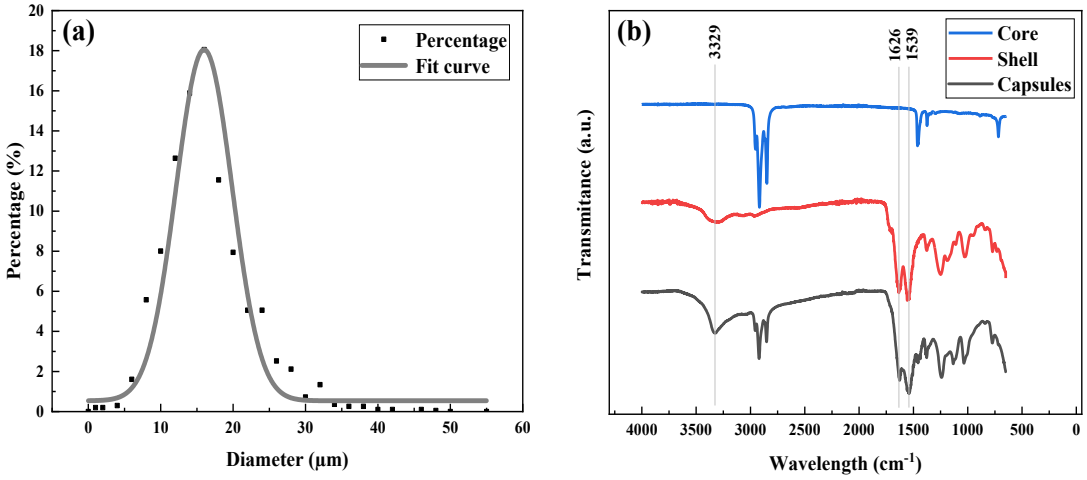

Figure 4-5. *(a) Size distribution of the PCM microcapsules and (b) the ATR-FTIR spectra corresponding to the shell material, PCM-filled microcapsules, and core material.*

We used FTIR to study the chemical structure of the PCM mixture, PUF shell, and the microcapsules (Figure 4-5b). The identified peaks of the formation of poly urea–formaldehyde (PUF) appeared as an N–H stretching vibration at about 1550 cm^{-1} and a C═O stretching vibration at 1640 cm^{-1}. The FTIR spectrum of the shell material contained a stretching vibration of the N–H and O–H bonds between 3100 and 3500 cm^{-1} [264,265]. The characteristic peaks of both the shell material and the PCM

mixture were observed in the spectrum of the microcapsules. Therefore, FTIR analysis confirmed that the PCM mixture was successfully encapsulated inside the PUF shell.

4.4.4 Incorporating the PCM microcapsules within the aqueous self-lubricating coating

It is essential to disperse the microcapsules uniformly within the matrix to improve PCM performance. Microcapsule agglomeration in some surface regions means that other surface sections do not contain PCM microcapsules; thus, in these cases of agglomeration, the greater number of microcapsules are required to ensure PCM microcapsules cover the entire surface. However, increasing the number of microcapsules favors greater mechanical failure and could increase the adhesion of ice on the surface related to greater surface roughness. To avoid this issue, we diluted the PDMS mixture with hexane to reduce the risk of agglomeration and enhance the flowability of the microcapsule mixture. We also used magnetic stirring to disperse microcapsules, produce a better PCM homogeneity within the coating, and prevent the destruction of microcapsules during homogenization process. The cross-sectional micrographs confirmed that the microcapsules were, to a large extent, dispersed uniformly throughout the elastomeric matrix (Figure 4-6).

Moreover, microcapsules were well covered by the matrix; therefore, the prepared PCM microcapsules were protected against mechanical stresses. The surface roughness of microcapsules enhances the adhesion between the microcapsules and the matrix to produce this protection (see Figure 4-4c and Figure 4-4d).

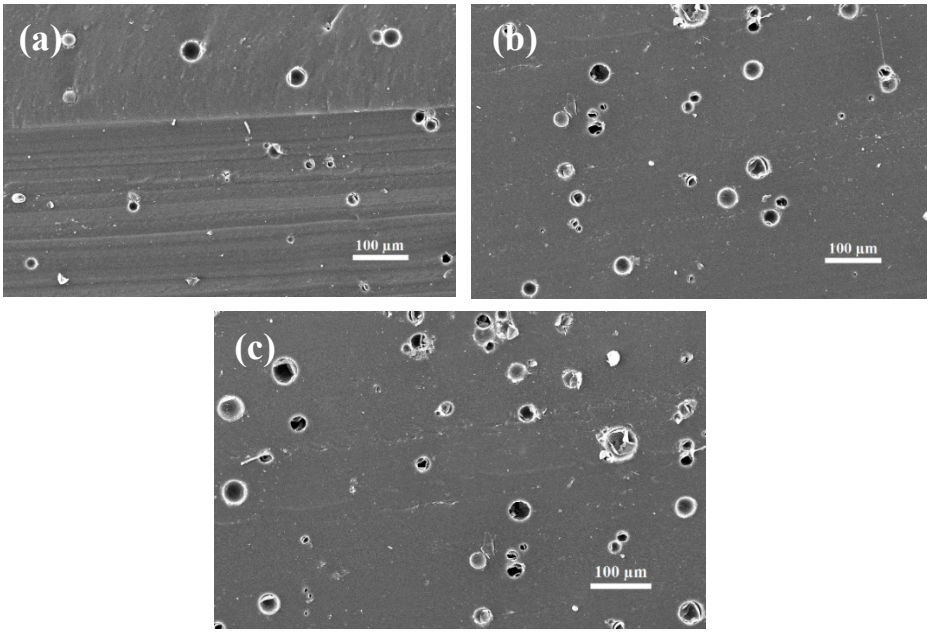

Figure 4-6. *Cross-sectional micrographs of samples (a) PP5, (b) PP10, and (c) PP15.*

4.4.5 Surface characterization

The surface parameters of the fabricated coatings are key for evaluating surface properties and icephobicity. The topographical maps of the samples (Figure 4-7) and their corresponding surface roughness values, expressed as the root mean square (RMS) roughness (S_q), were obtained by profilometry.

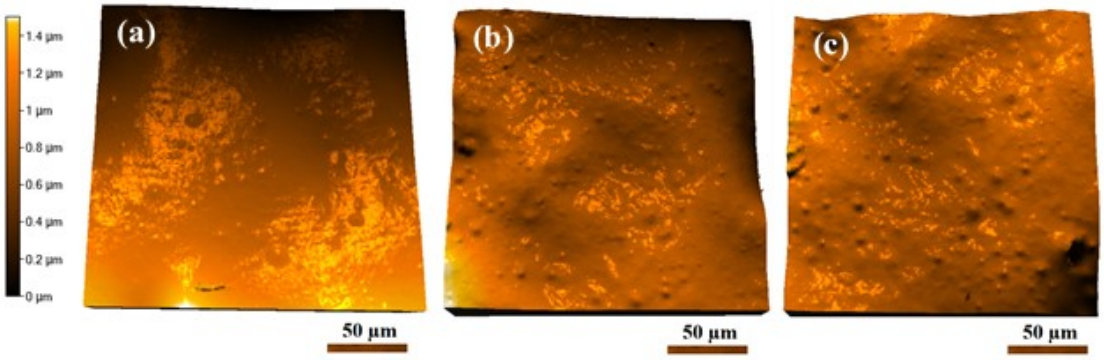

Figure 4-7. *The 3D topographical maps of the samples containing (a) 5%, (b) 10%, and (c) 15 wt.% PCM microcapsules.*

The S_q for samples containing 5%, 10%, and 15% PCM microcapsules was 102 ± 10, 163 ± 10, and 250 ± 20 nm, respectively. When we compare the S_q for samples with PDMS (S_q: 6.81 nm) and samples containing 2.5% PEG-PDMS copolymer (S_q: 9.45 nm), we note that the surface roughness of the samples increased with the addition of greater amounts of microcapsules. However, water contact angle (WCA) measurements showed that the presence of the microcapsules did not significantly affect sample wettability (Figure 4-8a). Indeed, the surface structure of the samples did not change as expected, e.g., a more effective trapping of air within the asperities, and acted as a superhydrophobic surface (WCA >150°). Furthermore, the contact angle hysteresis of the samples fluctuated between 30° and 35° without any meaningful trend among the samples.

4.4.6 Icephobicity characterization

4.4.6.1 Ice nucleation temperature and delay in complete freezing

Blending PEG-PDMS copolymer within the elastomeric matrix could reduce the ice nucleation temperature and delayed freezing. These effects likely stem from the liquid-like layer formed at the water–surface interface because of hydrogen bonds between the water and hydrophilic groups of the coating. We predicted that adding PCM microcapsules to the PDMS matrix containing the PEG-PDMS copolymer would further reduce the ice nucleation temperature and delay freezing. DSC analysis confirmed that the releasing/restoring heat capability of the PCM mixture was retained when the PCM was encapsulated and embedded within the coating as microcapsules (Figure 4-8b). Furthermore, the corresponding endothermic and exothermic curves of

the microcapsules and Sample PP15 had, to a large extent, similar onset and ending phase-changing temperatures.

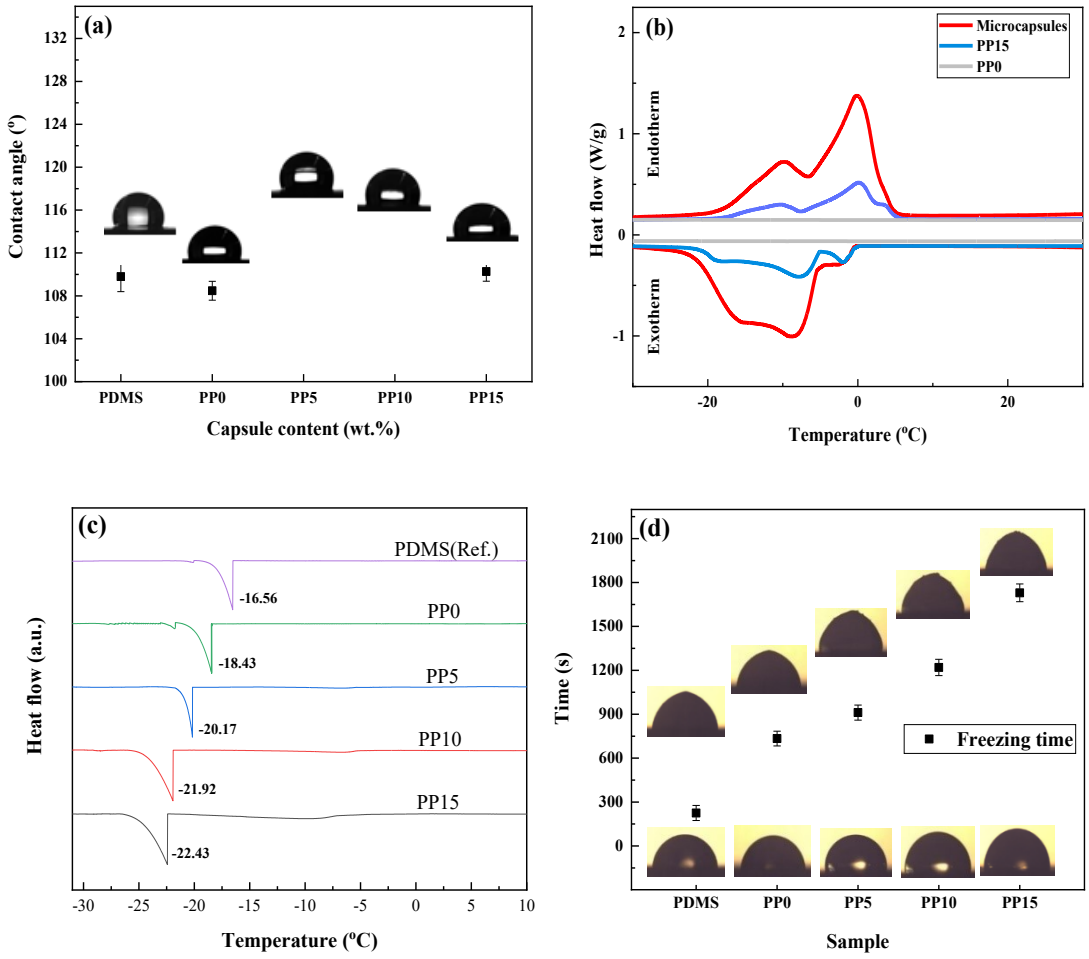

Figure 4-8. *(a) Relationship between water contact angle and PCM microcapsule content; (b) The evaluation of the phase change capability of PCM microcapsules, sample PP0, and PP15 (c) delayed ice nucleation temperature, evaluated using differential scanning calorimetry (DSC); (d) Freezing time on the prepared samples with the images of the water droplets at t = 0 s and at the instant of complete freezing.*

DSC analysis also confirmed that ice nucleation temperature shifted toward colder temperatures for PCM-microcapsule-containing samples (Figure 4-8c). Water

droplets on 15% PCM samples were frozen at −22.4 °C, whereas samples containing only 2.5% PEG-PDMS copolymer and lacking microcapsules had an ice nucleation temperature of −18.4 °C. Latent heat release by the PCM preserved the QLL at lower temperatures, thereby delaying ice nucleation. Freezing times also support this idea, as complete freezing time increased from 745 s for PP0 to 1541 s for the 15% PCM samples (Figure 4-8d).

Therefore, we confirmed that the PCM within the matrix enhances the anti-icing performance of the self-lubricating coatings, and greater amounts of microcapsules can promote this effect further by releasing latent heat to maintain the QLL at the interface. Because of the viscous effect of this layer, the nucleation process would be slowed while the QLL is present.

4.4.6.2 Ice accumulation

The static accumulation test (SAT) was performed at different angles to evaluate surface ice accumulation. A comparison of the surface containing the PEG-PDMS copolymer with the PDMS coating alone confirmed including the copolymer within the PDMS coating reduced ice accumulation on the surface of the inclined samples (Fig. 8a). The reduced ice accumulation is likely because of the lubricating effect of the created QLL on the hydrophilic group–containing sample combined with the gravitational force; greater inclination heightens the tangential component of the gravitational force—$W \cdot sin\alpha$ (W: ice weight, α: tilted angle)—and favors less ice accumulation at higher angles.

We then evaluated the effect of incorporating PCM microcapsules within the PEG-PDMS copolymer-containing coatings on ice accumulation. The microcapsule

presence further reduced ice accumulation on the sample surfaces (Figure 4-8a), observed at all angles (45° and 80°).

4.4.6.3 Ice adhesion measurements

Reduced ice adhesion affects the removal or accumulation of ice on a surface. We used the micro-push-off test to evaluate the ice adhesion strength of samples containing PCM microcapsules. Unlike the conventional test, this apparatus allows real-time monitoring of the freezing water droplet and the measuring of ice adhesion after a short period after complete freezing. This moment of complete freezing represents the moment of the temperature range at which PCM releases its latent heat, thereby affecting ice adhesion. Embedding PCM microcapsules within the self-lubricating matrix reduced ice adhesion (Figure 4-9a), and ice adhesion strength decreased with greater concentrations of incorporated PCM microcapsules. For samples containing 5% PCM microcapsules, we did not observe a clear reduction in ice adhesion; however, when the concentration of microcapsules was doubled, and for samples having 15% microcapsules, this reduction became apparent. The release of latent heat by PCM further lowered ice adhesion by preserving the existing QLL for a longer duration. The QLL already acts as a lubricant and reduces surface ice adhesion strength. The added PCM microcapsules release a large amount of heat during their phase change to add to the already lower ice adhesion strength. We observed a clear relationship between ice adhesion and ice accumulation, as a lower ice adhesion strength reduced the amount of accumulated ice on the surface.

4.4.7 Durability

The long-term durability of the fabricated coatings against multiple icing events is essential for applying anti-icing surfaces as a passive strategy. Therefore, we combined the micro-push-off method and 10 subsequent icing/de-icing tests to evaluate the long-term stability of the coating's icephobicity. Over the 10 cycles, we did not observe significant changes in the ice adhesion strength of all samples (Figure 4-9b). For sample PP15, however, the ice adhesion strength increased slightly after subsequent de-icing cycles. This reduced durability reflects the weaker mechanical properties of the coating with an increased microcapsule content.

The water contact angle of the fabricated coatings was measured after the 10^{th} icing/de-icing cycle (Figure 4-9c); the coatings presented no considerable change in wettability after the multiple cycles. We also conducted the tensile test to evaluate the mechanical properties of the fabricated coatings (Figure 4-9d).

We observed that blending the PEG-PDMS copolymer with the elastomeric matrix weakened the existing mechanical properties of the matrix (Young's modulus, toughness, and strain at break). This change relates to the low molecular weight of the copolymer (~4000 g/mol), which acts as a plasticizer. This reduction in modulus, and therefore an increased difference between mechanical properties of the matrix and the ice, lowers ice adhesion strength. Incorporating the PCM microcapsules within the PEG-PDMS copolymer matrix reduces the mechanical strength even further, as impregnating the soft matrix with rigid particles can promote stress concentration areas in the free film. These locations are the initial break points during tensile tests. Reduced mechanical properties can favor anti-icing properties; however, an excessive reduction in mechanical properties can result in coating failure and, consequently, reduced

durability. We note the obvious example of Sample PP15 that showed increased ice adhesion after 10 icing/de-icing cycles.

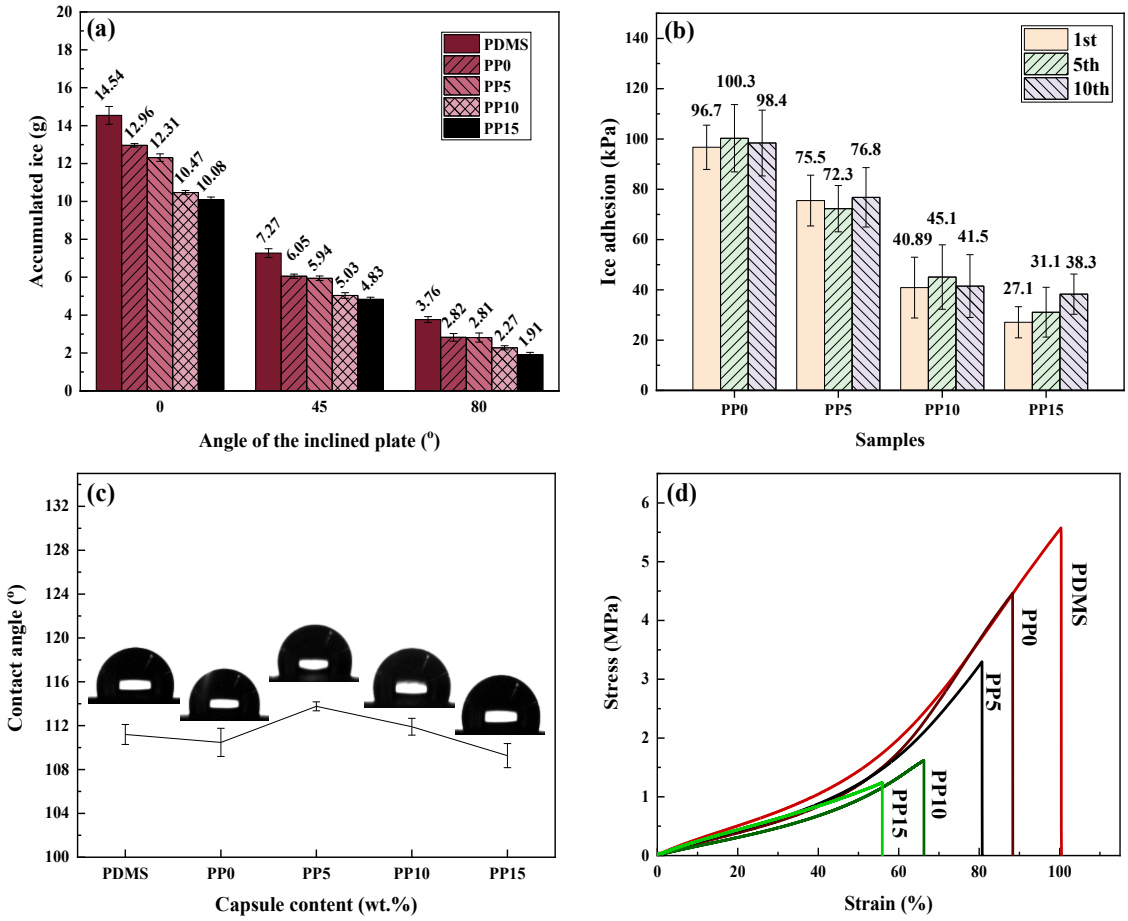

Figure 4-9. *(a) The amount of accumulated ice on the prepared coatings inclined at 0°, 45°, and 80° as measured by the static accumulation test (SAT); (b) the ice adhesion strength of the PCM-containing samples over 10 icing/de-icing cycles; the ice adhesion strengths of PDMS coating corresponding to first, fifth, and tenth cycles were measured as 379.4±49.3, 385.4±40.2, and 404.2±45.1 kPa, respectively; (c) water contact angle of the prepared samples after 10 icing/de-icing cycles; (d) stress–strain curves of samples differing in their PCM-microcapsule content.*

4.5 Conclusions

We have designed a new icephobic strategy by embedding PCM microcapsules within a self-lubricating coating containing a PEG-PDMS copolymer. We aimed to benefit from the anti-icing potential of the aqueous self-lubricating coatings and phase change materials as an integrated coating system. To attain the optimal anti-icing surface, we optimized the ratio of two PCMs, n-dodecane and n-tetradecane, and successfully encapsulated their optimized mixture within a UF shell. Afterward, the 10–20 μm PCM microcapsules were incorporated within a PDMS matrix containing 2.5 wt.% of hydroxyl-terminated PEG-PDMS copolymer. Although the PEG-PDMS copolymer–containing matrix presented anti-icing characteristics, such as reduced ice nucleation time, delayed freezing, and more limited ice accumulation, embedding PCM microcapsules into the matrix enhanced these properties. Latent heat released by the PCM mixture complements the viscous QLL of the PEG-PDMS copolymer that acts as an unfrozen lubricant on the surface; the QLL is produced by a strong hydrogen bonding between water molecules and the PEG. Indeed, the synergistic effect of combining aqueous self-lubricating coating (containing 2.5 wt.% PEG-PDMS copolymer) and phase change materials resulted in decreased ice adhesion strength from about 380 kPa (for PDMS) to 27 kPa (for PP15). It is noteworthy that the effect of the PCM presence on anti-icing performance was temporal. We found the PCM-embedded matrix maintained its icephobicity after 10 icing/de-icing cycles. We also noted that adding too many microcapsules weakens the matrix's mechanical properties, thereby reducing its long-term utility. To sum up, using each strategy, namely aqueous self-lubricating coating or phase change materials (PCMs) may have some limits; but, combing these strategies can considerably enhance icephobic performance of the

prepared coatings due to synergistic effect. This idea can provide a new solution to fabricate anti-icing surfaces for applying on many settings exposed to the harsh-weather conditions.

Acknowledgments

The authors acknowledge all support from the Natural Sciences and Engineering Research Council of Canada (NSERC), Hydro-Québec, and PRIMA Quebec. The authors would like to thank Ms Caroline Blackburn at the Anti-icing Materials International Laboratory (AMIL), UQAC, for helping carry out the SAT test. The authors would also like to thank Ms Hellene Gauthier Institut de recherche d′Hydro-Québec (IREQ), for all her support.

Chapter 5: Conclusions

In this chapter, the key findings of this research work are summarized as partial and general conclusions. First, the main results obtained in each paper are separately presented, and the general conclusion of the project is provided.

Icephobic properties of aqueous self-lubricating coatings containing PEG–PDMS copolymers

- We blended PEG–PDMS copolymers into an elastomeric matrix to obtain aqueous self-lubricating coatings. The copolymers had different molecular weights and terminated groups.
- The effects of copolymer type and content on wettability and surface morphology were evaluated. In general, increasing the copolymer percentage in the matrix decreased the water contact angle over time and consequently promoted surface wettability.
- Samples containing methoxy-terminated copolymers exhibited phase separation by increasing the copolymer content. We observed that the surface of samples containing this copolymer changed from homogeneous to heterogeneous by increasing the copolymer amount.
- Increased copolymer content improved the icephobic properties of the prepared coatings because of the produced hydrogen bonds between the surface and water molecules. This outcome resulted in the formation of a non-frozen quasi-liquid-like layer that delayed ice nucleation temperature and heightened freezing time.

- The ice adhesion strengths of the fabricated samples were evaluated via push-off and centrifuge tests. For the samples containing hydroxyl-terminated copolymers, the ice adhesion strength decreased from 90.3 kPa to 39.1 kPa and from 134 kPa to 99.5 kPa in the push-off and centrifugal tests, respectively, by increasing the copolymer percentage. In comparison, the corresponding values for the samples containing methoxy-terminated copolymer were reduced until the amounts of 5% (from 62.1 kPa to 53.2 kPa) and 2.5% (from 124.5 kPa to 85.5 kPa), followed by heightened ice adhesion strength.
- The ice adhesion strengths of the samples containing 1%–5% hydroxyl-terminated copolymer did not change remarkably over the seven icing/de-icing cycles. The values for thesamples containing 1%–5% methoxy-terminated copolymer remained at 72 kPa over the subsequent de-icing events.
- Differences between the mechanical characteristics of ice and the coating have an essential role in ice removal from the surface. However, an excessive reduction in hardness as a result of increased copolymer content can cause mechanical failure and consequently reduce the durability of the fabricated coatings.

An intelligent icephobic coating based on encapsulated phase change materials (PCM)

- In this article, we reported the encapsulation of a mixture of two PCMs, namely, *n*-dodecane and *n*-tetradecane (ratio of 3:7) via in situ polymerization within the UF shell. Then, different percentages of the prepared microcapsules were incorporated into a PDMS matrix.

- The microcapsules were spherical in shape and had a relatively wide size distribution curve. About 70% of them had a diameter between 5 and 15 μm. FTIR analysis showed that the peaks corresponding to each of the shell and core materials appeared in the FTIR spectrum of the microcapsules. The results confirmed that the PCM mixture was successfully encapsulated within the shell material.

- SEM images show that the PCM microcapsules were homogeneously dispersed in the matrix and bound very well with the PDMS matrix. Furthermore, the DSC investigation confirmed that the ability of the PCM to release latent heat was preserved after enclosure within the shell material.

- DSC analysis also showed that embedding PCM microcapsules within the PDMS matrix can decrease ice nucleation temperature due to latent heat release. Increasing the microcapsule percentages in the coating further decreased the ice nucleation temperature. In agreement with these results, the complete freezing time increased from 181.2 s (PDMS) to 1194.6 s (sample containing 30% microcapsules) when the microcapsule content increased as evaluated at −20 °C.

- Embedding the microcapsules improves the performance of the coating in reducing the amount of ice accumulation on the surface. The released latent heat by PCM increased the surface temperature of the samples, which likely contributed to the reduction of ice accumulation.

- The average ice adhesion strengths of the PCM-containing samples were generally lower than that of the reference (PDMS). Two possible mechanisms, namely, the formation of a quasi-liquid layer (QLL) and thermal expansion differences, were proposed to have stemmed from the release of PCM latent heat to justify the reduced ice adhesion.

A novel hybrid anti-icing surface combining an aqueous self-lubricating coating and phase-change materials

- We present a new approach to fabricate anti-icing coatings by incorporating PCM microcapsules within an aqueous self-lubricating coating. For this purpose, we optimized the ratios of the PCMs, *n*-dodecane and *n*-tetradecane, to obtain a desirable temperature range for latent heat release. Then, the selected mixture was encapsulated within the UF shell via in situ polymerization, and the produced microcapsules with diameters between 10 and 20 μm were embedded within a PDMS coating containing 2.5 wt.% PEG–PDMS copolymer.
- The synergistic effect of combining PEG–PDMS copolymer-containing coatings and PCMs led to the enhanced anti-icing and de-icing properties. Incorporating the PCM microcapsules within the coatings containing 2.5 wt.% PEG–PDMS copolymer decreased the ice nucleation temperature from −18.4 °C (for the reference) to −22.4 °C (for coating containing 15% microcapsules). In agreement with the DSC results, the complete freezing time increased from 745 s to 1541 s.
- The microcapsule in the aqueous self-lubricating coating caused a further reduction in ice accumulation on the sample surfaces. This result can be related to the decreased ice adhesion resulting from the combination of the lubricating effect of the QLL and the PCMs' latent heat release.
- Combining the micro-push-off test and 10 icing/de-icing cycles to evaluate coating durability confirmed that the samples containing PCM microcapsules did not show considerable changes over the subsequent de-icing trials. Furthermore, the

wettability of the fabricated samples did not vary substantially after 10 icing/de-icing cycles.

- Embedding the PCM microcapsules within the aqueous self-lubricating coatings reduced their mechanical characteristics. This outcome can be attributed to the increased stress concentration areas in the coatings due to presence of rigid particles within the elastomeric matrix.

General conclusions

In this work, we designed a novel icephobic coating using the synergistic effect of combining two anti-icing strategies, namely, aqueous self-lubricating coatings and PCMs. We first developed icephobic coatings using either method to identify the drawbacks and limits associated with each of the above-mentioned strategies. Therefore, we fabricated an aqueous self-lubricating coating inspired from the principles of ice skate sliding by incorporating PEG–PDMS copolymers into the PDMS matrix. We evaluated the surface characteristics of the prepared coatings, such as wettability, morphology, and topography. The samples containing hydroxyl-terminated copolymer showed no micro-scale immiscibility between the copolymer and matrix, whereas the sample containing methoxy-terminated copolymer had a saturation of copolymer in the mixture at lower concentrations. Furthermore, the presence of the PEG–PDMS copolymer can positively affect the icephobic characteristics of the prepared coatings. The increased content of these copolymers decreased the ice nucleation temperature and lengthened the freezing delay time. The ice adhesion measurements confirmed that incorporating PEG–PDMS copolymers within the PDMS matrix resulted in decreased ice adhesion strength, which was due to the

formation of the aqueous liquid-like layer on the surface. For samples containing methoxy-terminated copolymer, the immiscibility of the copolymer and the matrix with higher copolymer content heightened the surface roughness. Therefore, it promoted the possibility of mechanical interlocking between ice and the coating, resulting in increased ice adhesion strength. Higher copolymer content can have negative effects on mechanical properties and reduce the durability of the prepared coatings.

Second, we designed a smart icephobic coating by embedding the PCM microcapsules within the elastomeric matrix. The PCM mixture encapsulated within the UF shell releases its latent heat as the temperature decreases. A comprehensive set of icephobic characterization techniques was employed to assess the anti-icing and de-icing performances of the fabricated coatings. The latent heat release by the encapsulated PCM resulted in decreased ice nucleation temperature and increased complete freezing time. Incorporating PCM microcapsules reduced ice adhesion strength and consequently decreased ice accumulation on the surface via the formation of a liquid-like layer or by thermal expansion differences. Increasing the abundance of microcapsules within the matrix lowered the mechanical properties and reduced the durability of the coatings. It is noteworthy that the time period for latent heat release was limited, and as temperature stabilizes, the presence of microcapsules may increase adhesion strength as a result of increased surface roughness.

Finally, we presented an anti-icing strategy using the impregnation of an aqueous self-lubricating coating with PCM microcapsules. Given the results obtained in the previous steps, we selected the PDMS matrix containing 2.5 wt.% hydroxyl-terminated copolymer as the binder and then embedded various amounts of the PCM

microcapsules into the matrix. Measurements of ice nucleation temperature confirmed that the prepared coatings offered enhanced anti-icing performance compared with the self-lubricating coatings lacking PCM microcapsules. Moreover, the aqueous self-lubricating coatings showed further reduced ice adhesion strength and therefore reduced ice accumulation. These enhanced icephobic properties stemmed from the positive effect of latent heat release on the produced liquid-like layers.

Chapter 6: Recommendations

In this Ph.D. thesis, we developed smart icephobic coatings using two different approaches, namely, aqueous self-lubricating coatings and phase-change materials (PCMs). The coatings prepared using these methods alone or in combination demonstrated desirable icephobicity. Nevertheless, the following suggestions have been provided for further investigations.

- The main matrix has a remarkable effect on the mechanical properties of the coatings; therefore, other polymeric binders, such as polyurethane resins, could be selected to fabricate coatings with further mechanical robustness. Notably, the selected matrix must not have undesirable impact on the anti-icing and de-icing performances of the coating system.

- Parameters for encapsulation, such as optimum size distribution and shell thickness, could be further investigated in terms of process parameters, such as process temperature, agitation speed, and process time.

- In this work, we used a combination of two common PCMS, namely, n-dodecane and n-tetradecane. Other types of PCMs with sub-zero phase-change temperatures may release higher latent heat in comparison to the above-mentioned PCMs. Moreover, other shell materials, such as inorganic ones, show better thermal conductivity than organic-based shells.

- The thermal properties of the coating system can be considered for the future. Furthermore, incorporating some substances, such as TiO_2 nanoparticles, into the matrix is expected to have remarkable effects on improving the thermal conductivity

of the coatings. In fact, enhanced thermal conductivity could affect the icephobic performance of the prepared coatings.

- We tried to open a new avenue toward developing new smart icephobic coatings using the synergistic effects of the two icephobic strategies. Accordingly, other de-icing strategies, such as superhydrophobic surfaces, can also be combined with PCMs.

- The electrical properties of the prepared coatings can be evaluated to understand their potential in high-voltage insulator application. In this regard, the electrical characteristics of the coatings, including permittivity and loss factor, resistance against tracking and erosion, electrical performance under controlled humidity conditions, and flashover voltage, could be assessed.

References

[1] R. Menini, M. Farzaneh, Advanced icephobic coatings, J. Adhes. Sci. Technol. 25 (2011) 971–992. https://doi.org/10.1163/016942410X533372.

[2] M. Farzaneh, Ice accretions on high-voltage conductors and insulators and related phenomena, Philos. Trans. R. Soc. A Math. Phys. Eng. Sci. 358 (2000) 2971–3005. https://doi.org/10.1098/rsta.2000.0692.

[3] K. Maghsoudi, E. Vazirinasab, G. Momen, R. Jafari, Icephobicity and durability assessment of superhydrophobic surfaces: The role of surface roughness and the ice adhesion measurement technique, J. Mater. Process. Technol. 276 (2021) 116415. https://doi.org/10.1016/j.jmatprotec.2020.116883.

[4] K. Maghsoudi, E. Vazirinasab, R. Jafari, G. Momen, Evaluating the effect of processing parameters on the replication quality in the micro compression molding of silicone rubber, Mater. Manuf. Process. (2020). https://doi.org/10.1080/10426914.2020.1779942.

[5] Z. He, S. Xiao, H. Gao, J. He, Z. Zhang, Multiscale crack initiator promoted super-low ice adhesion surfaces, Soft Matter. (2017). https://doi.org/10.1039/c7sm01511a.

[6] Z. Wang, Recent progress on ultrasonic de-icing technique used for wind power generation, high-voltage transmission line and aircraft, Energy Build. 140 (2017) 42–49. https://doi.org/10.1016/j.enbuild.2017.01.072.

[7] Y. Cao, Z. Wu, Y. Su, Z. Xu, Aircraft flight characteristics in icing conditions, Prog. Aerosp. Sci. 74 (2015) 62–80. https://doi.org/10.1016/j.paerosci.2014.12.001.

[8] N. Dalili, A. Edrisy, R. Carriveau, A review of surface engineering issues critical to wind turbine performance, Renew. Sustain. Energy Rev. 13 (2009) 428–438. https://doi.org/10.1016/j.rser.2007.11.009.

[9] A.P. Broeren, S. Lee, C. Clark, Aerodynamic effects of anti-icing fluids on a thin high-performance wing section, J. Aircr. 53 (2016) 451–462. https://doi.org/10.2514/1.C033384.

[10] W.J. Jasinski, M.S. Selig, M.B. Bragg, N. Shawn C, Wind Turbine Performance Under Icing Conditions Aerospace sciences, Aerosp. Sci. 120 (1) (1997) 60–65. https://doi.org/10.1115/1.2888048.

[11] M. Lacavalla, P. Marcacci, A. Frigerio, Forecasting and monitoring wet-snow sleeve on overhead power lines in Italy, 2015 IEEE Work. Environ. Energy, Struct. Monit. Syst. EESMS 2015 - Proc. (2015) 78–83.

https://doi.org/10.1109/EESMS.2015.7175856.

[12] M. Ruan, J.W. Wang, Q.L. Liu, F.M. Ma, Z.L. Yu, W. Feng, Y. Chen, Superhydrophobic and anti-icing properties of sol–gel prepared alumina coatings, Russ. J. Non-Ferrous Met. 57 (2016) 638–645. https://doi.org/10.3103/S1067821216060122.

[13] E. Vazirinasab, K. Maghsoudi, R. Jafari, G. Momen, A comparative study of the icephobic and self-cleaning properties of Teflon materials having different surface morphologies, J. Mater. Process. Technol. 276 (2020) 116415. https://doi.org/10.1016/j.jmatprotec.2019.116415.

[14] M. Farzaneh, Atmospheric icing of power networks, 2008. https://doi.org/10.1007/978-1-4020-8531-4.

[15] J.W. Busby, K. Baker, M.D. Bazilian, A.Q. Gilbert, E. Grubert, V. Rai, J.D. Rhodes, S. Shidore, C.A. Smith, M.E. Webber, Cascading risks: Understanding the 2021 winter blackout in Texas, Energy Res. Soc. Sci. 77 (2021) 102106. https://doi.org/10.1016/j.erss.2021.102106.

[16] Arshad, G. Momen, M. Farzaneh, A. Nekahi, Properties and applications of superhydrophobic coatings in high voltage outdoor insulation: A review, IEEE Trans. Dielectr. Electr. Insul. 24 (2017) 3630–3646. https://doi.org/10.1109/TDEI.2017.006725.

[17] M. Farzaneh, W.A. Chisholm, Mitigation Options for Improved Performance in Pollution Conditions, in: Insul. Icing Polluted Environ., 2009. https://doi.org/10.1002/9780470496251.ch6.

[18] W. Liao, Z. Jia, Z. Guan, L. Wang, J. Yang, J. Fan, Z. Su, J. Zhou, Reducing ice accumulation on insulators by applying semiconducting RTV silicone coating, IEEE Trans. Dielectr. Electr. Insul. (2007). https://doi.org/10.1109/TDEI.2007.4401227.

[19] C. Challener, The intelligence behind smart coatings, JCT CoatingsTech. 3 (2006) 50–55.

[20] J. Thévenot, H. Oliveira, O. Sandre, S. Lecommandoux, Magnetic responsive polymer composite materials, Chem. Soc. Rev. 42 (2013) 7099–7116. https://doi.org/10.1039/c3cs60058k.

[21] M. Shamshiri, R. Jafari, G. Momen, Potential use of smart coatings for icephobic applications: A review, Surf. Coatings Technol. 424 (2021) 127656. https://doi.org/10.1016/j.surfcoat.2021.127656.

[22] A. Azimi Yancheshme, A. Allahdini, K. Maghsoudi, R. Jafari, G. Momen, Potential anti-icing applications of encapsulated phase change material–

embedded coatings; a review, J. Energy Storage. 31 (2020) 101638. https://doi.org/10.1016/j.est.2020.101638.

[23] Y. Yuan, H. Xiang, G. Liu, R. Liao, Fabrication of phase change microcapsules and their applications to anti-icing coating, Surfaces and Interfaces. 27 (2021) 101516. https://doi.org/10.1016/j.surfin.2021.101516.

[24] M. Shamshiri, R. Jafari, G. Momen, Icephobic properties of aqueous self-lubricating coatings containing PEG-PDMS copolymers, Prog. Org. Coatings. 161 (2021) 106466. https://doi.org/10.1016/j.porgcoat.2021.106466.

[25] M. Shamshiri, R. Jafari, G. Momen, An intelligent icephobic coating based on encapsulated phase change materials (PCM), Colloids Surfaces A Physicochem. Eng. Asp. 655 (2022) 130157. https://doi.org/10.1016/j.colsurfa.2022.130157.

[26] M. Shamshiri, R. Jafari, G. Momen, A novel hybrid anti-icing surface combining an aqueous self-lubricating coating and phase-change materials, Prog. Org. Coatings. 177 (2023) 107414. https://doi.org/10.1016/j.porgcoat.2023.107414.

[27] R. Carriveau, A. Edrisy, P. Cadieux, R. Mailloux, Ice adhesion issues in renewable energy infrastructure, J. Adhes. Sci. Technol. 26 (2012) 447–461. https://doi.org/10.1163/016942411X574592.

[28] S. Rønneberg, C. Laforte, C. Volat, J. He, Z. Zhang, The effect of ice type on ice adhesion, AIP Adv. 9 (2019). https://doi.org/10.1063/1.5086242.

[29] L.L. Shao, L. Yang, C.L. Zhang, Comparison of heat pump performance using fin-and-tube and microchannel heat exchangers under frost conditions, Appl. Energy. 87 (2010) 1187–1197. https://doi.org/10.1016/j.apenergy.2009.08.021.

[30] H. Habibi, L. Cheng, H. Zheng, V. Kappatos, C. Selcuk, T.H. Gan, A dual de-icing system for wind turbine blades combining high-power ultrasonic guided waves and low-frequency forced vibrations, Renew. Energy. 83 (2015) 859–870. https://doi.org/10.1016/j.renene.2015.05.025.

[31] M. Susoff, K. Siegmann, C. Pfaffenroth, M. Hirayama, Evaluation of icephobic coatings - Screening of different coatings and influence of roughness, Appl. Surf. Sci. 282 (2013) 870–879. https://doi.org/10.1016/j.apsusc.2013.06.073.

[32] Q. He, W. He, F. Zhang, Y. Zhao, L. Li, X. Yang, F. Zhang, Research Progress of Self-Cleaning, Anti-Icing, and Aging Test Technology of Composite Insulators, Coatings. 12 (2022) 1224. https://doi.org/10.3390/coatings12081224.

[33] T. Rashid, H.A. Khawaja, K. Edvardsen, Review of marine icing and anti-/de-icing systems, J. Mar. Eng. Technol. 15 (2016) 79–87. https://doi.org/10.1080/20464177.2016.1216734.

[34] Z. Liu, A. Li, Q. Wang, Y. Chi, L. Zhang, Experimental study on a new type of thermal storage defrosting system for frost-free household refrigerators, Appl. Therm. Eng. 118 (2017) 256–265. https://doi.org/10.1016/j.applthermaleng.2017.02.077.

[35] A. Amendola, G. Mingione, On the problem of icing for modern civil aircraft, Air Sp. Eur. 3 (3-4) (2001) 214–217. https://doi.org/10.1016/s1290-0958(01)90098-x.

[36] X. Huang, N. Tepylo, V. Pommier-Budinger, M. Budinger, E. Bonaccurso, P. Villedieu, L. Bennani, A survey of icephobic coatings and their potential use in a hybrid coating/active ice protection system for aerospace applications, Prog. Aerosp. Sci. 105 (2019) 74–97. https://doi.org/10.1016/j.paerosci.2019.01.002.

[37] X. Sun, V.G. Damle, S. Liu, K. Rykaczewski, Bioinspired Stimuli-Responsive and Antifreeze-Secreting Anti-Icing Coatings, Adv. Mater. Interfaces. 2 (5) (2015) 1400479. https://doi.org/10.1002/admi.201400479.

[38] X. Huang, N. Tepylo, V. Pommier-Budinger, M. Budinger, E. Bonaccurso, P. Villedieu, L. Bennani, A survey of icephobic coatings and their potential use in a hybrid coating/active ice protection system for aerospace applications, Prog. Aerosp. Sci. 105 (2019) 74–97. https://doi.org/10.1016/j.paerosci.2019.01.002.

[39] H. Sojoudi, M. Wang, N.D. Boscher, G.H. McKinley, K.K. Gleason, Durable and scalable icephobic surfaces: Similarities and distinctions from superhydrophobic surfaces, Soft Matter. 12 (2016) 1938–1963. https://doi.org/10.1039/c5sm02295a.

[40] M. Yamazaki, A. Jemcov, H. Sakaue, A review on the current status of icing physics and mitigation in aviation, Aerospace. 8 (2021) 188. https://doi.org/10.3390/aerospace8070188.

[41] Q. Li, Z. Guo, Fundamentals of icing and common strategies for designing biomimetic anti-icing surfaces, J. Mater. Chem. A. 6 (2018) 13549–13581. https://doi.org/10.1039/c8ta03259a.

[42] T.M. Schutzius, S. Jung, T. Maitra, P. Eberle, C. Antonini, C. Stamatopoulos, D. Poulikakos, Physics of icing and rational design of surfaces with extraordinary icephobicity, Langmuir. 31 (2015) 4807–4821. https://doi.org/10.1021/la502586a.

[43] X. Zhou, G. Yang, C. Li, J. Wu, Functional microdroplet self-dislodging icephobic surfaces: A review from mechanism to synergic morphology, Appl. Therm. Eng. 215 (2022) 118928. https://doi.org/10.1016/j.applthermaleng.2022.118928.

[44] Y. Shen, X. Wu, J. Tao, C. Zhu, Y. Lai, Z. Chen, Icephobic materials:

Fundamentals, performance evaluation, and applications, Prog. Mater. Sci. 103 (2019) 509–557. https://doi.org/10.1016/j.pmatsci.2019.03.004.

[45] Z. Zhang, X.Y. Liu, Control of ice nucleation: Freezing and antifreeze strategies, Chem. Soc. Rev. 47 (2018) 7116–7139. https://doi.org/10.1039/c8cs00626a.

[46] T. Kling, F. Kling, D. Donadio, Structure and Dynamics of the Quasi-Liquid Layer at the Surface of Ice from Molecular Simulations, J. Phys. Chem. C. 122 (2018) 24780–24787. https://doi.org/10.1021/acs.jpcc.8b07724.

[47] S. Takagi, Approximate thermodynamics of the liquid-like layer on an ice sphere based on an interpretation of the wetting parameter, J. Colloid Interface Sci. 137 (1990) 446–455. https://doi.org/10.1016/0021-9797(90)90419-O.

[48] M.P. Goertz, X.Y. Zhu, J.E. Houston, Exploring the liquid-like layer on the ice surface, Langmuir. 25 (2009) 6905–6908. https://doi.org/10.1021/la9001994.

[49] A. Amirfazli, C. Antonini, Fundamentals of Anti- Icing Surfaces, in: Non-Wettable Surfaces Theory, Prep. Appl. Non-Wettable Surfaces, Royal Society of Chemistry, 2016: p. 319−346.

[50] V. Hejazi, K. Sobolev, M. Nosonovsky, From superhydrophobicity to icephobicity: Forces and interaction analysis, Sci. Rep. 3 (2013) 2194. https://doi.org/10.1038/srep02194.

[51] H. Sojoudi, M. Wang, N.D. Boscher, G.H. McKinley, K.K. Gleason, Durable and scalable icephobic surfaces: Similarities and distinctions from superhydrophobic surfaces, Soft Matter. 12 (2016) 1938–1963. https://doi.org/10.1039/c5sm02295a.

[52] A.J. Meuler, G.H. McKinley, R.E. Cohen, Exploiting topographical texture to impart icephobicity, ACS Nano. 4 (2010) 7048–7052. https://doi.org/10.1021/nn103214q.

[53] T. Li, T. Ren, J. He, The Inspiration of Nature: Natural Counterparts with Self-cleaning Functions, RSC Smart Mater. 2017–Janua (2017) 1–24. https://doi.org/10.1039/9781782623991-00001.

[54] M.I. Jamil, A. Ali, F. Haq, Q. Zhang, X. Zhan, F. Chen, Icephobic Strategies and Materials with Superwettability: Design Principles and Mechanism, Langmuir. 34 (2018) 15425–15444. https://doi.org/10.1021/acs.langmuir.8b03276.

[55] Y. Zhuo, V. Håkonsen, Z. He, S. Xiao, J. He, Z. Zhang, Enhancing the Mechanical Durability of Icephobic Surfaces by Introducing Autonomous Self-Healing Function, ACS Appl. Mater. Interfaces. 10 (14) (2018) 11972–11978. https://doi.org/10.1021/acsami.8b01866.

[56] K. Golovin, S.P.R. Kobaku, D.H. Lee, E.T. DiLoreto, J.M. Mabry, A. Tuteja, Designing durable icephobic surfaces, Sci. Adv. 2 (2016) e1501496. https://doi.org/10.1126/sciadv.1501496.

[57] L.B. Boinovich, A.M. Emelyanenko, K.A. Emelyanenko, E.B. Modin, Modus Operandi of Protective and Anti-icing Mechanisms Underlying the Design of Longstanding Outdoor Icephobic Coatings, ACS Nano. 13 (2019) 4335−4346. https://doi.org/10.1021/acsnano.8b09549.

[58] Peyman Irajizad, S. Nazifi, H. Ghasemi, Icephobic surfaces: Definition and figures of merit, Adv. Colloid Interface Sci. 269 (2019) 203–218. https://doi.org/10.1016/j.cis.2019.04.005.

[59] K. Mirshahidi, K. Alasvand Zarasvand, W. Luo, K. Golovin, A high throughput tensile ice adhesion measurement system, HardwareX. 8 (2020). https://doi.org/10.1016/j.ohx.2020.e00146.

[60] P. Irajizad, S. Nazifi, H. Ghasemi, Icephobic surfaces: Definition and figures of merit, Adv. Colloid Interface Sci. 269 (2019) 203–218. https://doi.org/10.1016/j.cis.2019.04.005.

[61] L. Boinovich, A.M. Emelyanenko, V. V. Korolev, A.S. Pashinin, Effect of wettability on sessile drop freezing: When superhydrophobicity stimulates an extreme freezing delay, Langmuir. 30 (6) (2014) 1659–1668. https://doi.org/10.1021/la403796g.

[62] A. Marmur, C. Della Volpe, S. Siboni, A. Amirfazli, J.W. Drelich, Contact angles and wettability: Towards common and accurate terminology, Surf. Innov. 5 (2017) 3–8. https://doi.org/10.1680/jsuin.17.00002.

[63] J. Jeevahan, M. Chandrasekaran, G. Britto Joseph, R.B. Durairaj, G. Mageshwaran, Superhydrophobic surfaces: a review on fundamentals, applications, and challenges, J. Coatings Technol. Res. 15 (2018) 231–250. https://doi.org/10.1007/s11998-017-0011-x.

[64] J.W. Drelich, L. Boinovich, E. Chibowski, C. Della Volpe, L. Hołysz, A. Marmur, S. Siboni, Contact angles: History of over 200 years of open questions, Surf. Innov. 8 (2020) 3–27. https://doi.org/10.1680/jsuin.19.00007.

[65] S.A. Kulinich, M. Farzaneh, How wetting hysteresis influences ice adhesion strength on superhydrophobic surfaces, Langmuir. 25 (16) (2009) 8854–8856. https://doi.org/10.1021/la901439c.

[66] A.J. Meuler, J.D. Smith, K.K. Varanasi, J.M. Mabry, G.H. McKinley, R.E. Cohen, Relationships between water wettability and ice adhesion, ACS Appl. Mater. Interfaces. 2 (11) (2010) 3100–3110. https://doi.org/10.1021/am1006035.

[67] L. Gao, T.J. McCarthy, Teflon is hydrophilic. Comments on definitions of hydrophobic, shear versus tensile hydrophobicity, and wettability characterization, Langmuir. 24 (17) (2008) 9183–9188. https://doi.org/10.1021/la8014578.

[68] D. Chen, M.D. Gelenter, M. Hong, R.E. Cohen, G.H. McKinley, Icephobic surfaces induced by interfacial nonfrozen water, ACS Appl. Mater. Interfaces. 9 (2017) 4202–4214. https://doi.org/10.1021/acsami.6b13773.

[69] M. Nosonovsky, V. Hejazi, Why superhydrophobic surfaces are not always icephobic, ACS Nano. 9 (10) (2012) 8488–8491. https://doi.org/10.1021/nn302138r.

[70] L. Cao, A.K. Jones, V.K. Sikka, J. Wu, D. Gao, Anti-Icing superhydrophobic coatings, Langmuir. 25 (21) (2009) 12444–12448. https://doi.org/10.1021/la902882b.

[71] W. Li, Y. Zhan, S. Yu, Applications of superhydrophobic coatings in anti-icing: Theory, mechanisms, impact factors, challenges and perspectives, Prog. Org. Coatings. 152 (2021) 106117. https://doi.org/10.1016/j.porgcoat.2020.106117.

[72] H. He, Z. Guo, Superhydrophobic materials used for anti-icing Theory, application, and development, IScience. 24 (2021). https://doi.org/10.1016/j.isci.2021.103357.

[73] W. Huang, J. Huang, Z. Guo, W. Liu, Icephobic/anti-icing properties of superhydrophobic surfaces, Adv. Colloid Interface Sci. 304 (2022) 102658. https://doi.org/10.1016/j.cis.2022.102658.

[74] A.C. Ribeiro, B.G. Soares, J.G.M. Furtado, A.A. Silva, N.S.S.E. Couto, Superhydrophobic nanocomposite coatings based on different polysiloxane matrices designed for electrical insulators, Prog. Org. Coatings. 168 (2022) 106867. https://doi.org/10.1016/j.porgcoat.2022.106867.

[75] A. Aparna, A.S. Sethulekshmi, A. Saritha, K. Joseph, Recent advances in superhydrophobic epoxy based nanocomposite coatings and their applications, Prog. Org. Coatings. 166 (2022). https://doi.org/10.1016/j.porgcoat.2022.106819.

[76] A. Allahdini, G. Momen, F. Munger, S. Brettschneider, I. Fofana, R. Jafari, Performance of a nanotextured superhydrophobic coating developed for high-voltage outdoor porcelain insulators, Colloids Surfaces A Physicochem. Eng. Asp. 649 (2022) 129461. https://doi.org/10.1016/J.COLSURFA.2022.129461.

[77] T. Yang, Y. Li, H. Gui, D. Du, Y. Du, X.M. Song, F. Liang, Superhydrophobic Coating Derived from the Spontaneous Orientation of Janus Particles, ACS Appl. Mater. Interfaces. (2021). https://doi.org/10.1021/acsami.1c05571.

[78] S. Li, J. Qin, M. He, R. Paoli, Fast evaluation of aircraft icing severity using machine learning based on XGBoost, Aerospace. 7(4) (2020) 36. https://doi.org/10.3390/aerospace7040036.

[79] M. Kreutz, A. Ait-Alla, K. Varasteh, S. Oelker, A. Greulich, M. Freitag, K.D. Thoben, Machine learning-based icing prediction on wind turbines, Procedia CIRP. 81 (2019) 423–428. https://doi.org/10.1016/j.procir.2019.03.073.

[80] Y. Liu, H. Cheng, X. Kong, Q. Wang, H. Cui, Intelligent wind turbine blade icing detection using supervisory control and data acquisition data and ensemble deep learning, Energy Sci. Eng. 7 (6) (2019) 2633–2645. https://doi.org/10.1002/ese3.449.

[81] M. Fitzner, P. Pedevilla, A. Michaelides, Predicting heterogeneous ice nucleation with a data-driven approach, Nat. Commun. 11 (2020) 4777. https://doi.org/10.1038/s41467-020-18605-3.

[82] S. Ringdahl, S. Xiao, J. He, Z. Zhang, Machine learning based prediction of nanoscale ice adhesion on rough surfaces, Coatings. 11 (1) (2021) 33. https://doi.org/10.3390/coatings11010033.

[83] Y.H. Yeong, A. Milionis, E. Loth, J. Sokhey, Self-lubricating icephobic elastomer coating (SLIC) for ultralow ice adhesion with enhanced durability, Cold Reg. Sci. Technol. 148 (2018) 29–37. https://doi.org/10.1016/j.coldregions.2018.01.005.

[84] Y. Si, Z. Guo, Superhydrophobic nanocoatings: From materials to fabrications and to applications, Nanoscale. 7 (2015) 5922–5946. https://doi.org/10.1039/c4nr07554d.

[85] Y. Zhuo, S. Xiao, A. Amirfazli, J. He, Z. Zhang, Polysiloxane as icephobic materials – The past, present and the future, Chem. Eng. J. 405 (2021) 127088. https://doi.org/10.1016/j.cej.2020.127088.

[86] H. Murase, T. Fujibayashi, Characterization of molecular interfaces in hydrophobic systems, Prog. Org. Coatings. 31 (1997) 97–104. https://doi.org/10.1016/S0300-9440(97)00023-4.

[87] H. Murase, K. Nanishi, H. Kogure, T. Fujibayashi, K. Tamura, N. Haruta, Interactions between heterogeneous surfaces of polymers and water, J. Appl. Polym. Sci. 54 (1994) 2051–2062. https://doi.org/10.1002/app.1994.070541307.

[88] F. Arianpour, M. Farzaneh, R. Jafari, Hydrophobic and ice-phobic properties of self-assembled monolayers (SAMs) coatings on AA6061, Prog. Org. Coatings. (2016) 41–45. https://doi.org/10.1016/j.porgcoat.2015.12.008.

[89] S.N. Gorb, E. V. Gorb, Anti-icing strategies of plant surfaces: the ice formation on leaves visualized by Cryo-SEM experiments, Sci. Nat. 109 (2022) 24. https://doi.org/10.1007/s00114-022-01789-7.

[90] A. Marmur, Hydro- hygro- oleo- omni-phobic? Terminology of wettability classification, Soft Matter. 8 (2012) 6867–6870. https://doi.org/10.1039/c2sm25443c.

[91] N. Valipour M., F.C. Birjandi, J. Sargolzaei, Super-non-wettable surfaces: A review, Colloids Surfaces A Physicochem. Eng. Asp. 448 (2014) 93–106. https://doi.org/10.1016/j.colsurfa.2014.02.016.

[92] K. Maghsoudi, R. Jafari, G. Momen, M. Farzaneh, Micro-nanostructured polymer surfaces using injection molding: A review, Mater. Today Commun. 13 (2017) 126–143. https://doi.org/10.1016/j.mtcomm.2017.09.013.

[93] K. Maghsoudi, G. Momen, R. Jafari, M. Farzaneh, Direct replication of micro-nanostructures in the fabrication of superhydrophobic silicone rubber surfaces by compression molding, Appl. Surf. Sci. 458 (2018) 619–628. https://doi.org/10.1016/j.apsusc.2018.07.099.

[94] L. Bao, Z. Huang, N. V. Priezjev, S. Chen, K. Luo, H. Hu, A significant reduction of ice adhesion on nanostructured surfaces that consist of an array of single-walled carbon nanotubes: A molecular dynamics simulation study, Appl. Surf. Sci. 437 (2018) 202–208. https://doi.org/10.1016/j.apsusc.2017.12.096.

[95] E. Vazirinasab, R. Jafari, G. Momen, Application of superhydrophobic coatings as a corrosion barrier: A review, Surf. Coatings Technol. 341 (2018) 40–56. https://doi.org/10.1016/j.surfcoat.2017.11.053.

[96] R. Jafari, C. Cloutier, A. Allahdini, G. Momen, Recent progress and challenges with 3D printing of patterned hydrophobic and superhydrophobic surfaces, Int. J. Adv. Manuf. Technol. 103 (2019) 1225–1238. https://doi.org/10.1007/s00170-019-03630-4.

[97] R. Jafari, G. Momen, E. Eslami, Fabrication of icephobic aluminium surfaces by atmospheric plasma jet polymerisation, Surf. Eng. 35 (2019) 450–455. https://doi.org/10.1080/02670844.2018.1509813.

[98] K. Koch, B. Bhushan, W. Barthlott, Multifunctional surface structures of plants: An inspiration for biomimetics, Prog. Mater. Sci. 54 (2009) 137–178. https://doi.org/10.1016/j.pmatsci.2008.07.003.

[99] W. Barthlott, T. Schimmel, S. Wiersch, K. Koch, M. Brede, M. Barczewski, S. Walheim, A. Weis, A. Kaltenmaier, A. Leder, H.F. Bohn, The salvmia paradox: superhydrophobic surfaces with hydrophilic pins for air retention under water, Adv. Mater. 22 (2010) 2325–2328. https://doi.org/10.1002/adma.200904411.

[100] P. Perez Goodwyn, Y. Maezono, N. Hosoda, K. Fujisaki, Waterproof and translucent wings at the same time: Problems and solutions in butterflies, Naturwissenschaften. 96 (7) (2009) 781–787. https://doi.org/10.1007/s00114-009-0531-z.

[101] K. Liu, J. Du, J. Wu, L. Jiang, Superhydrophobic gecko feet with high adhesive forces towards water and their bio-inspired materials, Nanoscale. 4 (2012) 768–772. https://doi.org/10.1039/c1nr11369k.

[102] S.A. Kulinich, S. Farhadi, K. Nose, X.W. Du, Superhydrophobic surfaces: Are they really ice-repellent?, Langmuir. 27 (2011) 25–29. https://doi.org/10.1021/la104277q.

[103] Y. Wang, J. Xue, Q. Wang, Q. Chen, J. Ding, Verification of icephobic/anti-icing properties of a superhydrophobic surface, ACS Appl. Mater. Interfaces. 5 (2013) 3370–3381. https://doi.org/10.1021/am400429q.

[104] L.B. Boinovich, A.M. Emelyanenko, V.K. Ivanov, A.S. Pashinin, Durable icephobic coating for stainless steel, ACS Appl. Mater. Interfaces. 5 (2013) 2549–2554. https://doi.org/10.1021/am3031272.

[105] Glen Allen, Smart Coatings: The Next Big Opportunity in the Coatings Industry, N-Tech Res. (n.d.). https://www.pcimag.com/articles/102455-smart-coatings-the-next-big-opportunity-in-the-coatings-industry (accessed August 3, 2021).

[106] A.A. Nazeer, M. Madkour, Potential use of smart coatings for corrosion protection of metals and alloys: A review, J. Mol. Liq. 253 (2018) 11–22. https://doi.org/10.1016/j.molliq.2018.01.027.

[107] D. Sun, J. An, G. Wu, J. Yang, Double-layered reactive microcapsules with excellent thermal and non-polar solvent resistance for self-healing coatings, J. Mater. Chem. A. 3 (2015) 4435–4444. https://doi.org/10.1039/c4ta05339g.

[108] K. Uchino, Advanced piezoelectric materials: Science and technology, Woodhead Publishing Limited, 2010. https://doi.org/10.1533/9781845699758.

[109] K. Maghsoudi, G. Momen, R. Jafari, M. Farzaneh, Rigorous testing to assess the self-cleaning properties of an ultra-water-repellent silicone rubber surface, Surf. Coatings Technol. 374 (2019) 557–568. https://doi.org/10.1016/j.surfcoat.2019.05.073.

[110] E. Vazirinasab, R. Jafari, G. Momen, Evaluation of atmospheric-pressure plasma parameters to achieve superhydrophobic and self-cleaning HTV silicone rubber surfaces via a single-step, eco-friendly approach, Surf. Coatings Technol. 375 (2019) 100–111. https://doi.org/10.1016/j.surfcoat.2019.07.005.

[111] R. Ramachandran, M. Nosonovsky, Surface micro/nanotopography, wetting

properties and the potential for biomimetic icephobicity of skunk cabbage Symplocarpus foetidus, Soft Matter. 10 (2014) 7797–7803. https://doi.org/10.1039/c4sm01230e.

[112] A.R.O. Raji, T. Varadhachary, K. Nan, T. Wang, J. Lin, Y. Ji, B. Genorio, Y. Zhu, C. Kittrell, J.M. Tour, Composites of graphene nanoribbon stacks and epoxy for joule heating and deicing of surfaces, ACS Appl. Mater. Interfaces. 8 (2016) 3551–3556. https://doi.org/10.1021/acsami.5b11131.

[113] T. Wang, Y. Zheng, A.R.O. Raji, Y. Li, W.K.A. Sikkema, J.M. Tour, Passive Anti-Icing and Active Deicing Films, ACS Appl. Mater. Interfaces. 8 (2016) 14169–14173. https://doi.org/10.1021/acsami.6b03060.

[114] N. Karim, M. Zhang, S. Afroj, V. Koncherry, P. Potluri, K.S. Novoselov, Graphene-based surface heater for de-icing applications, RSC Adv. 8 (2018) 16815–16823. https://doi.org/10.1039/c8ra02567c.

[115] H. Wang, Z. Zhang, Z. Wang, Y. Liang, Z. Cui, J. Zhao, X. Li, L. Ren, Multistimuli-Responsive Microstructured Superamphiphobic Surfaces with Large-Range, Reversible Switchable Wettability for Oil, ACS Appl. Mater. Interfaces. 11 (2019) 28478–28486. https://doi.org/10.1021/acsami.9b07941.

[116] Y. Zhou, S. Huang, X. Tian, Magnetoresponsive Surfaces for Manipulation of Nonmagnetic Liquids: Design and Applications, Adv. Funct. Mater. 30 (2020) 1906507. https://doi.org/10.1002/adfm.201906507.

[117] H. Aono, H. Hirazawa, T. Naohara, H. Aono, H. Hirazawa, T.N. Heat, Heat generation ability in AC magnetic field of bead-milled nanosize Y 3 Fe 5 O 12 and preparation of microsphere for embolization therapy, in: 8th Int. Conf. Electromagn. Process. Mater., Cannes, France, 2015.

[118] B. Jeyadevan, Present status and prospects of magnetite nanoparticles-based hyperthermia, J. Ceram. Soc. Japan. 118 (2010) 391–401. https://doi.org/10.2109/jcersj2.118.391.

[119] A. Grigoryev, I. Tokarev, K.G. Kornev, I. Luzinov, S. Minko, Superomniphobic magnetic microtextures with remote wetting control, J. Am. Chem. Soc. 134 (2012) 12916–12919. https://doi.org/10.1021/ja305348n.

[120] P. Irajizad, M. Hasnain, N. Farokhnia, S.M. Sajadi, H. Ghasemi, Magnetic slippery extreme icephobic surfaces, Nat. Commun. 7 (2016) 13395. https://doi.org/10.1038/ncomms13395.

[121] X. Fan, J. Xiao, W. Wang, Y. Zhang, S. Zhang, B. Tang, Novel magnetic-to-thermal conversion and thermal energy management composite phase change material, Polymers (Basel). 10 (2018). https://doi.org/10.3390/polym10060585.

[122] Y. Gossuin, P. Gillis, A. Hocq, Q.L. Vuong, A. Roch, Magnetic resonance relaxation properties of superparamagnetic particles, Wiley Interdiscip. Rev. Nanomedicine Nanobiotechnology. 1 (3) (2009) 299–310. https://doi.org/10.1002/wnan.36.

[123] R. Ghosh, L. Pradhan, Y.P. Devi, S.S. Meena, R. Tewari, A. Kumar, S. Sharma, N.S. Gajbhiye, R.K. Vatsa, B.N. Pandey, R.S. Ningthoujam, Induction heating studies of Fe3O4 magnetic nanoparticles capped with oleic acid and polyethylene glycol for hyperthermia, J. Mater. Chem. 21 (2011) 13388–13398. https://doi.org/10.1039/c1jm10092k.

[124] T. Cheng, R. He, Q. Zhang, X. Zhan, F. Chen, Magnetic particle-based super-hydrophobic coatings with excellent anti-icing and thermoresponsive deicing performance, J. Mater. Chem. A. 3 (2015) 21637–21646. https://doi.org/10.1039/c5ta05277g.

[125] N. Tepylo, A Coupled Icephobic Coating and Piezoelectric Actuator System for Aircraft De-icing Applications, Carleton University, 2017. https://doi.org/10.22215/etd/2017-11986.

[126] V. Pommier-Budinger, M. Budinger, N. Tepylo, X. Huang, Analysis of piezoelectric ice protection systems combined with ice-phobic coatings, in: 8th AIAA Atmos. Sp. Environ. Conf., Washington, D.C., 2016. https://doi.org/10.2514/6.2016-3442.

[127] S. V. Venna, Y.J. Lin, Mechatronic development of self-actuating in-flight deicing structures, IEEE/ASME Trans. Mechatronics. 11 (2006) 585–592. https://doi.org/10.1109/TMECH.2006.882990.

[128] P.L. Dominique Broussoux, Michel C. Ceccaldi, Device for the removal of the ice formed on the surface of a wall, notably an optical or radio-electrical window, US Patent 5172024, 1992.

[129] T. Strobl, S. Storm, M. Kolb, J. Haag, M. Hornung, Development of a hybrid ice protection system based on nanostructured hydrophobic surfaces, in: 29th Congr. Int. Counc. Aeronaut. Sci. ICAS 2014, St. Petersburg, Russia, 2014.

[130] F. Z.Kamand, B. Mehmood, R. Ghunem, M.K. Hassan, A. El-Hag, L. Al-Sulaiti, A. Abdala;, Self-Healing Silicones for Outdoor High Voltage Insulation: Mechanism, Applications and Measurements, Energies. 15 (2022) 1677. https://doi.org/10.3390/en15051677.

[131] R.P. Wool, Self-healing materials: A review, Soft Matter. 4 (2008) 400–418. https://doi.org/10.1039/b711716g.

[132] D.Y. Wu, S. Meure, D. Solomon, Self-healing polymeric materials: A review of recent developments, Prog. Polym. Sci. 33 (2008) 479–522.

https://doi.org/10.1016/j.progpolymsci.2008.02.001.

[133] Y.C. Yuan, T. Yin, M.Z. Rong, M.Q. Zhang, Self healing in polymers and polymer composites. Concepts, realization and outlook: A review, Express Polym. Lett. 2 (2008) 238–250. https://doi.org/10.3144/expresspolymlett.2008.29.

[134] R.S. Trask, H.R. Williams, I.P. Bond, Self-healing polymer composites: Mimicking nature to enhance performance, Bioinspiration and Biomimetics. 2 (1) (2007) 1–9. https://doi.org/10.1088/1748-3182/2/1/P01.

[135] J.C. Cremaldi, B. Bhushan, Bioinspired self-healing materials: Lessons from nature, Beilstein J. Nanotechnol. 9 (2018) 907–935. https://doi.org/10.3762/bjnano.9.85.

[136] S.H. Cho, S.R. White, P. V. Braun, Self-healing polymer coatings, Adv. Mater. 21 (2009) 645–649. https://doi.org/10.1002/adma.200802008.

[137] P. Poornima Vijayan, M. Al-Maadeed, Self-Repairing Composites for Corrosion Protection: A Review on Recent Strategies and Evaluation Methods, Materials (Basel). 12 (2019) 2754. https://doi.org/10.3390/ma12172754.

[138] E. Tetteh, E. Loth, Reducing static and impact ice adhesion with a self-lubricating icephobic coating (SLIC), Coatings. 10 (2020) 262. https://doi.org/10.3390/coatings10030262.

[139] T. Chang, F. Panhwar, G. Zhao, Flourishing Self-Healing Surface Materials: Recent Progresses and Challenges, Adv. Mater. Interfaces. 7 (2020) 1901959. https://doi.org/10.1002/admi.201901959.

[140] Y. Zhuo, S. Xiao, V. Håkonsen, T. Li, F. Wang, J. He, Z. Zhang, Ultrafast self-healing and highly transparent coating with mechanically durable icephobicity, Appl. Mater. Today. 19 (2020) 100542. https://doi.org/10.1016/j.apmt.2019.100542.

[141] S. Wang, K. Liu, X. Yao, L. Jiang, Bioinspired surfaces with superwettability: New insight on theory, design, and applications, Chem. Rev. 115 (2015) 8230–8293. https://doi.org/10.1021/cr400083y.

[142] S.P. Dalawai, M.A. Saad Aly, S.S. Latthe, R. Xing, R.S. Sutar, S. Nagappan, C.S. Ha, K. Kumar Sadasivuni, S. Liu, Recent Advances in durability of superhydrophobic self-cleaning technology: A critical review, Prog. Org. Coatings. 138 (2020) 105381. https://doi.org/10.1016/j.porgcoat.2019.105381.

[143] S. Goharshenas Moghadam, H. Parsimehr, A. Ehsani, Multifunctional superhydrophobic surfaces, Adv. Colloid Interface Sci. 290 (2021) 102397. https://doi.org/10.1016/j.cis.2021.102397.

[144] L. Qin, Y. Chu, X. Zhou, Q. Pan, Fast Healable Superhydrophobic Material, ACS Appl. Mater. Interfaces. 11 (2019) 29388–29395. https://doi.org/10.1021/acsami.9b07563.

[145] Y. Li, B. Li, X. Zhao, N. Tian, J. Zhang, Totally Waterborne, Nonfluorinated, Mechanically Robust, and Self-Healing Superhydrophobic Coatings for Actual Anti-Icing, ACS Appl. Mater. Interfaces. 10 (2018) 39391–39399. https://doi.org/10.1021/acsami.8b15061.

[146] K. Fu, C. Lu, Y. Liu, H. Zhang, B. Zhang, H. Zhang, F. Zhou, Q. Zhang, B. Zhu, Mechanically robust, self-healing superhydrophobic anti-icing coatings based on a novel fluorinated polyurethane synthesized by a two-step thiol click reaction, Chem. Eng. J. 404 (2021) 127110. https://doi.org/10.1016/j.cej.2020.127110.

[147] K. Chen, S. Zhou, S. Yang, L. Wu, Fabrication of all-water-based self-repairing superhydrophobic coatings based on UV-responsive microcapsules, Adv. Funct. Mater. 25 (2015) 1035–1041. https://doi.org/10.1002/adfm.201403496.

[148] M. Shamshiri, A. Manaia, T. Vuchkov, A. Carvalho, G. Gaspar, A. Fernandes, S.H. Dolatabadi, F. Costa, A. Cavaleiro, Influence of laser structural patterning on the tribological performance of C-alloyed W-S coatings, Surf. Coatings Technol. 394 (2020) 125822. https://doi.org/10.1016/j.surfcoat.2020.125822.

[149] S. Heydarian, R. Jafari, G. Momen, Recent progress in the anti-icing performance of slippery liquid-infused surfaces, Prog. Org. Coatings. 151 (2021) 106096. https://doi.org/10.1016/j.porgcoat.2020.106096.

[150] A. Hozumi, L. Jiang, H. Lee, M. Shimomura, Toward Enviromentally Adaptive Anti-icing Coating, in: Stimuli-Responsive Dewetting/Wetting Smart Surfaces and Interfaces, Springer International Publishing AG, 2018: pp. 259–286.

[151] T.S. Wong, S.H. Kang, S.K.Y. Tang, E.J. Smythe, B.D. Hatton, A. Grinthal, J. Aizenberg, Bioinspired self-repairing slippery surfaces with pressure-stable omniphobicity, Nature. 477 (2011) 443–447. https://doi.org/10.1038/nature10447.

[152] N. Vogel, R.A. Belisle, B. Hatton, T.S. Wong, J. Aizenberg, Transparency and damage tolerance of patternable omniphobic lubricated surfaces based on inverse colloidal monolayers, Nat. Commun. 4 (2013) 2176. https://doi.org/10.1038/ncomms3176.

[153] P. Kim, T.S. Wong, J. Alvarenga, M.J. Kreder, W.E. Adorno-Martinez, J. Aizenberg, Liquid-infused nanostructured surfaces with extreme anti-ice and anti-frost performance, ACS Nano. 6 (2012) 6569–6577. https://doi.org/10.1021/nn302310q.

[154] J.D. Smith, R. Dhiman, S. Anand, E. Reza-Garduno, R.E. Cohen, G.H. McKinley, K.K. Varanasi, Droplet mobility on lubricant-impregnated surfaces, Soft Matter. 9 (2013) 1772–1780. https://doi.org/10.1039/c2sm27032c.

[155] A. Eifert, D. Paulssen, S.N. Varanakkottu, T. Baier, S. Hardt, Simple Fabrication of Robust Water-Repellent Surfaces with Low Contact-Angle Hysteresis Based on Impregnation, Adv. Mater. Interfaces. 1 (2014) 1300138. https://doi.org/10.1002/admi.201300138.

[156] H. Niemelä-Anttonen, H. Koivuluoto, M. Tuominen, H. Teisala, P. Juuti, J. Haapanen, J. Harra, C. Stenroos, J. Lahti, J. Kuusipalo, J.M. Mäkelä, P. Vuoristo, Icephobicity of Slippery Liquid Infused Porous Surfaces under Multiple Freeze–Thaw and Ice Accretion–Detachment Cycles, Adv. Mater. Interfaces. 5 (2018) 1800828. https://doi.org/10.1002/admi.201800828.

[157] Y.H. Yeong, C. Wang, K.J. Wynne, M.C. Gupta, Oil-infused superhydrophobic silicone material for low ice adhesion with long-term infusion stability, ACS Appl. Mater. Interfaces. 8 (2016) 32050–32059. https://doi.org/10.1021/acsami.6b11184.

[158] H. Zhao, Q. Sun, X. Deng, J. Cui, Earthworm-Inspired Rough Polymer Coatings with Self-Replenishing Lubrication for Adaptive Friction-Reduction and Antifouling Surfaces, Adv. Mater. 30 (2018) e1802141. https://doi.org/10.1002/adma.201802141.

[159] W. Federle, W.J.P. Barnes, W. Baumgartner, P. Drechsler, J.M. Smith, Wet but not slippery: Boundary friction in tree frog adhesive toe pads, J. R. Soc. Interface. 3 (2006) 689–697. https://doi.org/10.1098/rsif.2006.0135.

[160] T. Li, Y. Zhuo, V. Håkonsen, S. Rønneberg, J. He, Z. Zhang, Epidermal gland inspired self-repairing slippery lubricant-infused porous coatings with durable low ice adhesion, Coatings. 9 (2019) 602. https://doi.org/10.3390/coatings9100602.

[161] M.J. Coady, M. Wood, G.Q. Wallace, K.E. Nielsen, A.M. Kietzig, F. Lagugné-Labarthet, P.J. Ragogna, Icephobic Behavior of UV-Cured Polymer Networks Incorporated into Slippery Lubricant-Infused Porous Surfaces: Improving SLIPS Durability, ACS Appl. Mater. Interfaces. 10 (2018) 2890–2896. https://doi.org/10.1021/acsami.7b14433.

[162] Y. Zhuo, F. Wang, S. Xiao, J. He, Z. Zhang, One-Step Fabrication of Bioinspired Lubricant-Regenerable Icephobic Slippery Liquid-Infused Porous Surfaces, ACS Omega. 3 (2018) 10139–10144. https://doi.org/10.1021/acsomega.8b01148.

[163] L. Zhu, J. Xue, Y. Wang, Q. Chen, J. Ding, Q. Wang, Ice-phobic coatings based on silicon-oil-infused polydimethylsiloxane, ACS Appl. Mater. Interfaces. 5

(2013) 4053–4062. https://doi.org/10.1021/am400704z.

[164] C. Urata, R. Hönes, T. Sato, H. Kakiuchida, Y. Matsuo, A. Hozumi, Textured Organogel Films Showing Unusual Thermoresponsive Dewetting, Icephobic, and Optical Properties, Adv. Mater. Interfaces. 6 (2019) 1801358. https://doi.org/10.1002/admi.201801358.

[165] Y. Ru, R. Fang, Z. Gu, L. Jiang, M. Liu, Reversibly Thermosecreting Organogels with Switchable Lubrication and Anti-Icing Performance, Angew. Chemie - Int. Ed. 59 (2020) 11876–11880. https://doi.org/10.1002/anie.202004122.

[166] Y. Zhang, H. Guo, J. Gao, W. Wei, M. Liu, C. Zheng, P. Deng, Self-lubricated anti-icing MOF coating with long-term durability, Prog. Org. Coatings. 151 (2021) 106089. https://doi.org/10.1016/j.porgcoat.2020.106089.

[167] N.H. Fletcher, Surface structure of water and ice, Philos. Mag. 18 (1968) 1287–1300. https://doi.org/10.1080/14786436808227758.

[168] R. Rosenberg, Why is ice slippery, Phys. Today. 58 (2005) 50–55. https://doi.org/10.1063/1.2169444.

[169] R. Dou, J. Chen, Y. Zhang, X. Wang, D. Cui, Y. Song, L. Jiang, J. Wang, Anti-icing coating with an aqueous lubricating layer, ACS Appl. Mater. Interfaces. 6 (2014) 6998–7003. https://doi.org/10.1021/am501252u.

[170] D. Bonn, The physics of ice skating, Nature. 577 (2020) 173–174. https://doi.org/10.1038/d41586-019-03833-5.

[171] J. Chen, Z. Luo, Q. Fan, J. Lv, J. Wang, Anti-Ice coating inspired by ice skating, Small. 10 (2014) 4693–4699. https://doi.org/10.1002/smll.201401557.

[172] J.G. Constantin, M.M. Gianetti, M.P. Longinotti, H.R. Corti, The quasi-liquid layer of ice revisited: The role of temperature gradients and tip chemistry in AFM studies, Atmos. Chem. Phys. 18 (2018) 14965–14978. https://doi.org/10.5194/acp-18-14965-2018.

[173] J.S. Wettlaufer, Impurity effects in the premelting of ice, Phys. Rev. Lett. 82 (1999) 2516–2519. https://doi.org/10.1103/PhysRevLett.82.2516.

[174] T. Ikeda-Fukazawa, K. Kawamura, Molecular-dynamics studies of surface of ice Ih, J. Chem. Phys. 120 (2004) 1395–1401. https://doi.org/10.1063/1.1634250.

[175] Z. He, Y. Zhuo, Z. Zhang, J. He, Design of icephobic surfaces by lowering ice adhesion strength: A mini review, Coatings. 11 (2021). https://doi.org/10.3390/coatings11111343.

[176] K.A. Emelyanenko, A.M. Emelyanenko, L.B. Boinovich, Water and ice adhesion to solid surfaces: Common and specific, the impact of temperature and surface wettability, Coatings. 10 (2020) 648. https://doi.org/10.3390/coatings10070648.

[177] M.J. Kreder, J. Alvarenga, P. Kim, J. Aizenberg, Design of anti-icing surfaces: Smooth, textured or slippery?, Nat. Rev. Mater. (2016). https://doi.org/10.1038/natrevmats.2015.3.

[178] K. Li, S. Xu, J. Chen, Q. Zhang, Y. Zhang, D. Cui, X. Zhou, J. Wang, Y. Song, Viscosity of interfacial water regulates ice nucleation, Appl. Phys. Lett. 104 (2014). https://doi.org/10.1063/1.4868255.

[179] M.P. Goertz, J.E. Houston, X.Y. Zhu, Hydrophilicity and the viscosity of interfacial water, Langmuir. 23 (2007) 5491–5497. https://doi.org/10.1021/la062299q.

[180] R. Kent, Energy Management in Plastics Processing: Strategies, Targets, Techniques, and Tools, 3rd Ed., Elsevier Ltd, 2018. https://doi.org/10.1016/C2017-0-02035-9.

[181] B. Liu, K. Zhang, C. Tao, Y. Zhao, X. Li, K. Zhu, X. Yuan, Strategies for anti-icing: Low surface energy or liquid-infused?, RSC Adv. 6 (2016) 70251–70260. https://doi.org/10.1039/c6ra11383d.

[182] K.C. Jha, E. Anim-Danso, S. Bekele, G. Eason, M. Tsige, On modulating interfacial structure towards improved anti-icing performance, Coatings. 6 (2016) 3. https://doi.org/10.3390/coatings6010003.

[183] M. Kasuya, M. Hino, H. Yamada, M. Mizukami, H. Mori, S. Kajita, T. Ohmori, A. Suzuki, K. Kurihara, Characterization of water confined between silica surfaces using the resonance shear measurement, J. Phys. Chem. C. 117 (2013) 13540–13546. https://doi.org/10.1021/jp404378b.

[184] S. Bekele, M. Tsige, Interfacial properties of oxidized polystyrene and its interaction with water, Langmuir. 29 (2013) 13230–13238. https://doi.org/10.1021/la403099e.

[185] E.L. Hommel, J.K. Merle, G. Ma, C.M. Hadad, H.C. Allen, Spectroscopic and computational studies of aqueous ethylene glycol solution surfaces, J. Phys. Chem. B. 109 (2005) 811–818. https://doi.org/10.1021/jp046715w.

[186] J. Chen, R. Dou, D. Cui, Q. Zhang, Y. Zhang, F. Xu, X. Zhou, J. Wang, Y. Song, L. Jiang, Robust prototypical anti-icing coatings with a self-lubricating liquid water layer between ice and substrate, ACS Appl. Mater. Interfaces. 5 (2013) 4026–4030. https://doi.org/10.1021/am401004t.

[187] D.K. Chattopadhyay, K.V.S.N. Raju, Structural engineering of polyurethane coatings for high performance applications, Prog. Polym. Sci. 32 (2007) 352–418. https://doi.org/10.1016/j.progpolymsci.2006.05.003.

[188] J. Chen, K. Li, S. Wu, J. Liu, K. Liu, Q. Fan, Durable Anti-Icing Coatings Based on Self-Sustainable Lubricating Layer, ACS Omega. 2 (2017) 2047–2054. https://doi.org/10.1021/acsomega.7b00359.

[189] S. Chernyy, M. Järn, K. Shimizu, A. Swerin, S.U. Pedersen, K. Daasbjerg, L. Makkonen, P. Claesson, J. Iruthayaraj, Superhydrophilic polyelectrolyte brush layers with imparted anti-icing properties: Effect of counter ions, ACS Appl. Mater. Interfaces. 6 (2014) 6487–6496. https://doi.org/10.1021/am500046d.

[190] Y. Marcus, Effect of ions on the structure of water: Structure making and breaking, Chem. Rev. 109 (2009) 1346–1370. https://doi.org/10.1021/cr8003828.

[191] P. Ben Ishai, E. Mamontov, J.D. Nickels, A.P. Sokolov, Influence of ions on water diffusion-A neutron scattering study, J. Phys. Chem. B. 117 (2013) 7724–7728. https://doi.org/10.1021/jp4030415.

[192] P.A. Fokaides, A. Kylili, S.A. Kalogirou, Phase change materials (PCMs) integrated into transparent building elements: A review, Mater. Renew. Sustain. Energy. 4 (2015). https://doi.org/10.1007/s40243-015-0047-8.

[193] W.F. Wu, N. Liu, W.L. Cheng, Y. Liu, Study on the effect of shape-stabilized phase change materials on spacecraft thermal control in extreme thermal environment, Energy Convers. Manag. 69 (2013) 174–180. https://doi.org/10.1016/j.enconman.2013.01.025.

[194] N. Sarier, E. Onder, Organic phase change materials and their textile applications: An overview, Thermochim. Acta. 540 (2012) 7–60. https://doi.org/10.1016/j.tca.2012.04.013.

[195] J. Li, Y. Hu, Y. Hou, X. Shen, G. Xu, L. Dai, J. Zhou, Y. Liu, K. Cai, Phase-change material filled hollow magnetic nanoparticles for cancer therapy and dual modal bioimaging, Nanoscale. 7 (2015) 9004–9012. https://doi.org/10.1039/c5nr01744k.

[196] M. Kenisarin, K. Mahkamov, Solar energy storage using phase change materials, Renew. Sustain. Energy Rev. 11 (2007) 1913–1965. https://doi.org/10.1016/j.rser.2006.05.005.

[197] E. Oró, A. de Gracia, A. Castell, M.M. Farid, L.F. Cabeza, Review on phase change materials (PCMs) for cold thermal energy storage applications, Appl. Energy. 99 (2012) 513–533. https://doi.org/10.1016/j.apenergy.2012.03.058.

[198] A. Abhat, Low temperature latent heat thermal energy storage: Heat storage materials, Sol. Energy. 30 (1983) 313–332. https://doi.org/10.1016/0038-092X(83)90186-X.

[199] X.X. Zhang, Y.F. Fan, X.M. Tao, K.L. Yick, Crystallization and prevention of supercooling of microencapsulated n-alkanes, J. Colloid Interface Sci. 281 (2005) 299–306. https://doi.org/10.1016/j.jcis.2004.08.046.

[200] D. Zhou, C.Y. Zhao, Y. Tian, Review on thermal energy storage with phase change materials (PCMs) in building applications, Appl. Energy. 92 (2012) 593–605. https://doi.org/10.1016/j.apenergy.2011.08.025.

[201] L. Feng, J. Zheng, H. Yang, Y. Guo, W. Li, X. Li, Preparation and characterization of polyethylene glycol/active carbon composites as shape-stabilized phase change materials, Sol. Energy Mater. Sol. Cells. 95 (2011) 644–650. https://doi.org/10.1016/j.solmat.2010.09.033.

[202] S. Rostami, M. Afrand, A. Shahsavar, M. Sheikholeslami, R. Kalbasi, S. Aghakhani, M.S. Shadloo, H.F. Oztop, A review of melting and freezing processes of PCM/nano-PCM and their application in energy storage, Energy. 211 (2020) 118698. https://doi.org/10.1016/j.energy.2020.118698.

[203] H. Zhang, C. Xu, G. Fang, Encapsulation of inorganic phase change thermal storage materials and its effect on thermophysical properties: A review, Sol. Energy Mater. Sol. Cells. 241 (2022) 111747. https://doi.org/10.1016/j.solmat.2022.111747.

[204] S.A.A. Ghani, S.S. Jamari, S.Z. Abidin, Waste materials as the potential phase change material substitute in thermal energy storage system: a review, Chem. Eng. Commun. 208 (2021) 687–707. https://doi.org/10.1080/00986445.2020.1715960.

[205] X. Yao, J. Ju, S. Yang, J. Wang, L. Jiang, Temperature-driven switching of water adhesion on organogel surface, Adv. Mater. 26 (2014) 1895–1900. https://doi.org/10.1002/adma.201304798.

[206] D.W. Hawes, D. Feldman, D. Banu, Latent heat storage in building materials, Energy Build. 20 (1993) 77–86. https://doi.org/10.1016/0378-7788(93)90040-2.

[207] H. Peng, D. Zhang, X. Ling, Y. Li, Y. Wang, Q. Yu, X. She, Y. Li, Y. Ding, N -Alkanes Phase Change Materials and Their Microencapsulation for Thermal Energy Storage: A Critical Review, Energy and Fuels. 32 (2018) 7262–7293. https://doi.org/10.1021/acs.energyfuels.8b01347.

[208] A. Sharma, V. V. Tyagi, C.R. Chen, D. Buddhi, Review on thermal energy storage with phase change materials and applications, Renew. Sustain. Energy

Rev. 13 (2009) 318–345. https://doi.org/10.1016/j.rser.2007.10.005.

[209] E.M. Shchukina, M. Graham, Z. Zheng, D.G. Shchukin, Nanoencapsulation of phase change materials for advanced thermal energy storage systems, Chem. Soc. Rev. 47 (2018) 4156–4175. https://doi.org/10.1039/c8cs00099a.

[210] P.B. Salunkhe, P.S. Shembekar, A review on effect of phase change material encapsulation on the thermal performance of a system, Renew. Sustain. Energy Rev. 16 (2012) 5603–5616. https://doi.org/10.1016/j.rser.2012.05.037.

[211] R. Murty V. Bhamidipati, Methods and compositions for inhibiting surface icing, US 2008/0276837 A1, 2008.

[212] T. Zapletal, P. Sperka, I. Krupka, M. Hartl, The effect of surface roughness on friction and film thickness in transition from EHL to mixed lubrication, Tribol. Int. 128 (2018) 356–364. https://doi.org/10.1016/j.triboint.2018.07.047.

[213] B. Bhushan, Principles and Applications of Tribology, Second, John Wiley & Sons Ltd, New York, 2013.

[214] A.M. Goitandia, M.B. Miguel, A.M. Babiano, O.G. Miguel, Use of phase change materials to delay icing or to cause de-icing in wind-driven power generators, US 2018/0230972 A1, 2018.

[215] K. Zhu, X. Li, J. Su, H. Li, Y. Zhao, X. Yuan, Improvement of anti-icing properties of low surface energy coatings by introducing phase-change microcapsules, Polym. Eng. Sci. 58 (2018) 973–979. https://doi.org/10.1002/pen.24654.

[216] X. Yin, Y. Zhang, D. Wang, Z. Liu, Y. Liu, X. Pei, B. Yu, F. Zhou, Integration of Self-Lubrication and Near-Infrared Photothermogenesis for Excellent Anti-Icing/Deicing Performance, Adv. Funct. Mater. 25 (2015) 4237–4245. https://doi.org/10.1002/adfm.201501101.

[217] K. Chen, K. Gu, S. Qiang, C. Wang, Environmental stimuli-responsive self-repairing waterbased superhydrophobic coatings, RSC Adv. 7 (2017) 543–550. https://doi.org/10.1039/c6ra25135h.

[218] G. Zhang, Q. Zhang, T. Cheng, X. Zhan, F. Chen, Polyols-Infused Slippery Surfaces Based on Magnetic Fe3O4-Functionalized Polymer Hybrids for Enhanced Multifunctional Anti-Icing and Deicing Properties, Langmuir. 34 (2018) 4052–4058. https://doi.org/10.1021/acs.langmuir.8b00286.

[219] W. Wang, D. Shen, X. Li, Y. Yao, J. Lin, A. Wang, J. Yu, Z.L. Wang, S.W. Hong, Z. Lin, S. Lin, Light-Driven Shape-Memory Porous Films with Precisely Controlled Dimensions, Angew. Chemie - Int. Ed. 57 (2018) 2139–2143. https://doi.org/10.1002/anie.201712100.

[220] Wei Huang, An Introduction to Shape Memory Materials, AZoM. (n.d.). https://www.azom.com/article.aspx?ArticleID=5164 (accessed August 5, 2021).

[221] A. Lendlein, O.E.C. Gould, Reprogrammable recovery and actuation behaviour of shape-memory polymers, Nat. Rev. Mater. 4 (2019) 116–133. https://doi.org/10.1038/s41578-018-0078-8.

[222] L. Zhao, J. Zhao, Y. Liu, Y. Guo, L. Zhang, Z. Chen, H. Zhang, Z. Zhang, Continuously Tunable Wettability by Using Surface Patterned Shape Memory Polymers with Giant Deformability, Small. (2016) 3327–3333. https://doi.org/10.1002/smll.201600092.

[223] D. Zhang, Z. Cheng, Y. Liu, Smart Wetting Control on Shape Memory Polymer Surfaces, Chem. - A Eur. J. 25 (2019) 3979–3992. https://doi.org/10.1002/chem.201804192.

[224] C.M. Chen, S. Yang, Directed water shedding on high-aspect-ratio shape memory polymer micropillar arrays, Adv. Mater. 26 (2014) 1283–1288. https://doi.org/10.1002/adma.201304030.

[225] and L.J. Dongliang Tian, Linlin He, Thermal-Responsive Superwetting Surface, in: Stimuli-Responsive Dewetting/Wetting Smart Surfaces and Interfaces, Springer International Publishing AG, 2018: pp. 81–106.

[226] Y. Wang, Y. Sun, Y. Xue, X. Sui, F. Wang, W. Liang, Q. Dong, Multifunctional electro-thermal superhydrophobic shape memory film with in situ reversible wettability and anti-icing/deicing properties, Colloids Surfaces A Physicochem. Eng. Asp. 654 (2022) 129960. https://doi.org/10.1016/j.colsurfa.2022.129960.

[227] J. Ma, T. Ma, W. Duan, W. Wang, J. Cheng, J. Zhang, Superhydrophobic, multi-responsive and flexible bottlebrush-network-based form-stable phase change materials for thermal energy storage and sprayable coatings, J. Mater. Chem. A. 8 (2020) 22315–22326. https://doi.org/10.1039/d0ta07619h.

[228] F. Liu, Z. Wang, Q. Pan, Intelligent Icephobic Surface toward Self-Deicing Capability, ACS Sustain. Chem. Eng. 8 (2020) 792–799. https://doi.org/10.1021/acssuschemeng.9b04570.

[229] Z. He, Y. Zhuo, F. Wang, J. He, Z. Zhang, Design and preparation of icephobic PDMS-based coatings by introducing an aqueous lubricating layer and macro-crack initiators at the ice-substrate interface, Prog. Org. Coatings. 147 (2020) 105737. https://doi.org/10.1016/j.porgcoat.2020.105737.

[230] L. Wang, Q. Gong, S. Zhan, L. Jiang, Y. Zheng, Robust Anti-Icing Performance of a Flexible Superhydrophobic Surface, Adv. Mater. 28 (2016) 7729–7735. https://doi.org/10.1002/adma.201602480.

[231] Z.A. Dijvejin, M.C. Jain, R. Kozak, M.H. Zarifi, K. Golovin, Smart low interfacial toughness coatings for on-demand de-icing without melting, Nat. Commun. 13 (2022) 5119. https://doi.org/10.1038/s41467-022-32852-6.

[232] C. Urata, G.J. Dunderdale, M.W. England, A. Hozumi, Self-lubricating organogels (SLUGs) with exceptional syneresis-induced anti-sticking properties against viscous emulsions and ices, J. Mater. Chem. A. 3 (2015) 12626–12630. https://doi.org/10.1039/c5ta02690c.

[233] A. Marmur, Non-Wetting Fundamentals, in: R.H.A. Ras, A. Marmur (Eds.), Non-Wettable Surfaces Theory, Prep. Appl., Royal Society of Chemistry, 2017: pp. 1–11.

[234] T. Ougizawa, T. Inoue, Morphology of Polymer Blends, in: L.A. Utracki, C.A. Wilkie (Eds.), Polym. Blends Handb., 2nd ed., Springer Science+Business Media Dordrecht, 2014: pp. 875–918.

[235] L. Makkonen, Ice adhesion - Theory, measurements and countermeasures, J. Adhes. Sci. Technol. (2012). https://doi.org/10.1163/016942411X574583.

[236] G.M. Swallowe, Mechanical Properties and Testing of Polymers: An A–Z Reference, Springer Science & Business Media, 1999. https://doi.org/10.1007/978-94-015-9231-4.

[237] K.A.Z. Halar Memon, Kiana Mirshahidi, K. Golovin, K.-S.C. Davide S. A. De Focatiis, X. Hou, Comparative study on the influence of surface characteristics on de-icing evaluation, J. Mater. Sci. 56 (2021) 17337–17352. https://doi.org/10.1007/s10853-021-06407-x.

[238] K. Golovin, S.P.R. Kobaku, D.H. Lee, E.T. DiLoreto, J.M. Mabry, A. Tuteja, Designing durable icephobic surfaces, Sci. Adv. 2 (2016) e1501496. https://doi.org/10.1126/sciadv.1501496.

[239] S. Heydarian, K. Maghsoudi, R. Jafari, H. Gauthier, G. Momen, Fabrication of liquid-infused textured surfaces (LITS): The effect of surface textures on anti-icing properties and durability, Mater. Today Commun. 32 (2022) 103935. https://doi.org/10.1016/J.MTCOMM.2022.103935.

[240] F. Wang, W. Ding, J. He, Z. Zhang, Phase transition enabled durable anti-icing surfaces and its DIY design, Chem. Eng. J. 360 (2019) 243–249. https://doi.org/10.1016/j.cej.2018.11.224.

[241] R.A. Anayurt, C. Alkan, Recent applications of microencapsulated phase change materials, J. New Results Sci. 10 (2021) 24–37. https://dergipark.org.tr/en/pub/jnrs.

[242] R. Chatterjee, D. Beysens, S. Anand, Delaying Ice and Frost Formation Using

Phase-Switching Liquids, Adv. Mater. 31 (2019) 1807812. https://doi.org/10.1002/adma.201807812.

[243] R. Chatterjee, H. Bararnia, S. Anand, A Family of Frost-Resistant and Icephobic Coatings, Adv. Mater. 34 (2022) 2109930. https://doi.org/0.1002/adma.202109930.

[244] R. Murty V. Bhamidipati, Methods and compositions for inhibiting surface icing, US 2008/0276837 A, 2008.

[245] A.M. Goitandia, M.B. Miguel, A.M. Babiano, O.G. Miguel, Use of phase change materials to delay icing or to cause de-icing in wind-driven power generators, US 2018/0230972 A1, 2018.

[246] SAE International, ARP5485B: Endurance Time Test Procedures for SAE Type II/III/IV Aircraft Deicing/Anti-Icing Fluids, Society of Automotive Engineering, Warrendale, PA, USA, (2017).

[247] E.N. Brown, M.R. Kessler, N.R. Sottos, S.R. White, In situ poly(urea-formaldehyde) microencapsulation of dicyclopentadiene, J. Microencapsul. 20 (2003) 719–730. https://doi.org/10.3109/02652040309178083.

[248] Y. Zhuo, S. Xiao, A. Amirfazli, J. He, Z. Zhang, Polysiloxane as icephobic materials – The past , present and the future, 405 (2021) 127088.

[249] C. Wang, T. Fuller, W. Zhang, K.J. Wynne, Thickness dependence of ice removal stress for a polydimethylsiloxane nanocomposite: Sylgard 184, Langmuir. 30 (2014) 12819–12826. https://doi.org/10.1021/la5030444.

[250] P. Irajizad, S. Nazifi, H. Ghasemi, Icephobic surfaces: Definition and figures of merit, Adv. Colloid Interface Sci. 269 (2019) 203–218. https://doi.org/10.1016/j.cis.2019.04.005.

[251] E.M. Fayyad, M.A. Almaadeed, A. Jones, Preparation and characterization of urea– formaldehyde microcapsules filled with paraffin oil, Polym. Bull. 73 (2016) 631–646. https://doi.org/10.1007/s00289-015-1518-x.

[252] P. Irajizad, A. Al-Bayati, B. Eslami, T. Shafquat, M. Nazari, P. Jafari, V. Kashyap, A. Masoudi, D. Araya, H. Ghasemi, Stress-localized durable icephobic surfaces, Mater. Horizons. 6 (2019) 758–766. https://doi.org/10.1039/c8mh01291a.

[253] E. Vazirinasab, K. Maghsoudi, G. Momen, R. Jafari, On the icephobicity of damage-tolerant superhydrophobic bulk nanocomposites, Soft Matter. 18 (2022) 412–424. https://doi.org/10.1039/d1sm01399h.

[254] M. Shamshiri, R. Jafari, G. Momen, Potential use of smart coatings for icephobic

applications: A review, Surf. Coatings Technol. 424 (2021) 127656. https://doi.org/10.1016/j.surfcoat.2021.127656.

[255] R.H.A. Ras, A. Marmur, Non-wettable Surfaces: Theory, Preparation and Applications, The Royal Society of Chemistry, Cambridge, 2016. https://doi.org/10.1039/9781782623953.

[256] A. Allahdini, R. Jafari, G. Momen, Transparent non-fluorinated superhydrophobic coating with enhanced anti-icing performance, Prog. Org. Coatings. 165 (2022). https://doi.org/10.1016/j.porgcoat.2022.106758.

[257] X. Wang, J. Huang, Z. Guo, Overview of the development of slippery surfaces: Lubricants from presence to absence, Adv. Colloid Interface Sci. 301 (2022). https://doi.org/10.1016/j.cis.2022.102602.

[258] S. Heydarian, K. Maghsoudi, R. Jafari, H. Gauthier, G. Momen, Fabrication of liquid-infused textured surfaces (LITS): The effect of surface textures on anti-icing properties and durability, Mater. Today Commun. 32 (2022) 103935. https://doi.org/10.1016/j.mtcomm.2022.103935.

[259] Z. Hao, W. Li, A review of smart lubricant-infused surfaces for droplet manipulation, Nanomaterials. 11 (2021) 801. https://doi.org/10.3390/nano11030801.

[260] R.J. Mohammad Irfan Lone, A review on phase change materials for different applications, Mater. Today Proc. 40 (2021) 10980–10986. https://doi.org/10.1016/j.matpr.2021.02.050.

[261] J. Jaguemont, N. Omar, P. Van den Bossche, J. Mierlo, Phase-change materials (PCM) for automotive applications: A review, Appl. Therm. Eng. 132 (2018) 308–320. https://doi.org/10.1016/j.applthermaleng.2017.12.097.

[262] Zhiwei He, H. Xie, M.I. Jamil, T. Li, Q. Zhang, Electro-/Photo-Thermal Promoted Anti-Icing Materials: A New Strategy Combined with Passive Anti-Icing and Active De-Icing, Adv. Mater. Interfaces. 9 (2022) 2200275. https://doi.org/10.1002/admi.202200275.

[263] Hicham Farid, Prédiction de la rupture fragile de la glace atmosphérique des câbles et des conducteurs des réseaux aériens de transport de l'énergie électrique par le développement des critères de rupture, Université du Québec à Chicoutimi, 2016.

[264] L. Sánchez-Silva, V. Lopez, N. Cuenca, J.L. Valverde, Poly(urea-formaldehyde) microcapsules containing commercial paraffin: in situ polymerization study, Colloid Polym. Sci. 296 (2018) 1449–1457. https://doi.org/10.1007/s00396-018-4365-0.

[265] S. Lang, Q. Zhou, Synthesis and characterization of poly(urea-formaldehyde) microcapsules containing linseed oil for self-healing coating development, Prog. Org. Coatings. 105 (2017) 99–110. https://doi.org/10.1016/j.porgcoat.2016.11.015.

Publications

Journal Articles

1- M. Shamshiri, R. Jafari, G. Momen, **A novel hybrid anti-icing surface combining an aqueous self-lubricating coating and phase-change materials**, Prog. Org. Coatings. 177 (2023) 107414. https://doi.org/10.1016/j.porgcoat.2023.107414.

2- M. Shamshiri, R. Jafari, G. Momen, **An intelligent icephobic coating based on encapsulated phase change materials (PCM)**, Colloids Surfaces A Physicochem. Eng. Asp. 655 (2022) 130157. https://doi.org/10.1016/j.colsurfa.2022.130157.

3- M. Shamshiri, R. Jafari, G. Momen, **Icephobic properties of aqueous self-lubricating coatings containing PEG-PDMS copolymers**, Prog. Org. Coatings. 161 (2021) 106466. https://doi.org/10.1016/j.porgcoat.2021.106466.

4- M. Shamshiri, R. Jafari, G. Momen, **Potential use of smart coatings for icephobic applications: A review**, Surf. Coatings Technol. 424 (2021) 127656. https://doi.org/10.1016/j.surfcoat.2021.127656.

Conference papers

1- **Development of a smart PDMS icephobic coating using encapsulated phase change materials, Surfaces,** Interfaces and Coatings Technologies international conference in Lisbon, Portugal, 2023**.**

2- **Improving the icephobic characteristics of the PDMS coating using phase change microcapsules**, Canadian Chemical Engineering Conference, Vancouver, Canada, 2022.

3- **Fabrication of icephobic coatings using impregnating phase-change microcapsules,** IWAIS, Montreal, Canada, 2022.

4- **Aqueous self-lubricating icephobic coatings inspired by ice skating**, 36th international conference of the polymer processing society, Montreal, Canada, 2021.

5- **Fabrication of aqueous self-lubricating icephobic coatings containing PEG-PDMS copolymers,** 5th QCAM Annual Symposium, Montreal, Canada, 2021.

6- **A survey of stimuli-responsive coatings with icephobic applications**, 4th QCAM Annual Symposium, Montreal, Canada, 2020.